The Thesis Committee for Ryan Ziegler Sitzes
Certifies that this is the approved version of the following thesis:

On the Use of Hydrophobic Biopolymers and Hydrophobic Biopolymer-Coated Sands for the Removal of Naphthalene, Phenanthrene, and Pyrene from Contaminated Sediments

APPROVED BY
SUPERVISING COMMITTEE:

Supervisor:

Danny D. Reible

Desmond F. Lawler

On the Use of Hydrophobic Biopolymers and Hydrophobic Biopolymer-Coated Sands for the Removal of Naphthalene, Phenanthrene, and Pyrene from Contaminated Sediments

by

Ryan Ziegler Sitzes, B.S.

Thesis

Presented to the Faculty of the Graduate School of

The University of Texas at Austin

in Partial Fulfillment

of the Requirements

for the Degree of

Master of Science in Engineering

The University of Texas at Austin

December 2010

Dedication

I would like to dedicate this thesis to my father Gary, my mother Ann, and my sister Laura. Without their unbounded love and support, this thesis would not have been possible.

Acknowledgements

The author wishes to acknowledge the following entities and individuals for their generous assistance in this project:

- Dr. Danny Reible at the University of Texas at Austin for funding this project
- Warrenton Fiber (Warrenton, Oregon) for their donation of sitka spruce chips
- Dr. Donald R. Paul at The University of Texas at Austin Polymer Processing Facility for the use of the Wiley mill
- Jim McClelland of the University of Texas at Austin Marine Science Institute for total carbon and total nitrogen analysis
- Tony Smith, Patrick Dunlap, and Ellison Carter of the University of Texas at Austin for their valuable time in instructing me on how to operate various laboratory equipment
- Steve Sorey of the University of Texas at Austin Nuclear Magnetic Resonance (NMR) Laboratory for his assistance in analysis of NMR spectra

December 2010

Abstract

On the Use of Hydrophobic Biopolymers and Hydrophobic Biopolymer-Coated Sands for the Removal of Naphthalene, Phenanthrene, and Pyrene from Contaminated Sediments

Ryan Ziegler Sitzes, M.S.E.

The University of Texas at Austin, 2010

Supervisor: Danny D. Reible

The overall objective of the present study was to evaluate the effectiveness of using a variety of hydrophobic biopolymers and hydrophobic biopolymer-coated sands as technically and economically feasible in-situ sediment amendments or alternative capping materials on a laboratory scale. Cutin from tomato peels, cellulolytic enzyme lignin from sitka spruce chips, and keratin azure from commercially dyed sheeps wool were isolated, prepared, tested, and evaluated as feasible hydrophobic biopolymers for the removal of selected Polycyclic Aromatic Hydrocarbons (PAHs). Testing included chemical and physical characterization, as well as the measurement of kinetics and

equilibrium sorption parameters for the sorbates naphthalene, phenanthrene, and pyrene as model hydrophobic organic contaminants. Tomato peel cutin exhibited the largest overall affinity for PAHs, however, keratin azure was selected for further evaluation as the most feasible material due to its low preparation cost.

Amendment of industrial sand with a stable, uniform, cross-linked keratin azure derivative was achieved to produce hydrophobic biopolymer-coated sand products containing zero, moderate, and high mass fractions of sand. Chemical and physical material parameters, as well as kinetics and equilibrium sorption parameters for the sorbates naphthalene, phenanthrene, and pyrene, were then obtained for the coated sand products. This allowed simple finite difference modeling of PAH fate and transport through a thin cap comprised of the same, insight into the specific sorption mechanisms involved, and information which could prove useful in predicting potential of keratin products to provide a suitable capping material. Conclusions and recommendations for future research focus on the technical and economical feasibility of the prepared hydrophobic biopolymers and hydrophobic biopolymer-coated sand products as capping or in-situ sediment amendments.

Table of Contents

List of Tables

List of Figures

Chapter 1: Introduction

Sediment contamination in coastal and inland waterways remains a major human health and ecological concern in the United States. Approximately ten percent of the sediments underlying the nation's waterways have been found or estimated to be contaminated with metals and other toxic pollutants at levels that pose significant risk to aquatic organisms as well as wildlife and humans that consume such affected organisms. Drinking water sources and local economies that rely on such waterways for recreation and tourism are also affected (*1*). Sources of contamination may include municipal and industrial discharges, agricultural and urban runoff, and mine drainage, among others.

Among the myriad of compounds of concern to remediation efforts are Hydrophobic Organic Compounds (HOCs). Of particular interest to the present study are Polycyclic Aromatic Hydrocarbons (PAHs). Pollutants of this nature tend to be less bioaccumulative and recalcitrant than others such as heavy metals. However, PAHs remain difficult to remove due to their very strong affinity for the solid phase. Consequently, PAHs may remain in sediments at concentrations far above ambient concentrations for decades. Conventional treatment of sediments contaminated with PAHs in such environments typically includes one or more of the following:

- Monitored natural attenuation including abiotic or biotic fate processes

- In-situ treatment or containment through capping
- Physical removal by dredging followed by ex-situ remediation and/or disposal

Abiotic or biotic processes generally take advantage of microbial and/or chemical metabolism to reduce, eliminate, or transform contaminants in sediment to less toxic levels or less mobile forms. The contaminant(s) of concern must be chemically and/or biologically available, and the environmental conditions must encourage the contaminant transformations without harming the ecosystem or destroying the water body's value as a resource. Along with monitored natural attenuation, these processes are largely ineffective and unproven in cases where contaminants are strongly sorbed to the solid phase, such as with PAHs and other HOCs.

In-situ treatment is also difficult since chemical and biological reagents are often difficult to place and contain, and delivery of amendments often requires an annihilation of the benthic environment, compromising the typical advantages of an in-situ technology. Moreover, dredging is usually discouraged in areas where contamination is less localized due to its cost, tendency to re-suspend contaminated sediments, inherent difficulties in residuals management, disposal limitations, difficulty in differentiating between uncontaminated and contaminated areas, and its impact to the landscape and aquatic ecosystem for long periods of time following cleanup. For these reasons, in-situ capping remains a feasible and appropriate remedial option, and is implemented at demonstration or full-scale at more than 100 contaminated sites nationally and globally.

1.1 OBJECTIVES OF THE PRESENT STUDY

The present study seeks to investigate the effectiveness of using a variety of hydrophobic biopolymers and hydrophobic biopolymer-coated sands as technically and economically feasible capping materials for the removal of HOCs. The materials could also be employed as in-situ treatment approaches if the disruption of amendment delivery is acceptable. More specifically, the present study aims to achieve the following objectives:

- Isolate and prepare a number of low-cost hydrophobic biopolymers with an estimated larger sorption capacity for HOCs than conventional biopolymer products
- Chemically characterize the prepared hydrophobic biopolymers to make sure that the materials have similar organic carbon content and approximately the same ratios of hydrophobic to hydrophilic carbon regions as analogous materials obtained for this research and characterized in literature
- Obtain batch kinetics and equilibrium sorption data for selected PAHs onto the prepared hydrophobic biopolymers
- Using a decision matrix, select the most promising and cost feasible hydrophobic biopolymer for further investigation as a sorptive coating on sand particles.

- Produce a stable, uniform, cross-linked hydrophobic biopolymer coating on sand particles using the chosen hydrophobic biopolymer to yield hydrophobic biopolymer-coated sand products containing approximately zero percent (w/w), 15 percent (w/w), and 85 percent (w/w) sand/biopolymer concentrations
- Obtain chemical and physical parameters of the prepared hydrophobic biopolymer-coated sand products that, along with sorption data, will allow simple modeling of cap performance using the same
- Obtain batch kinetics and equilibrium sorption data for selected PAHs onto the prepared hydrophobic biopolymer-coated sand products
- Prepare a number of mixtures of conventional biopolymer products and active capping materials
- Obtain batch kinetics and equilibrium sorption data for selected PAHs onto the prepared conventional biopolymer products and active capping materials
- Compare sorption capacities of hydrophobic biopolymers and hydrophobic biopolymer-coated sand products to conventional biopolymer products and active capping materials
- Model the overall effectiveness of a simple capping system comprised of the prepared hydrophobic biopolymer-coated sand products in removing selected PAHs from contaminated sediment using numerical column studies
- Form conclusions and develop recommendations on the technical and economical feasibility of the prepared hydrophobic biopolymers and hydrophobic biopolymer-coated sand products as capping materials in industry

It may be noted that the nature of the present study is largely first-stage concept development using a broad range of hydrophobic biopolymers. Optimization of any or all process parameters and composition of hydrophobic biopolymer-coated sand products is not emphasized and is beyond the scope of the present study.

1.2 A BRIEF INTRODUCTION TO SEDIMENT CAPPING

Capping generally consists of placing one or more layers of clean, granular material over a contaminated sediment layer and may be classified as either passive or active. Figure 1.1 illustrates the typical components of a cap. In cases where upwelling velocity is low, contaminants are strongly sorbed to the solid phase, and hydraulic erosion is controllable, passive capping using largely insert and nonsorbing materials such as sand is most often used to achieve one or more of the following:

- Physical containment of underlying contaminated sediment
- Separation of the contaminants from biota at the sediment-water interface
- Shift of certain oxidation-reduction zones above the contaminated layer
- Isolation of the chemical contaminants from the overlying water
- Encouragement of habitat reconstruction in the surficial sediments

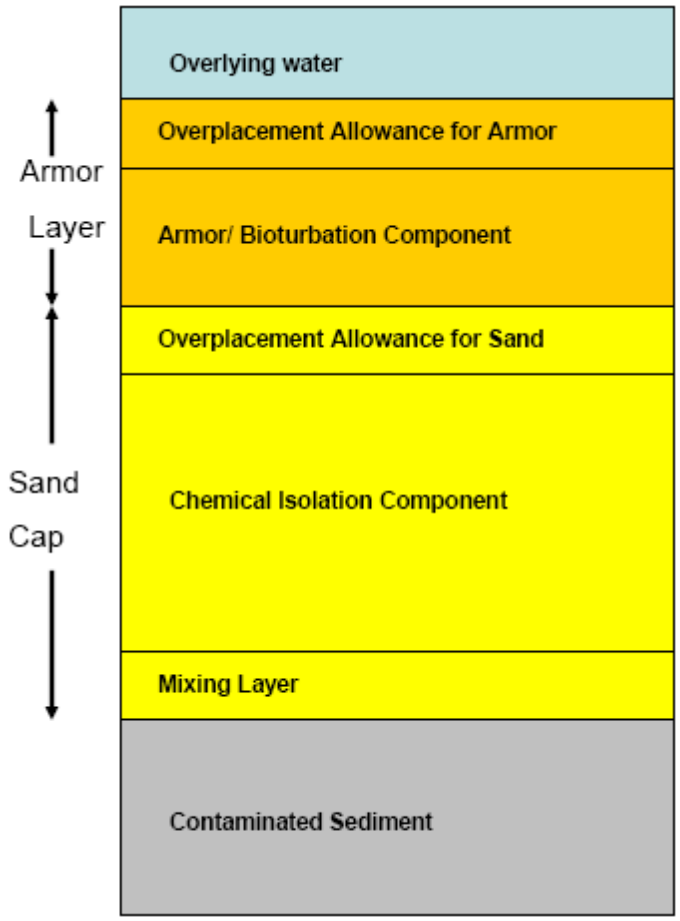

Figure 1.1: Capping Layers (*2*)

Active capping is the use of amendments to improve the performance of a cap through one or more of the following pathways:

- Encouragement of fate processes such as sequestration or degradation of contaminants beneath cap
- Increase of permeability control
- Increase of contaminant migration control (i.e. through sorption)

The most common material used for passive capping is sand, due to its low cost, high availability, and ease of placement. Active caps may include passive materials as well as active materials such as activated carbon, apatite, coke, organoclay, zero-valent iron, nanomaterials, oxygen or hydrogen releasing compounds, and/or biopolymers. In most cases, active capping is accomplished through the use of amendments to aid sorption or removal of contaminants from the mobile (interstitial water) phase. The amendments evaluated herein are focused solely on enhancing the sorption capacity of capping materials.

1.3 FEASIBILITY AND PERFORMANCE GOALS OF CAPPING MATERIALS

In order for the present study to be useful to industry, biopolymer products must be more feasible for implementation at contaminated sites than current, conventional capping materials. In the present study, a Capping Material A is defined as more feasible than a conventional Capping Material B if it removes (via sorption) more mass of contaminant per unit cost of material than Capping Material B. In other words, Capping Material A must have a lower unit contaminant removal cost than Capping Material B, where unit contaminant removal cost is defined as the cost per unit mass of sediment to reduce the sediment concentration to the desired amount. Unit contaminant removal cost may be reduced by decreasing the bulk material cost of the capping material, increasing sorptive capacity of the capping material, or both.

The bulk material cost may vary according to availability of raw materials and/or the presence of existing commercial infrastructure for production and transport. The true cost of using a certain capping material at any site may include costs in addition to bulk material cost, such as labor, equipment, and transportation to place the materials. In addition, secondary amendments or geotextiles are often required to hold in place, protect, or otherwise assist in implementing expensive or low-specific weight amendments, which also adds to total cost. Albeit these complexities associated with capping present a large degree of uncertainty in defining feasibility on a non site-specific basis, a general estimate of relative feasibility may be obtained for the sorbing amendments of interest here by comparing unit contaminant removal costs between capping materials.

Figure 1.2 presents relative orders of magnitudes of the overall solid-water partitioning coefficient, K_D, values for conventional capping materials. In Figure 1.2, K_{OC} is not material specific, and represents the equilibrium partitioning coefficient of the compound to natural organic matter in liters per kilogram. Also in Figure 1.2, f_{OC} is the fraction of organic carbon in the material.

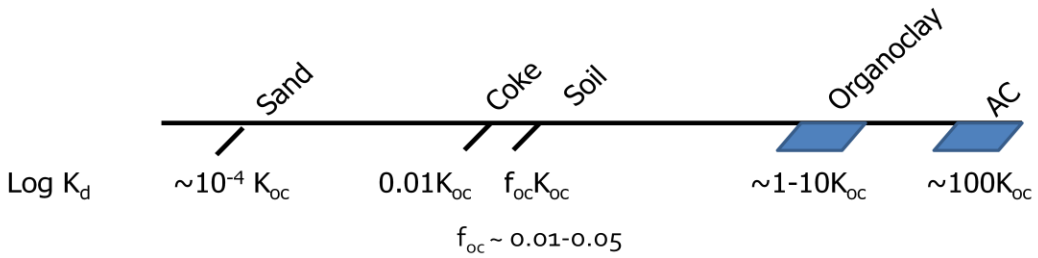

Figure 1.2: Relative Partitioning Coefficient Values (K_D values) of Various Capping Amendments (*2*)

For materials with organic carbon types very similar to natural organic matter, K_D is approximated by $f_{OC}K_{OC}$. For amendments which contain organic carbon types that are substantially more efficient or less efficient than natural organic carbon, the overall solid-water partitioning coefficient, K_D, may not be approximated by $f_{OC}K_{OC}$. As detailed later in this document, however, normalization of K_D by f_{OC} can still be used to obtain a material-specific "K_{OC}" value for comparison to the non specific K_{OC} value when determining the relative efficiency of the organic carbon present in the material.

As may be inferred from Figure 1.2, any alternative capping material would have to achieve a very high K_D value to compete with Activated Carbon (AC) or organoclay solely on the basis of sorptive capacity. It is thus reasonable to expect that the cost of the biopolymer products must be made as low as possible (i.e., by amending biopolymers with sand) to compensate for the lower sorptive capacity per mass of material.

Consider the closed system described in Figure 1.3, where an initially clean capping material is allowed to approach equilibrium with a contaminated sediment and overlying water. Also let $K_{D,sed}$ represent the overall solid-water partitioning coefficient for the sediment and $K_{D,cap}$ represent the overall solid-water partitioning coefficient for the capping material. Assuming $K_{D,sed}$ is less than $K_{D,cap}$, the mass of capping material required to remove a given fraction of the total contaminant mass from the sediment may be estimated from Equation 1.1, where M_{cap} is the mass of capping material, M_{sed} is the mass of contaminated sediment, $W_{sed,init}$ is the initial solid concentration of contaminant in the sediment, and $W_{sed,fin}$ is the final solid concentration of contaminant in the sediment at equilibrium.

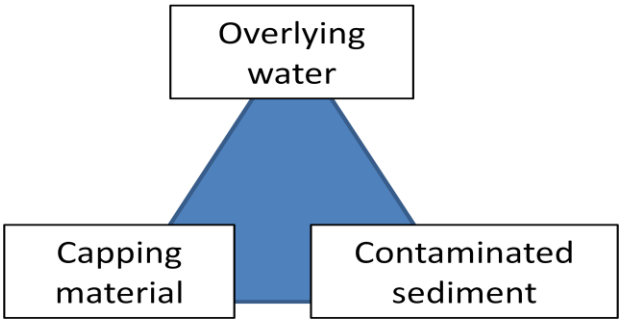

Figure 1.3: Example System

$$M_{cap} = M_{sed}\left(\frac{K_{D,sed}}{K_{D,cap}}\right)\left(\frac{W_{sed,init}}{W_{sed,fin}} - 1\right)$$

Equation 1.1: Removal Relationship

The mass may be converted to cost by assuming a unit cost of the capping material as shown in Equation 1.2, where UC_T is the total unit cost and UC_{cap} is the unit capping material cost in any appropriate cost units. It is appropriate to note here, however, that UC_{cap} may depend on M_{cap} (economy of scale exists). In such a case, an alternative relationship may be required for conversion to cost.

$$UC_T = M_{cap}(UC_{cap})$$

Equation 1.2: Conversion to Cost

Equations 1.1 and 1.2 are not without uncertainty, however. Equation 1.1 assumes that the porewater concentration is continuous from sediment to cap, and that the system is well-mixed. In a more realistic system, the assumption that the system is well-mixed may not be valid. A cap may only remove contaminants that migrate from the sediment up through a cap. "Removal," as it is used in this document, is relative to the contaminant concentration in the sediment. The mass of contaminant in the entire system remains constant if no other fate processes are present. In other words, the contaminants are sequestered, or immobilized in the cap, and are not completely removed from the overall system, as depicted in Figure 1.3. Considering these factors, an alternative to Equations 1.1 and 1.2 may be more useful in some cases. For example, comparison of relative feasibility of capping materials may be made simply by multiplying K_D by UC_{cap} to

obtain a pseudo-total unit cost factor. The resulting values would have little physical significance, but would serve as a suitable method of comparison.

Figure 1.4 presents solutions to Equations 1.1 and 1.2 for various unit costs typical of conventional materials. These unit costs, as well as the K_Ds are assumed for illustrative purposes and actual values may vary.

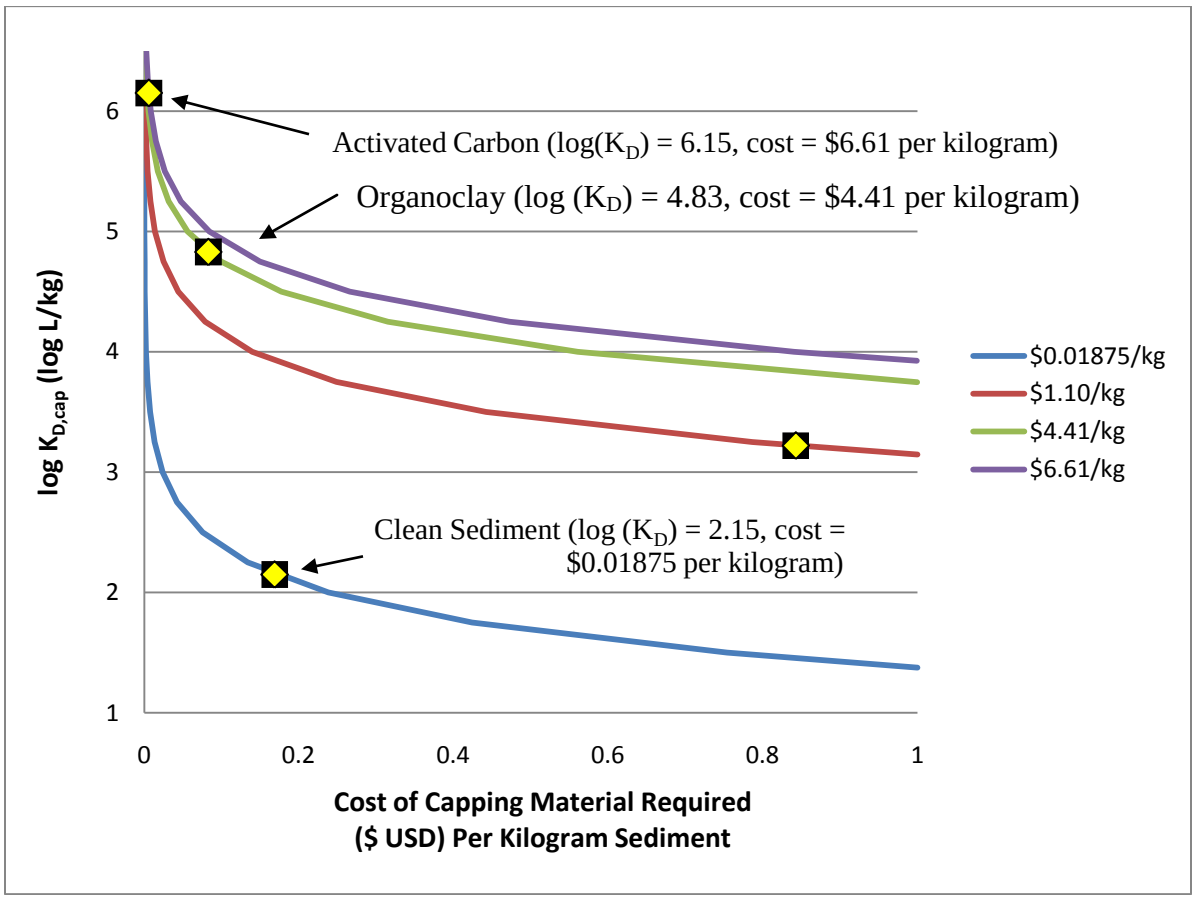

Figure 1.4: Comparative Cost of Various Capping Materials Used to Remove 90 Percent of Phenanthrene from One Kilogram of Contaminated Sediment

By choosing a maximum allowable cost per kg of sediment, one can get an estimate of the approximate cost and K_D value required to compete with conventional capping materials such as AC, organoclay, and sand. For example, consider a hydrophobic biopolymer-coated sand with a log(K_D) value of 4.25 log(liters per kilogram) for phenanthrene, which is approximately equal to that of bulk, unmodified cutin. Such a material would be more feasible than organoclay (log (K_D) = 4.83, cost = $4.41 per kilogram) if the unit cost was approximately $1.10 per kilogram, in terms of total cost required to remove the contaminant.

1.4 CHALLENGES OF USING CONVENTIONAL BIOPOLYMERS FOR THE REMOVAL OF HOCS FROM CONTAMINATED SEDIMENTS

Hydrophilic biopolymers such as chitins and gums have been investigated in the laboratory for their potential use in active capping applications (*3, 4*). Recent advancements in biomaterial technology have found that alginate and chitosan in particular have enormous potential as matrices for environmental applications because of their high biocompatibility, strong gel-forming tendencies, metal chelation and complexation capabilities, and versatility (*5, 6*). Chitosan and alginate have been applied extensively for heavy metal removal from aqueous solution (*7-10*). There are a number of drawbacks, however, associated with using hydrophilic biopolymers for sequestering hydrophobic contaminants. A first is instability in water at pH values not uncommon to the natural environment. A second is their very high bioavailability and susceptibility to

biotic degradation. Most important to the subject of the present study, however, is sorption capacity. The highly polar, polyhydroxyl structures of hydrophilic biopolymers offer a large number of H-bonding sites which produce a high affinity for water, limiting the accessibility of PAHs to internal hydrophobic domains (*11, 12*). Table 1.1 presents equilibrium sorption coefficients for phenanthrene and pyrene obtained from (*3, 4*) onto a clean, carbonate industrial sand, as well as the same sand amended with hydrophilic chitins and gums, and acid-washed sand amended with hydrophilic chitins and gums. Table 1.2 presents a description of the compositions of sand, sand amended with hydrophilic chitins and gums, and acid-washed sand amended with hydrophilic chitins and gums included in Table 1.1.

Table 1.1: Sorption of HOCs to Sand, Sand Amended with Hydrophilic Chitins and Gums, and Acid-Washed Sand Amended with Hydrophilic Chitins and Gums (*3, 4*)

Material	Equilibrium Sorption Coefficient, K_D (liters per kilogram)	
	Phenanthrene	Pyrene
Sand	3.19	27.01
CGB3	40.64	118.3
XCc	12.8	106.7
CGB3, Acid-Washed	~2.5	~11.0
XCc, Acid-Washed	~1.5	~18.0

Table 1.2: Description of Sand, Sand Amended with Hydrophilic Chitins and Gums, and Acid-Washed Sand Amended with Hydrophilic Chitins and Gums (*3, 4*)

Sample ID	Composition	Fraction Organic Carbon, f_{OC}	Porosity	Bulk Density (grams per milliliter)	Particle Density (grams per milliliter)	Hydraulic Conductivity (meters per year)
Sand	Not Available	0.003	0.378	1.515	Not Available	Not Available
CGB3	1.2% (w/w) sand, 49.4% (w/w) chitosan, 49.4% (w/w) guar gum	0.095	0.629	1.061	Not Available	179.82
XCc	1.2% (w/w) xanthan gum, 1.2% chitosan, 97.6% (w/w) sand	0.043	0.546	1.182	Not Available	72.37
CGB3, Acid-Washed	1.2% (w/w) acid-washed sand, 49.4% (w/w) chitosan, 49.4% (w/w) guar gum	Not Available	0.611	0.965	2.485	Not Available
XCc, Acid-Washed	1.2% (w/w) xanthan gum, 1.2% chitosan, 97.6% (w/w) acid-washed sand	Not Available	0.625	1.003	2.674	Not Available

The equilibrium sorption coefficients are substantially lower for the acid-washed sand mixtures when contrasted to the sand mixtures. This reduction in capacity may be mostly attributed to the removal of residual organic matter during the acid-washing process. All sands and coated sands exhibit poor sorption ability. Moreover, based on the fraction organic carbon measurements, each of the hydrophilic biopolymer products studied by (*3, 4*) are less efficient at sorbing HOCs than natural organic matter.

Although the mechanisms which decrease the sorption capacity of such biopolymers for hydrophobic, polyaromatic solutes may seem obvious, an increasing number of studies have shown that organic matter polarity is not necessarily the only dominating factor controlling sorption of HOCs. For example, a high correlation of aromatic moieties to the fraction of organic carbon-normalized K_D value, K_{OC}, has been widely observed for the sorption of aromatic HOCs to aromatic-rich organic matter, and is expected to be due to specific π-π interactions (*13-15*).

Other studies have observed a high correlation of both specific and non-specific HOC sorption to alkyl-C content in aliphatic-rich organic matter (*16, 17*). Consequently, generalized correlations for HOC sorption to alkyl-C content, aromatic content, or polarity have been strongly debated for the complex and highly varied forms of organic matter present in the environment. It is now generally suggested that any combination of specific and non-specific mechanisms may dominate sorption for any type of organic sorbent. Additionally, the hypothesis that sorbents may have a large abundance of polar-

C and still exhibit a high affinity for nonpolar solutes is becoming increasingly accepted on the basis that polar-C is not always available.

The roles of physical and chemical characteristics such as polarity, structure, and domain spatial arrangement on sorption of polyaromatic HOCs onto biopolymers are extensively discussed in (*15-24*), and generally conclude that K_{OC} values cannot be explained by polarity alone. Ideally, the arrangement and spatial positions of domains with high affinity for hydrophobic, polyaromatic solutes (i.e., alkyl-C and aromatic-C) as well as moieties with low affinity (i.e., alkyl-O and carbohydrate) must be positioned such that competition with polar, hydrophilic species such as water molecules is reduced.

Figure 1.5 illustrates the importance of chemical structure to sorption. Consider for comparison the structure of chitosan, alginate, guar gum, and xanthan gum presented in Figure 1.6, Figure 1.7, Figure 1.8, and Figure 1.9, respectively. In general, chitin is characterized by an amine functional group, while gums are composed of a variety of sugars and sugar derivatives.

As shown in the Figures 1.6 through 1.9, chitosan, alginate, guar gum, and xanthan gum have aliphatic domains characterized mostly by highly polar C and alkyl-O moieties in contrast to nonpolar, hydrophobic alkyl-C moieties. Such structures are not suitable for effective sorption of HOCs.

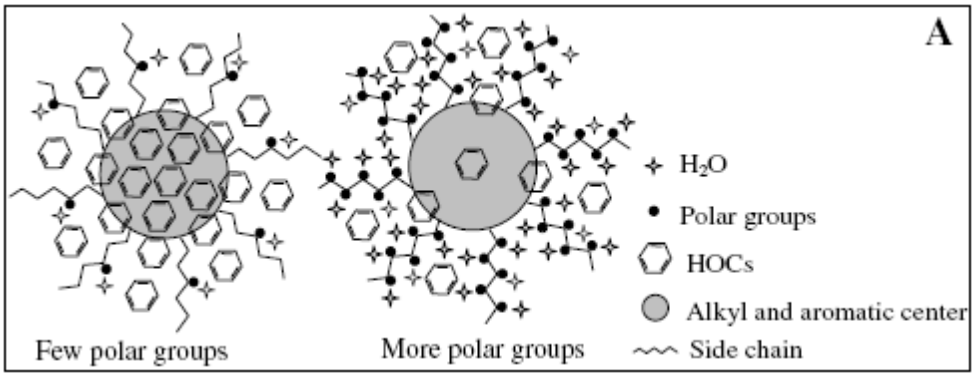

Figure 1.5: Effect of Polar Groups on Sorption of Hydrophobic Organic Contaminants (HOCs) (*15*)

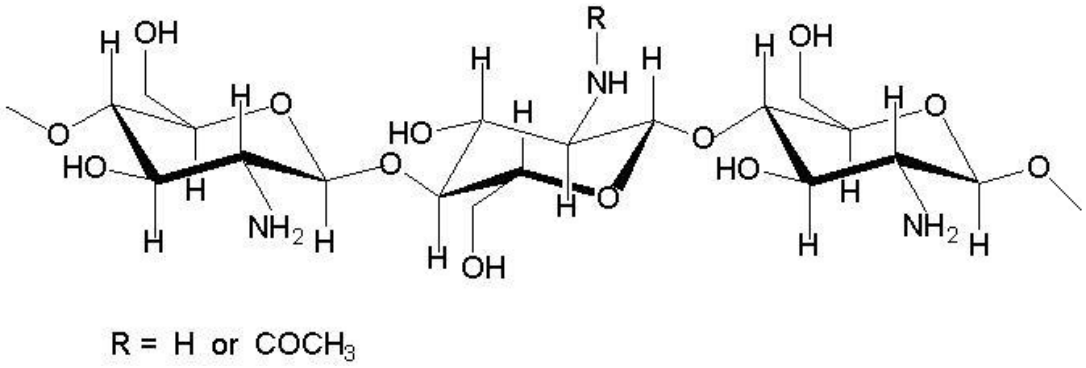

Figure 1.6: Chemical Structure of Chitosan (*25*)

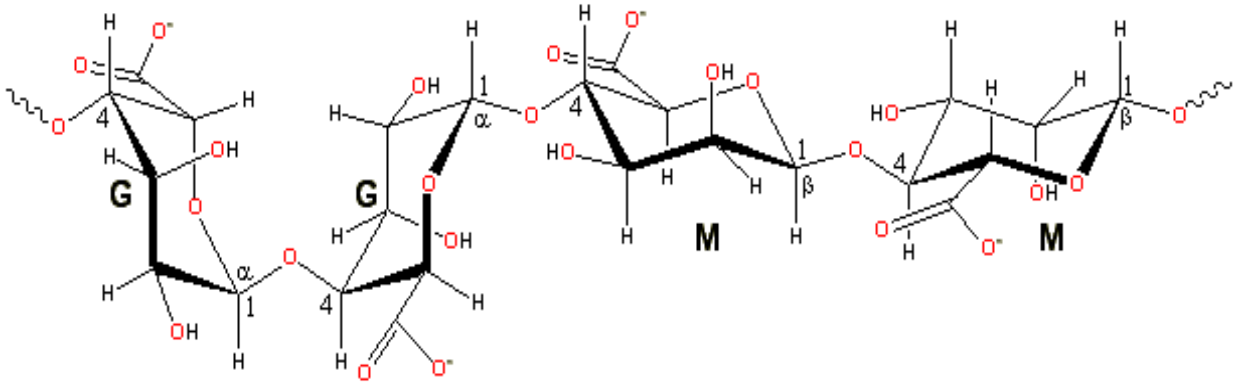

Figure 1.7: Chemical Structure of Alginate (*25*)

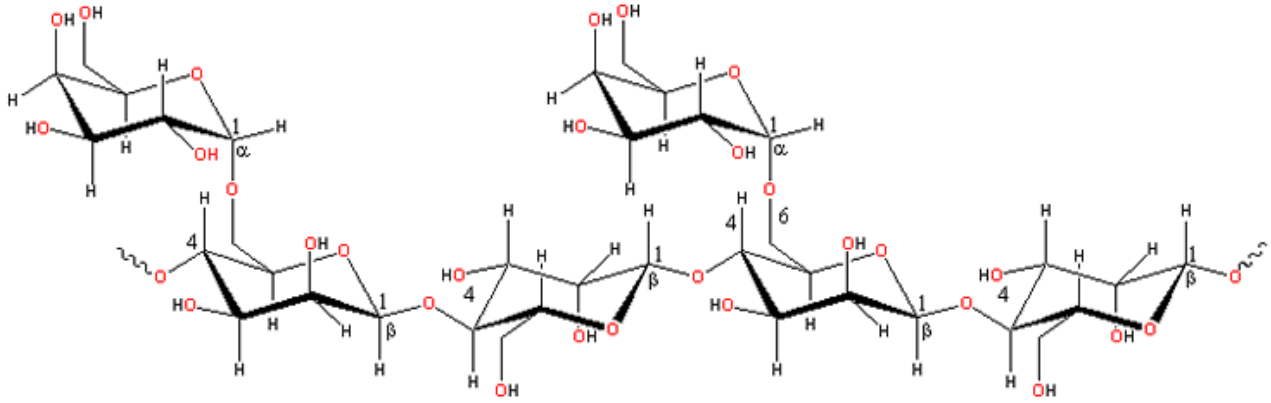

Figure 1.8: Chemical Structure of Guar Gum (*25*)

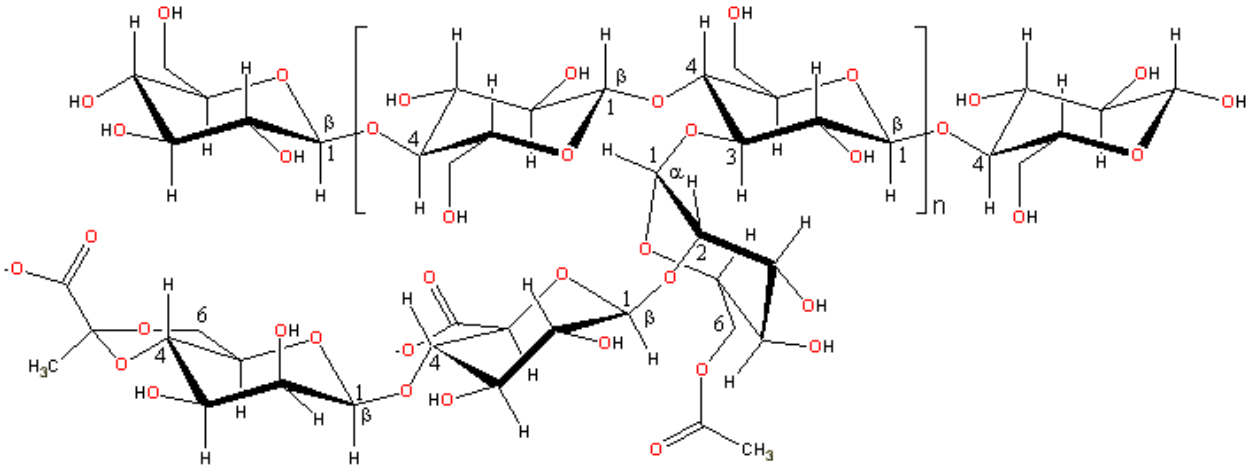

Figure 1.9: Chemical Structure of Xanthan Gum (*25*)

1.5 RATIONALE FOR THE PRESENT STUDY

Given the above discussion, investigation of a number of hydrophobic coatings on sand grains rather than hydrophilic coatings is necessary to explore the full potential of biopolymers as a low-cost, sorptive, and protective coating on conventional capping

amendments. To reiterate the rationale of amending capping materials using biopolymers, the following main advantages of coating materials are presented:

- Greater resistance of the desired amendment to variable flow, chemical composition, and environmental conditions typical to that of riverine surface environments
- Increased manageability of small-sized, high cost, or low specific-weight amendments during delivery, placement, and containment
- Increased overall surface area and sorption capacity of less-sorbing materials such as sand

Other advantages become apparent from the added versatility of immobilizing amendments in a biopolymer matrix. If left uncross-linked, the amendment-biopolymer composite may be introduced to a contaminated area via tremmie tubes suspended from floating barges. Increased throw mass and protection of amendments has also merited potential integration with water-jet injection technologies (*26*), which would allow injection of an amendment deep into sediment without destroying the amendment or large areas of the benthic or surficial environment. In dried, granular form, amendment-biopolymer composites may be placed in a conventional manner such as with a mechanical mixer, bucket or agricultural spreader attached to a floating barge, or between layers of geotextiles.

1.6 THREE POTENTIAL HYDROPHOBIC BIOPOLYMERS FOR INVESTIGATION IN THE PRESENT STUDY

Alternative biopolymers to chitins and gums (also known as "hydrocolloids") include starches, lignins, celluloses, peptins, hemicelluloses, proteins such as keratin, lipids, and cuticular materials such as suberins and cutins. Cellulose has been investigated by (*27*) as a potential sorbent for PAHs, and has been found to be roughly similar to chitins in both structural limitations and sorptive capacity for HOCs. However, the ability of plant cuticular materials and natural lignins to sorb a significant amount of hydrophobic organic pollutants has recently been demonstrated (*15-24, 28-31*). In cuticular materials, a significant impact on this sorbing ability is the presence of both crystalline and amorphous aliphatic regions. In lignins, sorption is mostly attributed to specific interactions with condensed, aromatic domains. The condensed lignin and long-chain cuticular material structures are also highly recalcitrant, which increases the potential for their use as capping materials. In the case of lignins, the highly aromatic-C, glassy structure with highly condensed hydrophobic domains mostly exhibit non-linear, Langmuir-type sorption of HOCs, contrasted to linear sorption typically associated with cutin's "rubbery" long-chain domains.

Unfortunately, cuticular plant biopolymers are not readily available commercially, but may be potentially available in the future from sustainable produce waste products using relatively simple and low cost production methods. Hydrophobic lignin products from organic biomass-to-energy and organic pulping processes have been commercially

available in the past, but have not been on the market since the dissolution of a company around the year 2007 that produced an organosolv pulping product, Alcell® lignin. The technology is currently owned by Lignol, who has developed a number of innovative applications for the process which are still in the pilot stages. Below is an excerpt from an email sent to the author in response to a request for hydrophobic lignin products from Lignol for testing, and illustrates the current state of availability of those products (*32*):

> …The organosolv lignin that you refer to was probably Alcell lignin that was made by an organosolv process (the Alcell Process) pioneered in the pulp and paper industry in the mid to late 1990's - this product was a highly hydrophobic material. It was commercially available at that time, but after the owner of the process went out of business, the technology was sold to our company, Lignol. We have continued development as part of an integrated biorefining process that produces cellulosic ethanol and biochemicals from biomass- an improved type of organosolv lignin, which we call HP-L Lignin is one of the proprietary products of Lignol's process. We have developed a number of applications for the material and we work with partners under Joint Development Agreements to tailor HP-L Lignin for specific applications - in many cases, these are hydrophobic materials too…

Conversely, less hydrophobic lignin products are widely commercially available in various forms from industrial pulping waste. The sorption capacity of these lignins has recently been shown to be rather minute for HOCs, however. Two good examples are kraft lignin and lignosulphonates, which are discussed further in later sections. Lignosulphonates are usually water-soluble, and are too polar for effective removal of HOCs. Kraft lignin is often water insoluble, but has a highly modified structure with relatively low accessibility for HOCs. This modification is due to exposure to strong

alkalis and bleaching chemicals in the pulping and kraft lignin recovery process. A good example of this phenomenon may be apparent from a study performed by (*33*), where water insoluble kraft lignin derived from softwood (spruce) and hardwood (birch) coniferous trees using the Lignoboost process (STFI-Packforsk) was mixed with fine clay sediment and added as a thin (two millimeter) cap to the surface of sediment contaminated with Polychlorinated BiPhenols (PCBs). Polychaete worms (*Hediste Nereis diversicolor*) were added for bioturbation and blue mussels (*Mytilus edulis*) were added to the water column. Results showed that compared to controls, PCB uptake by the blue mussels was decreased by 34 percent with sediment clay only, 50 percent with softwood kraft lignin and sediment clay, 77 percent with hardwood kraft lignin and sediment clay, and 90 percent with activated carbon and sediment clay. Normalization to fraction organic carbon values revealed that the kraft lignins used were as effective as activated carbon at removing PCBs, which shows the type of carbon to be promising.

Although the use of plant biopolymers is limited due to the aforementioned availability issues, biopolymers from animals may not be limited in terms of availability. For example, keratin is a highly hydrophobic protein found in animals that is widely commercially available as wool waste from the textile industry. Moreover, keratin may conceivably become widely available in the future from feather waste produced by large-scale poultry processing plants. The price for wool keratin for laboratory use is approximately $115 USD per five grams (Keratin Azure, Sigma-Aldrich, March 2010), which is still too high for use in active capping. The price of bulk feather keratin is

unknown, for obvious reasons. The high price of keratin may in large part be due to the lack of bulk production. However, if a market becomes available for bulk keratin in the future for active capping, keratin prices might decrease if production increases. Literature estimates for the sorption capacity of PAHs onto keratin are unavailable to the author's knowledge, however it is expected that sorption capacity may be analogous to or higher than that of cutins and lignins due to the highly hydrophobic nature of keratin.

In light of the previous discussion, three hydrophobic biopolymer materials were chosen for investigation in the present study: cutin from tomato peels, cellulolytic enzyme lignin from sitka spruce chips, and keratin azure from sheep's wool dyed with Remazol Brilliant Blue R (Reactive Blue 19). More advantages and disadvantages of using keratin, as well as cutin and lignin, are explained in the following sections detailing the chemistry of cutin, lignin, and keratin.

1.7 ORGANIZATION OF THESIS

In Chapter 2, the chemistry and sources of the three selected biopolymers are discussed in detail. In Chapter 3, materials used in the present study and methods used to obtain them are presented. Chapter 4 includes results and discussion, and Chapter 5 presents the conclusions of the present study as well as recommendations for future work.

Chapter 2: Occurrence, Uses, and Chemistry of Selected Hydrophobic Biopolymers

Modification to the chemical and physical properties of biopolymers desired for effective removal of HOCs is often unavoidable during their preparation for use as coatings on sand grains. Such modifications may include additional or altered functional groups due to the cleavage of chemical bonds, altered accessibility to polar or sorptive sites due to condensation or expansion of molecular linkages, changes in molecular weight, and/or the addition of byproducts or impurities.

In order to minimize modifications which may decrease the chemical, biological, or physical stability of the biopolymers, as well as decrease their sorption capacity for HOCs, a thorough understanding of the differences (if any) between biomaterials isolated from various sources is required so that suitable sources of raw or native biomaterials may be chosen. Furthermore, the most appropriate methods for preparing hydrophobic biopolymer products from those raw biomaterials must be identified. More specifically, consideration must be given to the many physical and chemical reaction mechanisms through which the following may be achieved:

- Preprocessing of raw or native biomaterial sources, which may include mechanical degradation of the sample via milling or grinding to decrease mass transfer limitations on chemical liberation and extraction
- Isolation and removal of the desired hydrophobic biopolymer from the biomaterial source. This typically includes chemical and/or biological cleavage of

molecular bonds which liberate desired constituents, solvent extraction of desired constituents into solution or suspension, and separation of desired hydrophobic biopolymer fractions from the solution or suspension via evaporation, filtration, and/or precipitation

- Purification of the hydrophobic biopolymer by a combination of washing and/or boiling in a combination of volatile and non-volatile solvents
- Amendment of the hydrophobic biopolymer onto sand particles, which may include dissolution and/or cross-linking

2.1 TOMATO PEEL CUTIN

Cutin is a waxy polymer which accounts for the main components of the plant cuticle. Cutin is produced at very large scales from the processing of fruits and vegetables for juices or sauces. Between 600-1200 million pounds of tomato waste were generated in the year 1994 alone from tomato processing (*34*), which contained approximately ten million pounds of cutin and cuticular materials. Currently, the primary use of these cuticular materials is academic, and no readily available commercial source of cutin exists. However, cutin may be useful in paints, coatings, drying oils, plasticizers, wetting agents, viscosity modifiers, or fat substitutes (*34*) if economical recovery processes are developed in the future.

Cutin is a highly hydrophobic polyester of cross-linked hydroxyl-fatty acids, hydroxyepoxy-fatty acids, and waxes with 16-18 carbons (*35*). The ends of these fatty acid carbon chains may contain carboxyl, aldehyde, or hydroxyl groups and cross-link via ester bonding. The ester linkages can accept, but not donate hydrogen bonds, making them highly hydrophobic. Cutan is similar to cutin, and is highly resistant to both acid and base hydrolysis. Cutan consists of polyethylene-like, long-chain fatty acids (greater than 30 carbons) attached to an aromatic core via ester linkages (*29, 30*). The main function of cutin is to render the plant cuticle impermeable to water, or at least regulate the flux of water across the cuticle. Cutin should not be confused with suberin, another waxy cuticular substance with a much different chemical structure. Suberins are possibly the most hydrophobic of all the cuticular materials, consisting of cross-linked polyaromatic and polyaliphatic domains. Hydroxyacids and diacids are common aliphatic domains, while polyaromatic domains are dominated by hydroxycinnamic acids and their derivatives (*36-38*). Figure 2.1 presents the general structure of the cutin macromolecule. As may be inferred from Figure 2.1, cutin is a sort of "irregular" biopolymer, in that it is characterized mostly by aliphatic lipids rather than a polysaccharide, peptide, or aromatic base.

Tomato peel methanolysates may be depolymerized via cleavage of ester bonds by alkaline hydrolysis, transesterification and other methods (*34, 35, 40*), typically in a methanol solution. Often, enzymatic degradation of lime fruit cuticular fractions is used to improve yields and/or break down cutin oligomers to monomers for enhanced

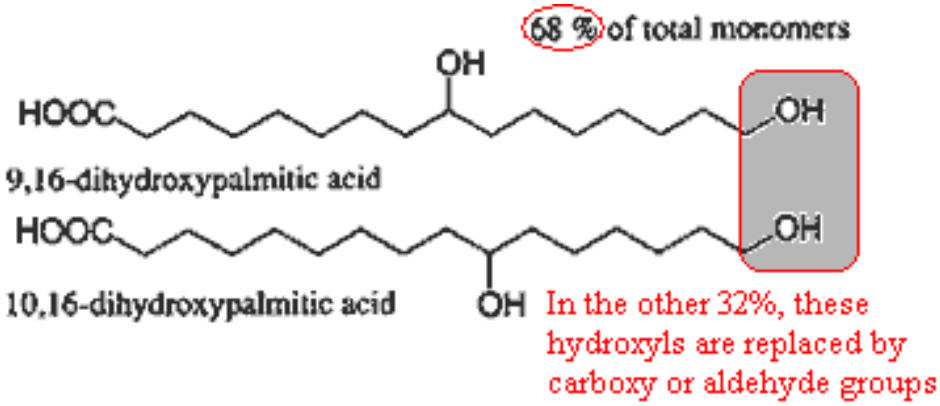

Figure 2.1: Chemical Structure of Cutin (*39*)

solubility and/or NMR analysis (*41, 42*). Filtration of the resulting mixture removes a large fraction of unwanted cuticular lipids and polar compounds such as carbohydrates and proteins. Cutin monomers and oligomers may be isolated from the filtrate by dissolution in an acidic aqueous solution followed by chloroform extraction. The leftover residues contain the remaining carbohydrate impurities may be discarded. Research by (*34*) reveals that cutin monomers of comparable purity may be obtained using an acidified aqueous methanolic monomer mixture with hexane. Cutin methanolysate may be precipitated by neutralization, and extraction of polar compounds is achieved via addition of water. Such an alternative would be much more economical and environmentally preferable; however, yields are only 40 percent of chloroform extraction yields.

In nature, cutin monomers and oligomers cross-link via esterification reactions between terminal and secondary hydroxyl groups in mid-chain positions. Recent research by (*43*) has shown that cutin monomers may self-assemble into layers, providing for a molecular orientation which facilitates the nucleophilic attack and the release of a water molecule required for an esterification reaction. Such self-cross-linking properties of cutin may prove useful in the inexpensive recross-linking of dissolved (or liquid-state) cutin onto sand grains. However, as discussed later in this document, cutin polymers exhibit a waxy consistency which is difficult to confine to a well-defined, rigid granular form in bulk. Cutin may thus conceivably form a non rigid capping layer with or without amendment to sand. However, its ability to maintain a granular product with a reasonably high porosity and/or permeability is debatable without further investigation.

2.2 CELLULOLYTIC ENZYME LIGNIN

Lignin is the principle component of plant cell walls, and rivals only cellulose as the most abundant biopolymer on earth. Figure 2.2 presents the general structure of the lignin macromolecule. Industrial uses for both water-soluble and water-insoluble waste lignin are many, and include adhesives and resins (*44-48*), polyurethane foams (*49*), coatings (*50*), materials for enhanced oil recovery (*51, 52*), concrete admixtures (*53*), coagulation/flocculation agents (*54, 55*), pesticide carriers (*56*), gel permeation matrices (*57*), thickening agents (*58*), and surfactants (*59*), among others.

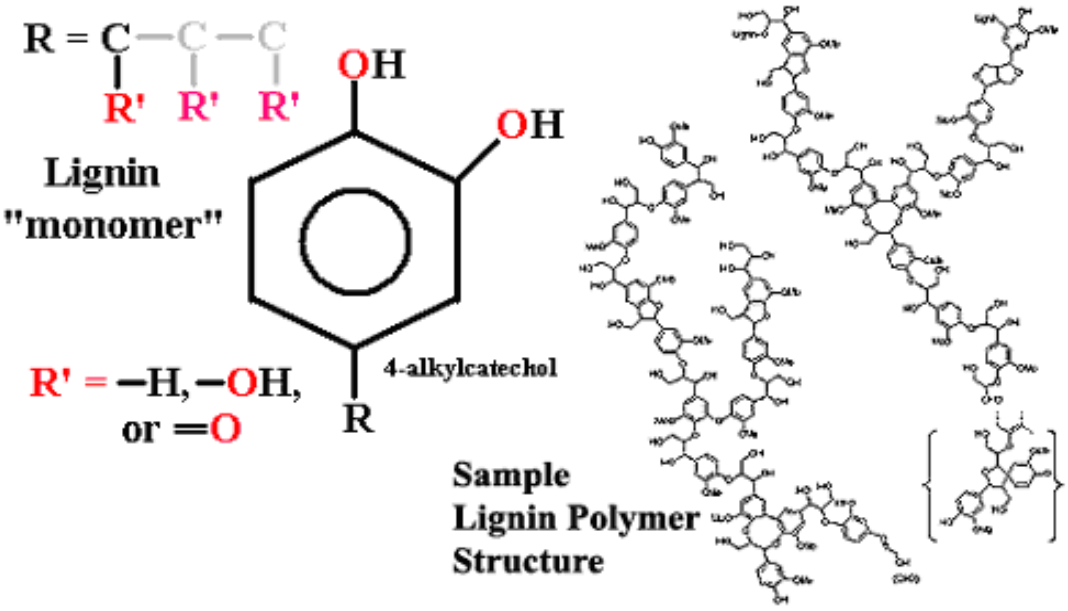

Figure 2.2: Chemical Structure of Lignin (*39*)

Lignin has been extensively investigated as a phenol reducer for phenol/formaldehyde resins in the wood processing industry because of the high cost, toxicity, and reduction in availability of phenol (*44-48*). The lignin is often substituted for phenol at a certain percentage and is subsequently cross-linked with the addition of formaldehyde. In the year 1996 alone, $600 million (USD) worth of lignin-based materials were sold globally, most of which were by-products of the pulping industry (*53*).

As may be inferred from Figure 2.2, lignins are highly complex, and may include aldehyde, carboxyl, keto, hydroxyl, methoxy, and/or phenolic functional groups. Lignin

is constructed via oxidative coupling of mostly three p-hydroxycinnamyl alcohol monomers, or monolignols, that differ only by their degree of methoxylation:

- p-coumaryl alcohol
- coniferyl alcohol
- sinapyl alcohol

These monolignols produce, respectively, the following units in the lignin oligomer (*60*):

- p-hydroxyphenol (H) phenylpropanoid
- guaiacyl (G) phenylpropanoid
- syringyl (S) phenylpropanoid

These units are illustrated in Figure 2.3.

Research has shown that lignin is often derived from monomers other than the three previously described (*62, 63*). Consequently, lignin may be broadly described as a phenylpropanoid polymer, which is lignified by radical coupling of phenols. Therefore, any hydroxyphenylpropanoid and its conjugate that can incorporate itself as a monomer into such polymers via these radical coupling reactions may be considered a lignin monomer (*62*). Examples of such alternative monolignol components are presented in Figure 2.4, and may include, among others (*62*):

- acylated (H), (G), and (S) monolignols

- ferulates and diferulates
- mutants and transgenics
- technical monolignols

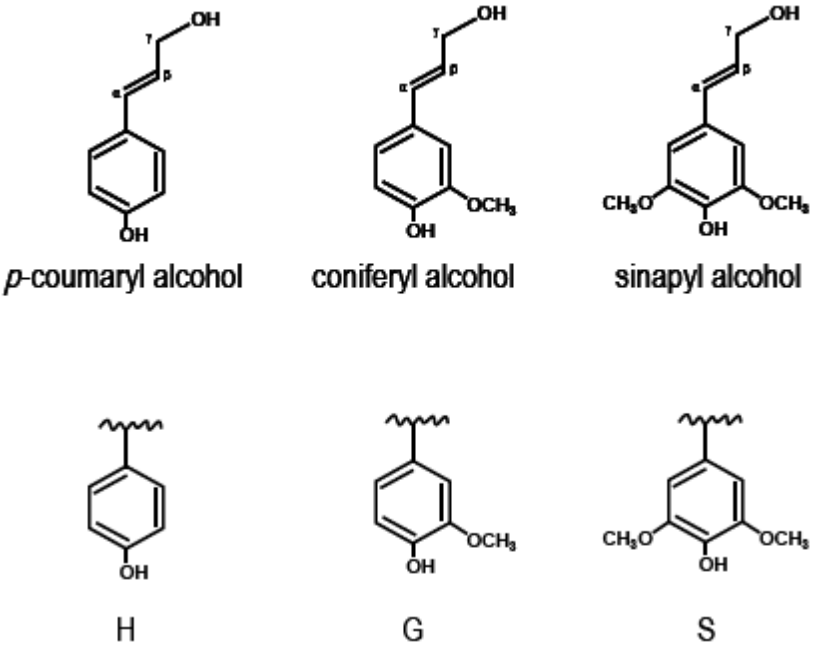

Figure 2.3: Three Basic Monolignols (*61*)

Acylated (H), (G), and (S) monolignols are common monomers involved in the radical coupling lignification process. Acylation is the process of adding an acyl group to a compound. An acyl group is formed from removing the hydroxyl group from an oxoacid, such as a monolignol. Various acylated monolignols include acetates, p-coumerates, and p-hydroxybenzoates, which always attach to the γ-carbon of the lignin

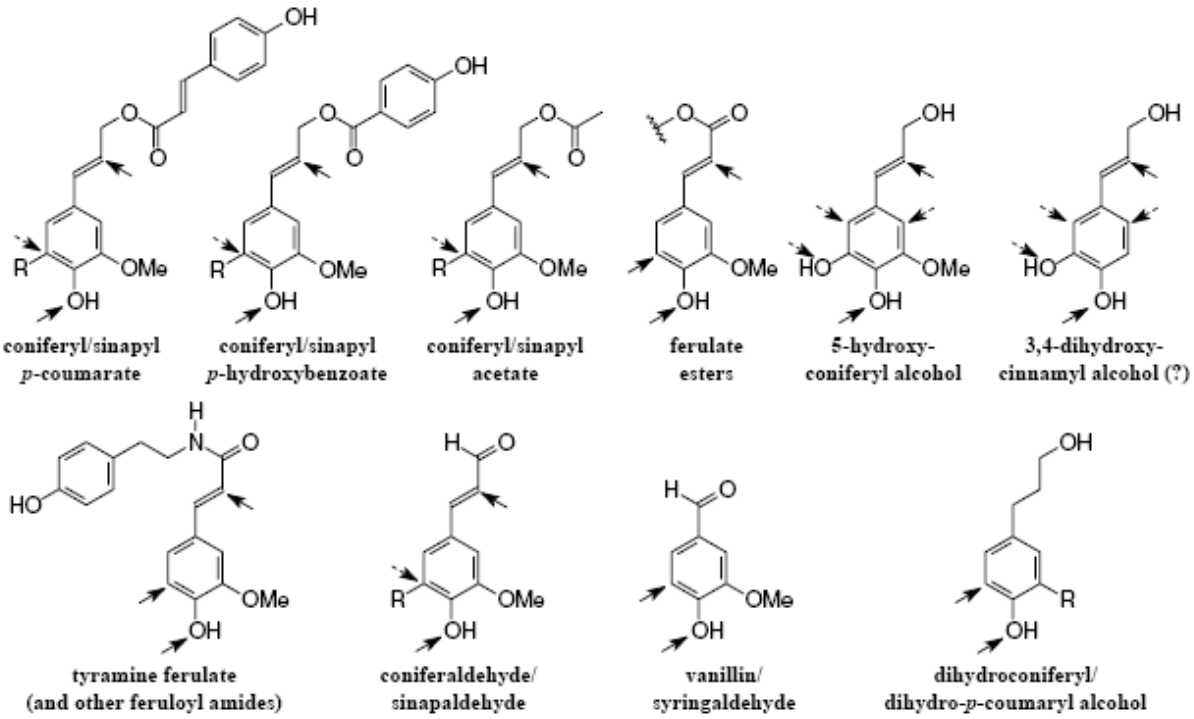

Figure 2.4: Conjugates of the Three Basic Lignin Monomers (*62*)

side chain. It has been somewhat ambiguously demonstrated that acylated monomers are pre-acylated at the monolignol level before polymerization into acylated lignin (*62, 64*).

Ferulates and diferulates are a group of monomers and/or dimers which have been shown to act as nucleation sites for lignification and bridge molecules between lignins and polysaccharides in plant cell walls (*65-69*). Ferulic acid is a bifunctional hydroxycinnamic acid that is easily oxidized by the peroxidase enzyme to create ferulate esters. An ester is formed when a hydroxyl group in an organic or inorganic aid is replaced by a –O-alkyl group. Ferulate esters may combine to form diferulates and

dehydro-dimers, or react to form a variety of structures, including tyramine ferulate and vanillin. Ferulate forms ether bonds with lignin at the α-carbon position of the propanoid side chains of lignin, and ester bonds at the C5-hydroxyl of α-L-arabinose sidechains of xylans. The types of bonds formed by ferulates and their derivatives can only be formed between ferulates and monolignols, and not with preformed lignin oligomers. In general, ferulation occurs at the arabinose or galactose side chains of pectic polysaccharides.

Mutant and transgenic monomers are derived from natural or biogenetic up- or down- regulation of key genes responsible for enzymes which control monolignol biosynthesis. They may incorporate precursors or derivatives of the three basic monolignols and components other than the three basic monolignols, and include dihydro-monolignols, tyramine hydroxycinnamates, aldehydes (including their products such as vanillin), and 5-hydroxyconiferyl alcohols, among countless others (*62, 70*).

"Technical", or industrial, lignin monomers are most often co-products of pulping, biomass-to-energy, or similar commercial processes that are aimed at converting woody materials into fibrous materials and/or extracting certain chemicals. Generally, industrial lignin products are highly modified and may contain significant amounts of non-lignin materials. They may include hydrolysis (acid) lignins, kraft lignins, lignosulfonates, organosolv lignins, and steam explosion lignins (*71-78*).

Hydrolysis (acid) lignin products are produced during the acid hydrolysis of wood. They are insoluble in water, highly modified, and contain high amounts of sugar degradation products, wood extractives, and inorganic compounds. Kraft lignins are produced during the reaction of woody material with NaOH and Na_2S at high temperatures, and are precipitated out of the system via acidification or ultrafiltration. Often, kraft lignins are sulfomethylated to solubilize for commercial interests. A disadvantage of kraft lignin as it pertains to the present study is its highly polar, modified structure that isn't immediately obvious due to its higher insolubility in water. Lignosulfonates are both soluble in water and highly modified. They are produced from acid sulfite pulping, bisulfate pulping, neutral sulfite semi chemical process, or alkaline sulfite-anthraquinone pulping. The chemical behavior and physical properties of a lignosulfonate may be varied according to its base and source. Bases may be a sodium, calcium, magnesium, or ammonium ion. Sources may include softwoods, hardwoods, or grasses. In general, lignosulfonates produced from hardwoods and grasses have a lower molecular weight than lignosulfonates produced from softwoods. Lignosulfonates generally contain highly modified sulfonated lignin polymers, sugar polymers, sugars, sugar acids, wood extractives, and inorganic compounds. Organosolv lignins are generally produced through organic solvent extraction processes, including ethanol/water pulping (Alcell®), Alkaline Sulfate Anthraquinone Methanol pulping (ASAM), Methanol pulping followed by methanol, NaOH and anthraquinone pulping (Organocell), and acetic acid/hydrochloric acid pulping (Acetosolv). The products obtained through these processes are generally insoluble, highly purified, only mildly modified, and contain a

high percentage of lignin. Steam explosion lignins are produced through high temperature, high pressure separation of fibers with steam. The products obtained are insoluble and typically include carbohydrate and wood extractive impurities. A disadvantage of this process is that acid hydrolysis reactions may reduce molecular weight.

Although technical, or "industrial" lignins are often widely available at reasonable cost, of most interest to the present study are lignins from native sources which are as unmodified as possible. Possibly the simplest method of "natural" lignin extraction is hydrolysis of woody material in an alcoholic solvent (*79*), which yields only a small amount of a combined lignin-carbohydrate fraction (approximately three to four percent of the total Klason lignin content in wood). Klason lignin is the total amount of lignin materials isolated through the strong acid degradation of woody materials, and the Klason lignin procedure is often used to quantify the amount of lignin in woody materials (*80*). The lignin structure is markedly changed by the drastic conditions used in this treatment, however, and the lignin material is left unusable afterward for the purposes of this study. Other wet chemical methods for the determination of lignin content in wood are less commonly employed and also highly modify the lignin structure (*80-86*).

The Brauns ("native") (*87*) solvent extraction method yields a slightly smaller amount of a much more purified lignin fraction and is one of the most effective methods used to isolate and prepare relatively unmodified, very hydrophobic lignin materials for

non-industrial applications. Brauns lignins exhibit properties very close to natural lignins, however, yield is on the order of two to three percent of the total Klason lignin content in wood. Yields may be improved to approximately 25 percent of the total Klason lignin content in wood using milling techniques developed by Bjorkman (*88*). Furthermore, yield purity may be significantly improved by increasing the cleavage of lignocellulose bonds using cellulolytic enzyme treatment (*89*). A disadvantage of cellulolytic enzyme treatment is the low availability and high cost of effective enzymes. Cellulolytic mold, although sparsely studied, may be an effective alternative to using cellulolytic enzymes (*90, 91*). Use of cellulolytic mold is not without its own disadvantages, however, as it may be subject to such unique requirements as advanced mycological culturing techniques and ability to use longer incubation times, for example.

Association of carbohydrate complexes within the cell wall of lignins affects yield and the structure of extractable lignin. The lignin-carbohydrate complex has been well-documented (*92, 93*). Investigations performed by (*89, 94-99*) have shown that the use of cellulolytic enzymes prior to the solvent extraction of milled wood lignins greatly increases molecular weight, and produces lignins that are more representative of those found naturally in plants. Some methods of lignin extraction in dioxane, a chemically indifferent solvent most used for lignin extraction and dissolution, are improved by slight acidification of the dioxane when used as an extraction solvent (*100*). However, acidic dioxane does not isolate a form of the lignin with a composition that is as close to natural lignin as methods which do not employ acidification. Methods that include the use of

alternative solvents, some of which may be more economically and environmentally feasible than dioxane, are described in (*101-104*).

The effects of various milling techniques and milling times have also been studied (*105-109*); and it has been shown that milling significantly affects the chemical structure and molecular weight of lignins obtained. Milling reduces polymerization and increases the free-phenolic groups through cleavage of β-aryl ether linkages and the formation of α-carbonyl groups via side-chain oxidation (*108*). Milling also condenses many bonds when heat is generated in the process, and generally affects the side-chain structure of the C9 phenyl-propane units in lignin the most. The use of ultrasonics has been employed to shorten milling and extraction times, as well as aid in the cleavage of lignin-cellulose bonds (*110, 111*). For the purposes of this study, however, cellulolytic enzyme lignins without ultrasonics are estimated to meet both yield and yield purity requirements for sorption experiments.

Softwoods such as sprucewood remain to be one of the most commonly used source for native lignin in academic studies, possibly due to their high availability. Since it is an objective of the present study to investigate the use of lignin from common waste products, spruce chips may be a preferred source of lignin materials for HOC sorption studies because of their high rate of use in paper pulping plants. The composition and structure of sprucewood lignin, as well as the differences between various softwood and hardwood lignins are generally known (*112, 113*). However, modern NMR techniques

allow much more detailed characterization of any lignin fraction used in the present study and are recommended (*114, 115*).

By re-dissolving the solid, purified cellulolytic lignin material into the same solvent(s) used to extract it, lignin monomers may cross-link to form lignin oligomers, and lignin oligomers may cross link to form lignin polymers. In general, there are three possible main reactive sites, or sites with free hydrogens, on a lignin monomer: the phenolic hydroxyl radical, the carboxyl group on the end of the aliphatic chain, and the ortho position to the phenolic hydroxyl radical. Lignin cross-linking may be achieved in one or both of the following ways: (i) phenolic (non-condensed) ether bonding, and (ii) non-phenolic (condensed) carbon-carbon bonding. Phenolic cross-linking requires expensive cross-linking agents, but exhausts polar hydroxyl groups, which would increase the hydrophobicity of the lignin for PAH sorption. Condensation of lignin does not necessarily make free hydroxyl groups unavailable for further reactions, and may significantly alter functionality and domain spatial arrangement. Oftentimes condensation reactions require heating or addition of mineral acids, which may additionally cause structural damage or charring to lignins.

Figure 2.5 presents examples of phenolic cross-linking between some lignin monomers, including an (A) β-O-4’ alkyl-aryl ether bond and a (B) 4-O-5’ aryl-aryl ether bond (*61*). Figure 2.6 presents examples of non-phenolic cross-linking between some lignin monomers, including linkages between two side chains such as the β-β’/α-O-γ’/γ-

O-α' resinol bond (C), linkages between a side chain and an aromatic ring such as the β-1' (D) and phenylcoumaran β-5'/α-O-4' bonds (E), or biphenyl linkages between two aromatic rings such as the dibenzodioxocin 5-5'/α''-O-4/β''-O-4' (F) and spirodienone β-1'/α-O-α' (I) bonds (*61*).

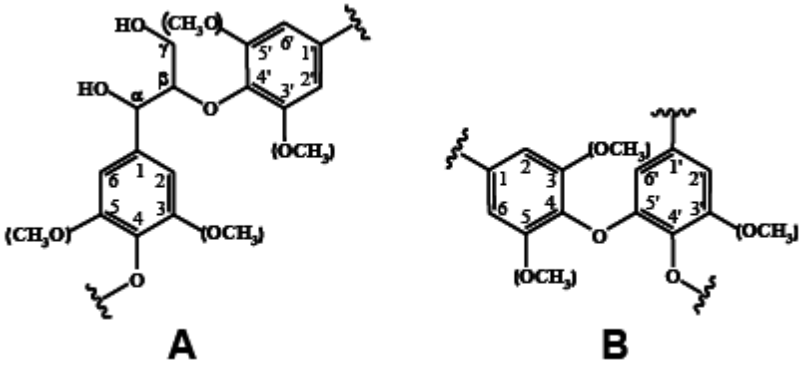

Figure 2.5: Non-Condensed Monolignol Bonds (*61*)

Phenolic cross-linking of lignin may be achieved by bridging the free phenolic hydroxyl groups with bi-functional organic compounds and/or polyvalent metal cations, with or without pre-phenolation to provide for more reactive sites. Aliphatic chains of halogen- or epoxide- containing bifunctional organic compounds such as epichlorohydrin, di-epoxide, polyoxyalkylene dihalide, dichlorohydrin, 1,2,3,4-diepoxybutane, bis-epoxypropyl ether, ethylene glycol-bis-epoxypropyl ether, and 1,4-butane-diol-bis-epoxy-propyl ether have been used to achieve phenolic cross-linking of lignins in industry (*56, 57, 116*).A disadvantage of using such compounds, however, is that they are all highly toxic and not suitable for environmental applications.

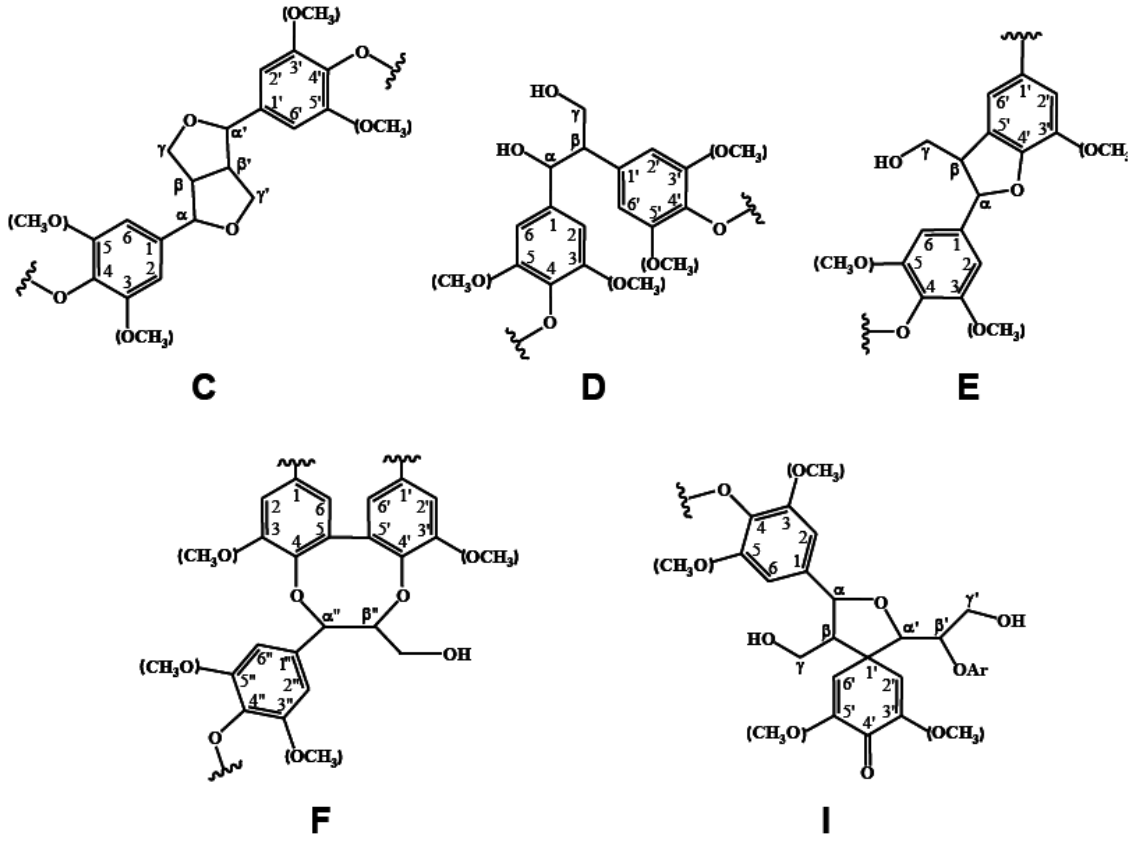

Figure 2.6: Condensed Monolignol Bonds (*61*)

Positive, polyvalent cations are more environmentally friendly, however, and have been shown to complex with lignins and materials similar to lignins, such as humic acids (*117-122*). In fact, the metal-lignin complex provides the driving force behind several coagulation aids and ion exchange resins used in industrial effluent treatment and coagulation of excess humic substances in drinking water treatment (*123-126*) Unless a water-soluble lignin is used initially, however, positive metal ion complexation requires

much modification to the lignin structure prior to cross-linking to provide enough reactive sites (i.e. hydroxyls) for significant bonding. This would be highly undesirable for sorption of HOCs, and would render lignin unsuitable for providing a stable coating on sand grains in an aqueous system. Cation-lignin bond stabilities also tend to be much more dependent than bifunctional organic agents on the chemistry of the surrounding aqueous phase. Choosing a cation which would provide for a stable, sufficiently strong bond throughout the wide range of pH values, ionic strengths, and competing cations not uncommonly present in riverine environments is a very difficult and complex task. If the structure of the modified lignin may be assumed to be approximately similar to humic substances in both size and number/types of reactive groups, models such as the Non-Ideal Competitive Adsorption (NICA)-Donnan and Model-V may be used to make predictions on cation-lignin bond stability under various environmental conditions (*127-140*). However, such assumptions are rarely valid. In addition to the complex nature of cation binding to water-soluble lignins, effects of cation complexation on the sorption of HOCs to natural organic matter, including lignins, have also been observed (*141-145*). Such effects include a decrease or increase in total sorption capacity, as well as enhanced sorption nonlinearity, sorption/desorption hysteresis, and competition between multiple solutes. Therefore, for the purposes of this study, phenolic cross-linking of lignin would seem undesirable.

Non-phenolic methods of cross-linking lignins mostly include the use of aldehydes, specifically formaldehyde or formaldehyde-forming agents, with or without

prior chemical modifications such as oxidation, methylolation, phenolation, or similar reactions to produce more active sites for cross-linking, as formaldehyde alone is typically not strong enough. Non-phenolic cross-linking with formaldehyde requires a free ortho or para position to a phenolic hydroxyl group along the aromatic ring. Consequently, formaldehyde treatment alone often results in a small, inadequate amount of cross-linking in the case a large number of syringyl units are present in the lignin. This, along with the consideration of the toxicity of formaldehyde, suggests that formaldehyde alone may not be suitable for use as a cross-linking agent in environmental applications. Glyoxal, a non-toxic aldehyde, has been shown to be suitable for cross-linking lignin (*56, 146*) and would be suitable for the present study, however. Other forms of non-phenolic cross-linking may include the use of ferulates and diferulates as previously mentioned to provide nucleation sites for radical-radical cross-linking and peroxidase-mediated phenol oxidative coupling of lignin-lignin and lignin-carbohydrate fractions (*65-69*). Association of ferulates and diferulates in the cross-linking of pectin, proteins, and gelatin have also been observed, which shows the effectiveness and versatility of using ferulate-mediated cross-linking of an entire host of biopolymer types (*147-149*).

Lignin reactivity is often improved prior to cross-linking by chemical modification. Such modifications may include oxidation and/or reduction (*116*), methylolation (*46, 56*), phenolation (*44*), or a combination of both (*116*). The first method, oxidation, generates free radical intermediates which combine to form biphenol

structures. Oxidative coupling with oxidizing agents such as hydrogen peroxide, alkali metal persulfates, permanganates, and perborates may be facilitated by oxidative enzymes capable of catalyzing oxidative reactions, such as peroxidases (hydrogen peroxide as substrate) and oxidases (molecular oxygen as substrate) are employed. The second, methylolation, uses methylolating agents such as formaldehyde, paraformaldehyde, glyoxal, glutaric dialdehydeformalin, hexa methylene-tetramine, or other compounds which readily decompose to formaldehyde to introduce methylol groups to the lignin compound. After methylolation, a phenolic cross-linking agent such as phenol, cresol, catechol, resorcinol, or bifunctional organic compound capable of phenolic cross-linking may be used to react with the methylol groups, condensing the mono- and poly-methylol monomers to form methylene ethers which further react to form methylene bridged polymers. The third, phenolation, consists of adding phenol-like groups to the lignin compounds to increase the number of aromatic rings with available ortho positions relative to the hydroxyl group. After phenolation, formaldehyde or formaldehyde-forming compound are added to condense the monomers via C-C bonding.

2.3 KERATIN AZURE

Keratin is a naturally abundant fibrous protein found in animals that rivals only chitin as one of the toughest biomaterials known. Keratin has many useful properties such as “self-healing” that have made it an excellent biomaterial for the medical fields, where it has served as a material for medical implants, diffusion membranes for drug delivery,

tissue-engineering scaffolds, and wound dressings (*150-152*). Keratins have also been employed outside of the medical industry in electronics (*153*), food products (*154*), cosmetic products (*155*), and as substitutes for petroleum-based components in plastics (*156*), among others.

The keratin macromolecule has an average molecular weight of approximately 60,000 grams per mole and may generally be described as a polypeptide consisting of approximately 18 amino acids that connect to form larger three-dimensional structures (*157*). Figure 2.7 presents a simple representation of the keratin macromolecule. The amino acid composition of keratin from human hair, lamb wool, and hen feathers in particular are presented in Table 2.1, which has been reproduced without permission from (*159*).

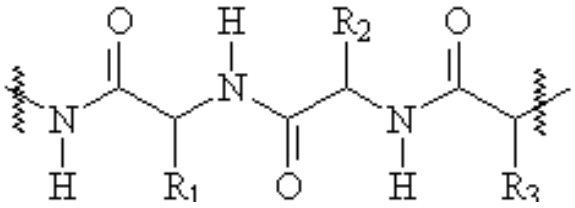

Figure 2.7: Chemical Structure of Keratin (*158*)

In general, amino acids contain an amine group, a carboxylic group, and a side chain which varies between individual amino acids. It is vitally important to understand what the particular composition of the side chains are in any polypeptide used for sorption of HOCs, along with what carbon the amine group attaches to in the overall

TABLE I

Amino Acid Composition of Some Eukeratins

Protein	Nitrogen	Sulfur	Histidine	Lysine	Arginine	Cystine	Tyrosine	Tryptophane	Phenylalanine	Glycine
	per cent	*per cent*	*per cent*	*per cent*	*per cent*	*per cent*	*per cent*	*per cent*	*per cent*	*per cent*
Human hair	15.4	5.0	0.6	2.5	8.0	15.5	3.0	0.7	2.6	4.3
Chimpanzee hair (5)†	16.7	4.3	0.6	2.0	8.1	15.5	3.3	1.4		
Goat hair	16.2	3.1	0.7	3.2	8.1	8.9	3.0	0.9	4.6	6.3
Cow " (5)	15.3	3.7	0.7	2.0	7.5	13.4	3.3	1.4	3.9	10.3
Lamb wool	15.4	3.6	0.7	2.5	8.7	13.1	4.5	0.7	4.0	6.5
Camel "	15.1	3.1	0.6	2.7	8.6	11.0	3.1	0.8	4.1	9.2
Cattle horn	16.1	2.6	0.6	2.4	8.6	8.2	3.7	0.7	4.0	9.8
Rhinoceros horn	15.6	2.3	0.6	2.6	8.2	8.7	8.6	1.7	5.0	7.4
Finger nails (7)	14.9	3.8	0.5	2.6	8.5	12.0	3.0	1.1	2.5	
Porcupine quills	15.8	3.0	0.6	2.6	7.6	9.4	3.3	0.9	3.6	5.7
Echidna quills	15.2	3.8	0.5	1.8	6.8	11.9	9.1	2.2	6.8	
Hen feathers	15.5	2.3	0.3	1.6	6.0	6.8	2.2	0.7	5.3	9.5
Snake skin	15.2	2.2	0.4	1.9	5.4	6.6	5.2	0.9	3.9	13.1
Egg shell membrane (4)	16.6	3.8	0.9	3.7	9.9	12.7	2.5	2.6	2.0	

* The cystine values have been calculated as cysteine.

† Bibliographic reference number.

Table 2.1: Amino Acid Composition of Various Eukeratins (*159*)

amino acid molecule. Such factors may determine a protein's secondary, tertiary, and quaternary structure, as well as affect the macromolecule's overall chemical functionality and affinity for hydrophobic solutes in aqueous systems. For example, some amino acids found in keratins contain charged polar side chains, such as histidine and lysine. Others such as serine, tyrosine, and threonine have non-charged polar side chains, while leucine

and methionine contain nonpolar side chains (*160*). These side chains may interact with themselves, as well as water molecules in the surrounding environment, to produce the particular micro- and macro-molecular shape of a protein and its specific affinity for dissolved solutes. All amino acids, however, since they contain both amine and carboxylic acid functional groups, are both acids and bases. When the number of protonated, or positively charged groups (i.e. ammonium groups) equal the number of deprotonated, or negatively charged groups (i.e. carboxylate groups), the amino acid has no overall electric charge and is at a pH known as the isoelectric point. Amino acids have minimum aqueous solubility at their specific isoelectric points, and may exist at the isoelectric point in both solid matrices and in polar, liquid solutions.

There are two major secondary forms of keratin, alpha- (α-) keratin and beta- (β-) keratin (*160-162*). Alpha- (α-) keratins consist of α-helically coiled, single polypeptide chains, and are the primary keratin found in mammalian skin and the cortex of mammalian hair. They are highly flexible, elastic, moderately water-soluble, and very fibrous. Alpha- (α-) keratins often occur in superhelical structures comprised of a large number of α-helical keratin fibers woven together. Beta- (β-) keratins consist of β-pleated polypeptide sheets which are stacked and/or twisted together to yield a highly rigid structure. Beta- (β-) keratins are the primary keratin found in mammalian hooves, fingernails, and horns, as well as the feathers, beaks, and claws of birds, and the shells and claws of reptiles, among others.

The differences in the physical and chemical behavior of these two types of keratin may be attributed to the particular combination of bond types present both within and between their associated polypeptide chains. In polypeptides such as keratins, the type of bonding generally may be reduced to the side chain and amino acid composition of each (*160, 161*). For example, some amino acid groups such as cysteine form covalent bonds between each other to make disulfide bonds. Other groups may form one of two main types of hydrogen-bonded groups: (-O-H-O-) and (-O-H-N-). (-O-H-O-) groups result from water-water and water-hydroxyl interaction while (-O-H-N-) groups result from amide-amide, amide-carboxyl, and amide-carboxylic acid interactions between side chains. Van der Waals forces between polypeptide chains also play a particularly large role in keratin bonding. Interactions between hydrophobic keratin domains in the presence of water are responsible for the formation of double α-helically coiled ropes which make up intermediate filaments in hair. The last major type of bond interaction in keratins may be classified as coulombic, occurring between basic or acidic side chains ($-NH_3^+$) and ($-COO^-$).

Each of the aforementioned bonds, however, has a different associated strength, or total energy required to perturb the distance between the atoms a certain amount. Such a distance is also relatively specific for each type of bond. The result is that there is a very wide range of natural and synthetic keratin structures, each with a different chemical behavior in aqueous systems than the other. Such a concept is illustrated in Figure 2.8, which has been reproduced without permission from (*161*). As may be inferred from

Figure 2.8, covalent bonds are much stronger than weaker interactions such as hydrogen, coulombic, or Van der Waals, but form with much smaller distances between atoms.

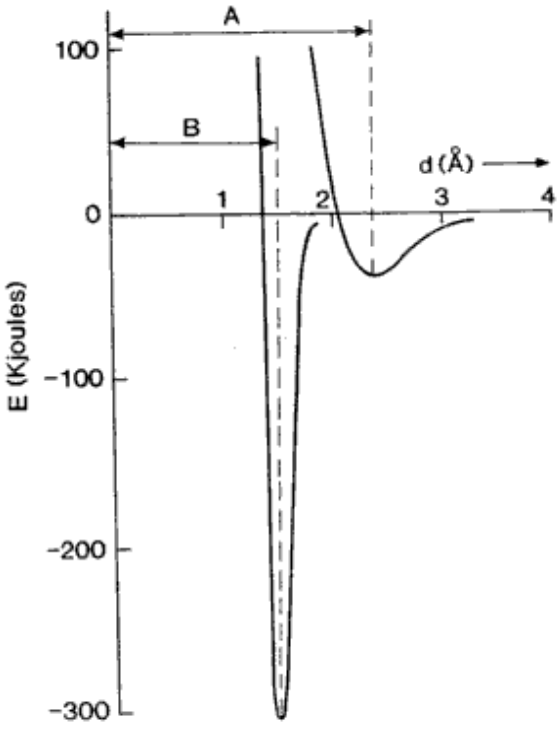

Figure 1.7
An illustration of the energy-distance relationship between two covalently bonded atoms and two atoms bonded by weaker interactions. The equilibrium interatomic distance B (covalent bonds) is shorter, the energy 'well' deeper and very much narrower than for weaker interactions with the interatomic distance A. This results in the much stronger covalent bonds being ineffective except in a very narrow band of distance.

Figure 2.8: Energy-Distance Relationship Between Covalent and Weaker Bonded Atoms (*161*)

Strongly bound and largely insoluble β-keratins often contain a high proportion of glycine, which contains a single hydrogen atom as a side chain and is the smallest amino acid group found in keratins. In some cases, β-keratins also tend to contain a high

percentage of the next smallest amino acid found in keratins, alanine, whose functional side group is the small and uncharged methyl group. This results in sterically unhindered hydrogen bonding between amino and carboxyl groups of neighboring peptide chains, and thus facilitates their closer alignment. Consequently, hydrogen bonds in β-sheets form mostly not within the polypeptide backbone, but between neighboring peptides (*160*). Alpha- (α-) keratins not only tend to have a higher relative abundance of inter-molecular hydrogen bonding than β-keratins, but they generally have more complex, less neutral side groups, which results in more sterically-hindered hydrogen bonding and larger spacing between adjacent protein chains.

In general, β-keratins also contain a higher relative abundance of the amino acid cysteine when compared to α-keratins (*161-162*). This is especially true for sheep's wool, as the β-keratins found within the exocuticle of hair keratin contain roughly 35% cysteine, while the α-keratins found in the endocuticle (cortex) contain only three percent (*161*). Hair may not be representative of all keratins, however, as they have the highest overall percentage of cysteine with respect to most other major keratin types. In fact, hen feathers have been shown to have a smaller total sulfur content, as well as cysteine percentage than lamb wool (*159*). Cysteine itself is characterized by the thiol functional group, -SH, which is comprised of a sulfur atom and a hydrogen atom. The thiol groups tend to pair up and, through oxidation, form a covalent sulfur-sulfur (disulfide) bond with the loss of two protons and two electrons. Expressed more formally, when cysteine is

oxidized it can form cystine, which is two cysteine residues joined by a disulfide bridge (cys-S-S-cys). Disulfide bridges confer additional strength and rigidity to keratins by permanent, thermally-stable intra-molecular crosslinking. Extensive disulfide bonding contributes to the insolubility of keratins, except in dissociating or reducing agents.

Modern techniques used to render keratin soluble in polar solvents may take advantage of such cysteine functionality. Due to keratin's resilience to dissolution, however, these methods are usually invasive and not always reversible, yielding at best a keratin-like substance with properties similar to the native keratin. Modern techniques used to dissolve or cross-link keratins usually employ hydrolysis coupled with oxidation (*163*), reduction (*154, 155, 164*), or both oxidation and reduction (*150, 151*). Typically, these hydrolysis reactions decrease sulfur content and leave charged residues, although molecular weight and solubility generally remain the same (*164*). In order to decrease chemical alteration of keratin, some studies have successfully employed enzymes to aid in hydrolysis (*155*). Cross-linking may also be achieved without reduction or oxidation using bifunctional compounds (*152*).

Oxidation of native keratin cleaves cysteine-cysteine disulfide linkages to form cysteic acid ($R\text{-}CH_2SO_3H$) residues. Reduction cleaves cysteine-cysteine disulfide linkages (cystine) to form cysteine residues with thiol (R-SH) groups. Thiols (aka mercaptans) give the resulting material properties similar to alcohols, which may allow alcohol-water mixtures as a reducing solvent. Both residues add hydrophilic sites to the

polypeptide chains and aid in increasing solubility. However, the cysteine residues with thiol groups do not readily participate in hydrogen bonding, a property common to nucleophiles such as thiols. When reduced native keratin is oxidized, thiol groups will reform hydrophobic cystine linkages. However, once formed, the cysteic acid residues are permanent and left unchanged with further reduction (or oxidation). Accordingly, to form a soluble keratin product that may be recross-linked back into a hydrophobic, non-wetting material, oxidation of the cystine linkages must be avoided in the dissolution step.

Given the above discussion, it is obvious that cysteine-rich, hydrophobic β-keratins would be more effective than α-keratins at sequestering hydrophobic solutes. Two potential sources of native keratin that could potentially meet those requirements may be poultry feathers and sheep's wool. Although not currently marketed commercially, poultry feathers are produced in bulk as a waste byproduct at poultry processing facilities, and contain over 90 percent (w/w) native keratin, most of which is of the β-keratin type. If a market appears for such a product, poultry feathers may easily be made available commercially at very reasonable costs and used in either bulk or modified forms. The cysteine content in feathers, although roughly half that of sheep's wool, is still high enough to achieve effective dissolution and cross-linking.

A commercially available alternative to poultry feathers may be found in sheep's wool, such as the keratin azure used in the present study, and may also be economically

feasible if the bulk price is low enough. Wool is high in cysteine groups and has a low β-keratin fraction in its native, bulk form. However, by taking advantage of the high affinity of hair cortex α-keratin for polar solvents such as water, the β-keratin fraction in wool may be increased to over 80 percent (*151*). For example, the α-keratin fraction, when at least partially homogenized with the β-keratin fraction in a reducing or oxidizing environment, may be at least partially exposed to and subsequently removed to the aqueous phase where it may be separated from the remaining β-enriched keratin by decantation. As it is commercially available from the textile industry, keratin azure would thus potentially be a candidate for such modification. However, when the decrease in total mass of keratin required for removal of most of the α-keratin is considered, keratin azure may ironically be most feasible in its bulk, unmodified-form. In other words, if the increase in sorption capacity for HOCs is relatively small with modification, removal of the α-keratin fraction would be an unnecessary cost. If the native keratin will be chosen to amend additional amendments such as sand, however, solubilization of the keratin must be achieved regardless, and partial to full removal of the alpha fraction may be achieved with little to no additional cost.

Removal of the α-keratin fraction is not the only modification which may be required for keratin azure to be suitable for use in active capping environments, due to the fact that keratin azure comes pre-reacted, or dyed with Remazol Brilliant Blue-R (Reactive Blue 19). Remazol Brilliant Blue is very commonly used in the wool textile industry and is the potassium salt of the sulphato ethyl sulfone derivative of an

anthraquinone sulfonic acid. Its vinyl sulfone derivative has been found to bind covalently and stoichiometrically to primary and secondary amines and to alcohol and sulfhydryl groups (*165*). Generally, any carboxylic acid side chain or amino group such as lysine, cysteine, histidine, threonine, serine, tyrosine, methionine, and N-terminal may confer affinity for reactive dyes, including Remazol Brilliant Blue-R (*157, 166*). Also, two-thirds of the amino bonds formed with reactive dyes are lysine and histidine groups (*167*). Remazol Brilliant Blue-R is a monofunctional dye which does not additionally cross-link or change the solubility of wool (*168*). General mechanisms of dye-wool reactions are described by (*169*).

Studies have shown that up to 20 percent of reactive dye molecules present on dyed wool may be unfixed, or non-covalently linked (*170*), which may cause the partitioning of reactive dyes such as Remazol Brilliant Blue-R into the polar phase when submerged in water. Furthermore, once in the aqueous phase, Remazol Brilliant Blue-R has been observed to undergo oxidative reactions in the presence of catalysts such as ultraviolet light to liberate anthraquinone groups which degrade to form naphthalene and other toxic aromatic intermediates (*170-173*). Such occurrences may be obvious from Figure 2.9, which is reproduced without permission from (*172*). As may be inferred from Figure 2.9, the anthraquinone group contains a phenanthrene-like domain which may easily be cleaved via oxidation reactions and released into the aqueous phase. Thus, it would obviously seem clear that keratin azure would require additional removal of non-covalently linked dye molecules before its raw, or bulk form could be used “as-is” in a

capping environment. (*167*) has included methods to remove the non-covalently linked dye which would be suitable for use in the present study.

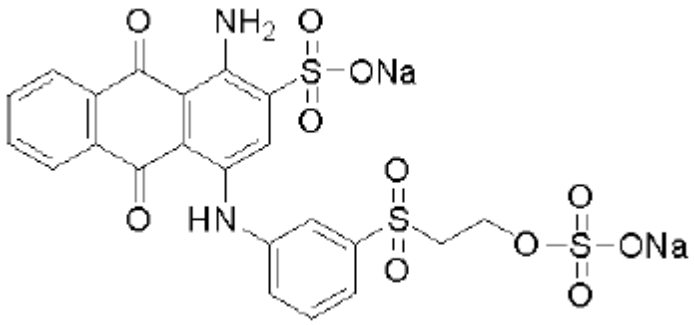

Figure 2.9: Chemical Structure of Remazol Brilliant Blue-R (*172*)

Chapter 3: Materials and Methods

The prepared hydrophobic biopolymers included cutin from tomato peels, cellulolytic enzyme lignin from spruce chips, commercially available keratin azure, and purified keratin azure. Following their isolation and preparation, the biopolymers were subjected to one or more chemical analyses, including Total Carbon and Total Nitrogen (TC and TN), Loss-On-Ignition (LOI), and/or Solution-State Nuclear Magnetic Resonance (SS-NMR). Results were used to determine if the prepared hydrophobic biopolymers materials had a similar chemical composition to that expected from the literature. Comparisons were based on proportions of certain chemical groups present and overall elemental content as estimated from literature. Batch kinetics and equilibrium sorption studies using the selected hydrophobic biopolymers then allowed determination of the amount of time required for a number of non-competing PAHs to reach physiochemical equilibrium between the aqueous and solid biopolymer phases, and the calculation of equilibrium partition coefficients for the same.

It was concluded using a decision matrix that keratin azure had the greatest potential for success at providing a stable, uniform, and sorptive coating on sand grains. Hydrophobic biopolymer-Coated Sand Products (CSPs) were then constructed to yield modified keratin azure-containing products with low, moderate, and high sand concentrations. The CSPs were then subjected to additional batch kinetics and equilibrium sorption studies, physical analysis, and chemical characterization. Results

were used to evaluate and discuss the chemical and physical mechanisms by which sorption was achieved, identify parameters that may be optimized for rendering the CSPs most effective and suitable for use as active capping materials, and simulate via simple modeling the performance of selected hydrophobic biopolymer-CSPs in a thin-layer sediment cap with respect to their ability to feasibly and efficiently remove PAHs. Preparations of conventional active capping amendments, including hydrophilic biopolymers, were prepared and similarly tested for comparison to the hydrophobic biopolymer-CSPs.

The experimental approach and general procedures employed to complete such efforts are described in the following sections:

3.1 Isolation and Preparation of Selected Hydrophobic Biopolymers

3.2 Construction of Hydrophobic Biopolymer-Coated Sand Products

3.3 Physical and Chemical Characterization of Selected Hydrophobic Biopolymers and Hydrophobic Biopolymer-Coated Sand Products

3.4 Batch Kinetics and Equilibrium Sorption Tests of Selected Hydrophobic Biopolymers, Hydrophobic Biopolymer Coated Sand Products, and Other Amendments

3.5 Feasibility Analysis of Hydrophobic Biopolymers and Hydrophobic Biopolymer-Coated Sand Products

3.6 Finite Difference Simulation of the Transport of Naphthalene through a Thin-Layer Cap Comprised of Hydrophobic Biopolymer-Coated Sand Products

3.1 ISOLATION AND PREPARATION OF SELECTED HYDROPHOBIC BIOPOLYMERS

Presented below are procedures for the preparation and isolation of cutin from tomato peels (CUT), cellulolytic enzyme lignin (CEL) from spruce wood chips, keratin azure (KER) from dyed sheep's wool, and purified keratin azure (KER PUR).

3.1.1 Tomato Peel Cutin

According to a method adapted from (*34, 40*), commercial tomatoes were first boiled in water for 25-30 minutes in order to achieve manual separation of the peels from the flesh of the tomatoes. The peels were then washed three times with deionized water and dried overnight in a drying oven at 60 degrees Celsius.

To remove an initial fraction of the cuticle lipids and monosaccharides, the dried tomato peels were exhaustively extracted at room temperature in methanol (Fisher, 99.9% w/v) overnight on a rotary shaker at approximately 100 rounds per minute, using approximately 50 milliliters of methanol for every 2.5 grams of dried tomato peels. The solution containing the suspended tomato peels was then separated from the extracted peels by filtration using 45-micrometer glass-fiber microfilters (Whatman). The procedure was repeated on the extracted tomato peels until no residue was obtained from the filtrates.

In a similar manner, the extracted tomato peels were then exhaustively extracted overnight at room temperature in 1.5M KOMe on a rotary shaker at 100 rounds per minute, prepared by dissolving 84.16 grams KOH (Fisher, 87.3% w/w) per liter of methanol. Cutin methanolysates were isolated by first filtering the solution using 45-micrometer glass-fiber microfilters, washing the retentate with methanol, and diluting the combined filtrates with two volumes of deionized water. The solution was then chilled, adjusted to pH 3.5 with concentrated hydrochloric acid (Fisher, 34-37% w/v), and extracted twice in a separatory funnel with trichloromethane (EMD, 99.8% w/v). In order to avoid localized pH extremes due to using concentrated hydrochloric acid to adjust pH, the solution containing the diluted, combined filtrates was kept under continuous, rigorous stirring while the acid was added slowly in dropwise fashion. After combining the extracts and back-extracting with deionized water, the solution was concentrated to dryness on a rotary evaporator using a bath temperature of 40 degrees Celsius and a rotation speed of 30 rounds per minute. According to (*34, 40*), the trichloromethane soluble fraction was estimated to contain greater than 90 percent cutin monomers. The residues obtained from filtering contain greater than 95 percent carbohydrates and were discarded as waste. As noted by (*34, 40*), dichloromethane may be successfully substituted for trichloromethane due to the reduced toxicity of dichloromethane.

3.1.2 Cellulolytic Enzyme Lignin

Sitka spruce (*Picea sitchensis*) chips were first obtained from Warrenton Fiber (Warrenton, Oregon) and dried at room temperature. According to a method adapted from (*88*), the chips were then ground in a Wiley mill (University of Texas at Austin Polymer Processing Facility) to pass a 40-mesh sieve. Following the preparation of milled wood, a fraction of the total amount of cellulose was released from the lignin contained within the spruce chips, according to a method adapted from (*89*).

In order to achieve this, an Enzyme Buffer Solution (EBS) containing 0.05 molar sodium acetate and 0.05 molar acetic acid at a pH of approximately 4.5 was prepared by adding 4.10 grams of sodium acetate (anhydrous, Fisher, 99.1% w/w) to a 1000 milliliter volumetric flask, diluting to approximately halfway using DI water, adding an additional 2.89 milliliters of glacial acetic acid (Fisher, >99% w/v), and diluting to the remainder of the 1000 milliliter volume with deionized water while under continuous stirring. The EBS was then diluted to two liters with deionized water, stirred, and divided evenly into two 1000 milliliter flasks. One of the 1000 milliliter flasks was stored for later use in the dark at four degrees Celsius, while the following target masses of materials were added to the remaining flask, along with three drops of toluene for preservation:

- 100 grams sitka spruce chips (40 mesh)
- 20 grams Onozuka 3S cellulase (Yakult Pharmaceutical, Japan)
- 20 grams Onozuka Y-NC hemicellulase (Yakult Pharmaceutical, Japan)

After agitation on a rotary shaker at 120 rounds per minute at 50 degrees Celsius for three days, the mixture was filtered through 45-micrometer glass-fiber microfilters. An additional three drops of toluene (EM Science, 99.99% w/v), 20 grams of Onozuka 3S, and 20 grams of Onozuka Y-NC were added with the residue and suspended in the unused 1000 milliliter flask of EBS. The agitation process was then repeated for an additional three days at 50 degrees C and 120 rounds per minute. Following the second agitation/incubation, the suspension was once again filtered through 45-micrometer glass-fiber microfilters. The residue was then rinsed three times with deionized water, dried at room temperature, and stored at room temperature in the dark.

During a first extraction event, a portion of the residue, or treated wood meal, was exhaustively extracted in a soxhlet extractor for 36 hours in 96% (v/v) aqueous dioxane, prepared by adding 12.5 milliliters deionized water to every 300 milliliters concentrated 1,4 dioxane (Mallinckrodt Chemicals, 99.0+% w/v). Boiling stones were added to the boiling flasks to increase overall evaporative flux to the condensing units, and glass microfiber thimbles (Whatman, 19x90 millimeters) were used to contain the treated wood meal during operation. The mass of treated wood meal added to each thimble was 3.5-4.0 grams. A number of issues arose with continued use of the soxhlet extractor, however, including precipitation of material inside the boiling flask and flooding resulting from the continual flow of tap water required to cool the condenser coils. A second extraction event was performed without the use of a soxhlet extractor by stirring a portion of the residue (approximately 36 grams) in a 2000 milliliter volumetric flask for 36 hours under

no heat in 96 percent (v/v) aqueous dioxane. No precipitate was formed. Following each extraction, the solutions obtained were filtered through 45-micrometer glass-fiber microfilters and retained for further processing. The residue was kept for re-dissolution and extraction. The extractions were each repeated once, for a total of two extractions during each event. The extractions were not repeated more than once due to the relatively insignificant amount of material obtained after the first extractions. Both extraction events produced a translucent, light yellow-colored solution of similar characteristics.

Filtrates from each event were evaporated to dryness using a rotoevaporator under a steady stream of air and a slight vacuum. Evaporation flask temperature and rotating speed was set at 55 degrees Celsius and 45 rounds per minute, respectively. The residues were purified by rinsing first with water and then by petroleum ether, and repeating for a total of three times. Petroleum ether readily evaporated from even the smallest pores in the purified residues at room temperature. Cellulolytic Enzyme Lignin (CEL) obtained from the purified residue was identical for both extraction events, and samples from each were used in further experiments.

3.1.3 Keratin Azure and Purified Keratin Azure

Initially, two keratinous materials were tested in order to investigate both “as-is” and “pseudo-as-is” states of a commercially-available wool, keratin azure. Alternatively, the first material may be described as the bulk form of keratin azure, and the second

material may be described as the bulk form of keratin azure with the non-covalently attached dye molecules removed. When obtained, keratin azure (Sigma Aldrich, 98% w/w) was divided into a first fraction designated as the first, or bulk keratin azure (KER), and a second, larger fraction designated as the second, or bulk "purified" keratin azure (KER PUR). KER PUR was then obtained from KER using a method adapted from (*167*).

An extraction solution consisting of a one-to-one mixture of pyridine (Fisher, 99.9% w/v) and deionized water was prepared and brought to pH 6.5-7.0 by dropwise addition of concentrated hydrochloric acid (Fisher, 37.4% w/v) under constant stirring. The amount of concentrated hydrochloric acid used per 667 milliliters was approximately 0.4 milliliters. The solution was then brought to a temperature of 70 degrees Celsius while stirring on a heat/stir plate in a well-ventilated fume hood. When the temperature had remained stable for 30 minutes, a mass of keratin azure was added to the solution and extracted for one hour. To extract a 4.5 gram batch of keratin azure, two-thirds of a liter of extraction solution was typically used in order to account for the very small bulk density of the wool. Grinding the KER into a more powdered material for use of a smaller amount of solvent was not possible without the use of a Wiley mill. Milling, or grinding, is also generally discouraged because of estimated effects on such parameters as the aqueous stability, manageability, and the release rate of previously stable dye molecules. Also, grinding or milling has been observed in some studies to affect the cysteine content of wool (*174*). As described later in this document, changing the

cysteine content of the wool may render the keratin less able to form stable coatings on sand grains, as disulfide linkages are necessarily manipulated in order to render the keratin soluble and recross-link.

Following extraction, the mixture was filtered using 45-micrometer glass-fiber microfilters and the retained fibers were rinsed thoroughly (five times) with deionized water. The procedure was repeated until the largest fraction possible of noncovalently-linked Remazol Brilliant Blue-R was removed, or until the extraction solution remained clear. This proved to be approximately three times for each batch extracted. After the last extraction, the fibers were left on aluminum foil to air-dry at room temperature under a fume hood. The resulting material was labeled as KER PUR.

3.2 CONSTRUCTION OF HYDROPHOBIC BIOPOLYMER-COATED SAND PRODUCTS

According to dissolution and cross-linking methods adapted from (*151*), hydrophobic biopolymer-Coated Sand Products (CSPs) were prepared in two major stages from purified keratin azure (KER PUR). In the first stage, partial reduction of the disulfide bonds in the keratin fibers was achieved in a nitrogen atmosphere containing approximately one to two parts-per-million (ppm) hydrogen for oxygen scavenging. Such reduction allowed the partial dissolution of the keratin material, yielding a form of the keratin which may be used to coat sand particles. A reducing solution was prepared prior to beginning the reaction by adding 31.03 milliliters of concentrated ammonium

hydroxide (Fisher, 29.46% w/w as NH_3) to approximately 75 milliliters deionized water and diluting, using deionized water, to 150 milliliters, yielding 150 milliliters of three-normal ammonium hydroxide. A solution containing 15.7 milliliters of ammonium thioglycolate (Acros Organics, 70% (w/w) in water) per 75 milliliters of the three-normal ammonium hydroxide was then prepared and brought to a stir on a heat/stir plate.

In an initial batch, the reducing solution was immediately allowed to approach a constant 60 degrees Celsius. After the temperature had remained steady for 30 minutes, purified keratin azure were added and reduced for two hours. Approximately 272.1 milliliters of reducing solution was initially needed to completely cover a 4.0-5.0 gram batch of keratin fibers, once again due to the density of the bulk keratin. However, upon the onset of reaction, the keratin quickly condensed, and after six hours, was able to be covered with as little as 90.7 milliliters of reducing solution. Subsequent batches did not add heat to the reducing solution until after the keratin had been under stirring and no heat for one hour. Following one hour, the heat was allowed to increase to 60 degrees Celsius until two hours of total reaction time was reached. The gradual addition of heat greatly aided in regulating the rate of cleavage of disulfide linkages at the start of the reduction when the reaction rate was highest, and therefore decreased the occurrence of rapid and large hydrogen sulfide releases to a constant, lower rate of release which could be managed. Additional measures taken to reduce the possibility of dangerous hydrogen gas buildup included periodically purging approximately one-third of the total volume of the glovebox in which the atmosphere was maintained (Coy Laboratory Products) and

replacing the volume with fresh mixed gas. Oxygen-scavenging catalysts and sulfide traps placed within the glovebox aided in oxygen removal and sulfur sequestration from the hydrogen sulfide released. Vermiculite placed in tubs throughout the glovebox aided in moisture removal.

Ammonium hydroxide aids in the deprotonation of carboxylic acids and the cysteine thiol groups, which forms a polyanionic keratin material with increased aqueous solubility (*151*). In addition, the ammonium in the ammonium hydroxide partially swells the protein, allowing less mass transfer limitations on the thioglycolic acid reaction with disulfide bridges (*151*). Following the first two hours of reaction, the reducing suspension was removed from heat and filtered without vacuum using fine glass-fiber filter paper (Whatman, P5). The partially-reduced keratin fibers were removed and rinsed three times with deionized water. The rinsed, partially-reduced keratin fibers were then resuspended in deionized water which had been purged with nitrogen gas before bringing into the glovebox to remove oxygen. While suspended in the oxygen-free deionized water, the fibers were removed from the glovebox and partially homogenized for ten minutes using a commercial food processor (Cuisinart Mini Prep Plus®) under a well-ventilated fume hood. Immediately following the homogenization, the fibers were returned to the glovebox while remaining suspended in the deionized water. The rationale for removing the fibers from the glovebox was used due to safety concerns of operating an electric device not rated for laboratory use in an environment which may possibly reach dangerous levels of hydrogen sulfide gas during homogenization. Initially,

homogenization using a ceramic mortar and pestle inside the glovebox was attempted without success, as the keratin fibers remained too tough to grind even after six hours of reaction. The fiber did not seem to be oxidized much from being possibly briefly exposed to oxygen. The homogenized wool keratin was then removed from the suspension by filtration through 45 micrometer glass-microfiber filters under vacuum, rinsed three times with deionized water, and resuspended in fresh reducing solution. The reaction was then continued with heat for an additional four hours, for a total of six reaction hours.

Partial homogenization of the alpha and beta keratin fractions contained within the wool fibers is necessary in order to decrease mass transfer of the reducing solution to internal cysteine linkages and allow the more polar alpha keratin fractions to be dissolved into the polar phase where they may be filtered off with the reducing solution. A much more hydrophobic, dissolution-resistant wool-keratin fraction remains afterwards, which contains a higher percentage of beta keratin than previously. After the homogenized keratin fractions are returned to the reducing solution, any disulfide bridges which may have re-formed during the ten minutes outside of the glovebox could presumably be reduced once again in a similar amount of time.

After six total reaction hours, the reducing suspension was filtered and the reducing solution was replaced once more in similar fashion. The retained keratin material was then resuspended and reacted for an additional 12 hours, for a total of 18 hours of reaction. Such periodic replacement of the reducing solution provided the

additional advantage of increasing the removal of dye molecules released to the polar liquid phase during the partial reduction of keratin. In fact, dye molecules which had previously been permanently attached to the keratin fiber were significantly removed to the point of there being no observable dye left on the partially-reduced keratin material. Following 18 total hours of reduction, the reducing suspension containing the partially reduced keratin fibers was poured evenly into several 50 milliliter centrifuge tubes and allowed to settle 12 hours, or overnight. The reducing solution was then decanted using a glass pipet, leaving a more concentrated suspension. Following decantation, the concentrated suspension was placed on filter paper overnight in the glovebox over a beaker to filter off remaining liquids without a vacuum, leaving a beta-enriched wool keratin fraction which is resistant to dissolution and relatively free of dye molecules.

While filtration of the reducing suspension to recover the partially-reduced keratin material remained possible after only six hours of reaction, filtration was not possible following 12 hours of reaction due to clogging of the filter paper. Thus, settling of the suspension in centrifuge tubes seemed necessary. In an original method, a centrifuge was used to speed up the settling for ten minutes at 5200 rounds per minute. However, a number of tubes broke using the method, and the suspension remaining in the intact tubes did not settle any faster than suspensions in tubes that were allowed to settle without the aid of the centrifuge.

In the second stage of the preparation of hydrophobic biopolymer-coated sand products, the partially-reduced keratin material was combined with industrial/play sand grains to provide a coating, and oxidized in the presence of an oxygen-containing atmosphere to reform the disulfide links, cross-linking the keratin. Upon complete removal of the reducing solution, the partially-reduced keratin material was removed from the oxygen-free glovebox and immediately acidified to pH 2.0 (checked with litmus paper) by addition of a volume of concentrated formic acid (Fisher, 90.2% w/v). Acid was added in dropwise fashion very slowly to prevent generation of copius amounts of heat, under a fume hood under continuous stirring with a glass stir rod. Approximately 2.5 milliliters of formic acid were used per 4.0-5.0 gram batch of keratin azure partially degraded in the reducing solution. Formic acid swells the keratin matrix, enhancing the solubility (*151*). The acidified, partially-reduced keratin slurry was then added to petri dishes containing individual masses of industrial/play sand (mostly carbonate sand with ~0.1% organic matter) and thoroughly mixed to yield homogeneous mixtures of approximately low (~0% w/w) , moderate (~15% w/w/) , and high (~85% w/w) sand content. Petri dishes were then allowed to oxidize under a fume hood for 48 hours, after which they were moved to a drying oven at 60 degrees Celsius. Following 24 additional hours in the drying oven, materials were broken up and coarsely ground with a ceramic mortar and pestle to yield granular materials. Following their grinding, coated sand products were returned to the oven for 24 hours of additional drying. After 96 total hours of oxidation, or drying, the coated sand products were no longer decreasing in total mass due to the volatilization of solvents, and were removed from the drying oven.

Purification of the coated sand products was achieved by boiling in deionized water for 30 minutes. The products were then removed by filtration using 45-micrometer glass-fiber microfilters, resuspended in fresh deionized water, and the boiling process was repeated for a total of three times. The purified coated sand products were then placed in a drying oven for 12 hours, or overnight to dry. The final concentrations of sand were calculated by recording the masses of sand added to each petri dish prior to addition of acidified and reduced keratin, as well as the final total masses of dried hydrophobic biopolymer-coated sand products containing the same. Such concentrations were very close to the target concentrations. Accordingly, products containing zero percent sand were labeled 0% CSP, products containing 15.4 percent sand were labeled 15.4% CSP, and products containing 87 percent sand were labeled 87% CSP.

Air drying achieves several tasks in addition to oxidation of cysteine residues. Namely, it removes water and residual solvents such as ammonium thioglycolate, ammonium hydroxide, and pyridine. Boiling in water further removes any thioglycolate from the products, rendering a very safe, pure keratin-containing material for environmental use. (*151*) describes the use of medical implants produced using the dissolution and cross-linking methods employed in this study. Thus, toxicity of potential residual solvents and/or unfixed dye molecules is not of great concern in this study.

3.3 PHYSICAL AND CHEMICAL CHARACTERIZATION OF SELECTED HYDROPHOBIC BIOPOLYMERS AND HYDROPHOBIC BIOPOLYMER-COATED SAND PRODUCTS

The following sections of this document include general procedures used in the chemical and physical analysis of hydrophobic biopolymers and hydrophobic biopolymer-coated sand products isolated and prepared for use in the present study, namely:

- Solution-State ^{1}H and ^{13}C Nuclear Magnetic Resonance (SS-NMR) of tomato peel cutin and cellulolytic enzyme lignin
- Elemental Analysis of tomato peel cutin, cellulolytic enzyme lignin, and 0% hydrophobic biopolymer-coated sand products
- Loss-On-Ignition (LOI) test for tomato peel cutin, cellulolytic enzyme lignin, purified keratin azure, and 0% hydrophobic biopolymer-coated sand products
- Bulk porosity, bulk density, specific density, particle size distribution, and estimated hydraulic conductivity of hydrophobic biopolymer-coated sand products (0%, 15.4%, and 87%) and industrial/play sand

3.3.1 Solution- State ^{1}H and ^{13}C Nuclear Magnetic Resonance

Samples of tomato peel cutin and cellulolytic enzyme lignin were prepared for SS-NMR analysis by first adding approximately 25.0 milligrams of material to a small beaker along with one milliliter of deuterated solvent. For tomato peel cutin, chloroform-

d (Cambridge Isotope Laboratories, 99.8% w/v, TMS added) was used as the solvent. In the case of cellulolytic enzyme lignin, however, Dimethyl Sulfoxide (DMSO) (d6, Cambridge Isotope Laboratories, 99.9% w/v, without TMS added) was used, which required addition of TMS prior to analysis for a reference. The beaker and its contents were then sonicated and/or vortex mixed for approximately 20 minutes, or until all material was completely dissolved. A small amount of "clean" (unbleached) cotton was then inserted into a disposable glass pipet tip and packed securely in place with a glass stir rod. Following preparation of the pipet tip, the deuterated biopolymer solution was filtered through the cotton to remove any water impurities into a five millimeter glass tube (Fisher, seven inch) for analysis. The one milliliter volume of deuterated solution filled the five millimeter glass tube up to approximately two inches, which is the required length of tube required to easily use in the SS-NMR machine.

Quantitative ^{1}H spectra and qualitative ^{13}C spectra were obtained using a 500 MHz Varian INOVA SS-NMR analyzer (University of Texas at Austin NMR Laboratory). A flip angle of 15 degrees and a recycle/delay time of approximately six seconds were used for the ^{1}H scan, while a flip angle of 30 degrees and a recycle/delay time of approximately four seconds were used for the ^{13}C scan. Signal peaks within the ^{13}C spectra were correlated to specific carbon types as presented in Table 3.1. Chemical shift ranges for analysis of the ^{1}H spectra were approximately analogous to ^{13}C ranges by relation of groups to each other, but are more difficult to generalize. Tomato peel cutin

and cellulolytic enzyme lignin spectra were compared to that obtained by (*40, 28, 29, 22, 18*) and (*15*), respectively.

Table 3.1: ^{13}C Chemical Shift Ranges

Carbon Type	^{13}C Chemical Shift Range (parts per million)
Alkyl (Paraffinic)-C	0-50
Amorphous ("rubbery") Paraffinic-C	28-30.5
Crystalline ("glassy") Paraffinic-C	30.5-33
Substituted Alkyl-C (Alkyl-O, Alkyl-N, etc)	50-112
Aromatic-C	112-145
Phenolic-C	145-163
Carboxyl-C	163-190
Carbonyl-C	190-215
Total Polar-C	(50-112) + (145-215)
Aliphaticity	(0-112)/(0-163)
Aromaticity	(112-163)/(0-163)

3.3.2 Elemental Analysis

Total Carbon and Total Nitrogen were determined for tomato peel cutin, cellulolytic enzyme lignin, and zero percent coated sand products using a Carbon-Hydrogen-Nitrogen (CHN) elemental analyzer coupled to an isotope ratio mass spectrometer (University of Texas Marine Science Institute). Total organic carbon content was assumed to be approximately equal to total carbon content, due to the carbon in cutin, lignin, and keratin being almost exclusively associated with organic matter. In

order to further support this assumption, organic matter content of each of the hydrophobic biopolymers was determined by Loss-On-Ignition (LOI) tests, which are described in the following section of this document. The organic carbon content was also assumed to have been relatively unchanged in keratin azure with pyridine extraction, alkaline reduction, and air oxidation. Therefore, the organic carbon content of both keratin azure and purified keratin azure was assumed to be approximately equal to that of the zero percent coated sand product. Fraction of organic carbon was calculated for hydrophobic biopolymers and hydrophobic biopolymer-coated sand products by Equation 3.1, using the total carbon results, where f_{OC} represents the fraction of organic carbon in the sample, $M_{tot,C}$ is the mass of total [organic] carbon in milligrams, and $M_{tot,samp}$ is the total sample mass in milligrams. As discussed later in this document, the fraction of organic carbon obtained for the zero percent coated sand product must be normalized to the fraction of hydrophobic biopolymer when applied to obtain a fraction of organic carbon for coated sand products with a nonzero mass fraction of sand.

$$f_{OC} = \frac{M_{tot,C}}{M_{tot,samp}}$$

Equation 3.1: Fraction of Organic Carbon

Total nitrogen content of the zero percent coated sand product was used to determine the effectiveness of drying and boiling on removal of nitrogen-containing solvents in the coated sand product preparation process. Such evaluation is useful in

analyzing for any potential environmental toxicity of keratin-coated sands produced in this manner. Total nitrogen content of purified keratin azure was estimated from (*159*) and compared to total nitrogen of the zero percent keratin-coated sand product.

3.3.3 Loss-On-Ignition

Organic matter content was measured for tomato peel cutin, cellulolytic enzyme lignin, purified keratin azure, and zero percent coated sand product by Loss-On-Ignition (LOI). Hydrophobic biopolymers and hydrophobic biopolymer-coated sand products were first dried overnight (or 12 hours) in a drying oven at 105-110 degrees Celsius. Upon removal from the drying oven, the samples were allowed to cool to room temperature inside of a dessicator in order to minimize the effects of atmospheric moisture on sample mass. A mass of each hydrophobic biopolymer and hydrophobic biopolymer-coated sand product was then placed into a small aluminum weigh boat and combusted for 12 hours at 550 degrees Celsius in a combustion oven. Following combustion, samples were removed from the oven and allowed to return to room temperature once more in a dessicator. The mass of material remaining on each aluminum weigh boat was then recorded and used as the mass of total inorganic carbon present in each sample. Fraction of Organic Matter was calculated by Equation 3.2, where f_{OM} represents the fraction of organic matter, M_{IC} is the mass of inorganic carbon in milligrams, and $M_{tot,samp}$ is the total sample mass in milligrams.

$$f_{OM} = 1 - \frac{M_{IC}}{M_{tot,samp}}$$

Equation 3.2: Fraction Organic Matter

3.3.4 Bulk Porosity, Bulk Density, Specific Density, Particle Size Distribution, and Estimated Hydraulic Conductivity

Samples of hydrophobic biopolymers and industrial/play sand were allowed to dry in a drying oven at 105-110 degrees Celsius for 12 hours or overnight. Dry mass of each sample was then measured following removal from the oven and cooling to room temperature in a dessicator. Dry bulk density was measured by recording the mass of dried material required to fill a given graduated cylinder volume. For the purposes of this study, wet bulk density was assumed to be approximately equal to dry bulk density, as all materials tested are highly hydrophobic. The relation used to calculate dry bulk density is given by Equation 3.3, where $\rho_{b,d}$ denotes dry bulk density in grams per milliliter, M_d represents dry mass in grams, and V denotes dry volume in milliliters.

$$\rho_{b,d} = \frac{M_d}{V}$$

Equation 3.3: Dry Bulk Density

Specific density was measured by first recording the dry mass of a certain quantity of sample following removal of moisture at 105-110 degrees Celsius for 12

hours (or overnight) and cooling in a dessicator as before. Secondly, the sample was immersed in a given volume of deionized water in a graduated cylinder. The change in volume in the graduated cylinder was then recorded immediately for calculation of dry specific density as presented in Equation 3.4, where $\rho_{s,d}$ represents dry specific density in grams per milliliter, M_d represents dry mass in grams, and Δv_0 denotes change in volume at time zero in milliliters. The volume at some time greater than zero, however, would not significantly differ from the change in volume at time zero, or immediately after immersion. This is due, once again, to the non-swelling behavior of the hydrophobic biopolymer-coated sand products. For this reason, wet specific density and dry specific density are approximately equal to each other as well. Dry specific weight was obtained by multiplying specific density by the acceleration of gravity as shown by Equation 3.5, where γ_d represents the dry specific weight of sample in newtons per cubic meter, $\rho_{s,d}$ represents dry specific density in grams per milliliter, and g represents the acceleration of gravity in meters per second squared.

$$\rho_{s,d} = \frac{M_d}{\Delta v_0}$$

Equation 3.4: Dry Specific Density

$$\gamma_d = 1000(\rho_{s,\mathrm{d}})(g)$$

Equation 3.5: Dry Specific Weight

Dry (or wet) bulk porosity was calculated for samples of hydrophobic biopolymers and industrial/play sand using values obtained for dry (or wet) bulk and specific densities as given by Equations 3.3 and 3.4, respectively. Equation 3.6 presents the relationship used for such calculations, where $\eta_{b,d}$ denotes dry (or wet) bulk porosity, $\rho_{b,d}$ denotes dry (or wet) bulk density in grams per milliliter, and $\rho_{s,d}$ denotes dry (or wet) specific density in grams per milliliter.

$$\eta_{b,d} = 1 - \frac{\rho_{b,d}}{\rho_{s,d}}$$

Equation 3.6: Dry/Wet Bulk Porosity

Particle size distribution of each of the hydrophobic biopolymer-coated sand products and industrial/play sand in bulk were determined by sieve analysis. A mass of material was first placed in the top of several consecutively finer sieves stacked on top of a bottom pan, including US standard sieve sizes No. 10, No. 20, No. 40, No.50, No. 60, No. 100, No. 140, and No. 200, respectively. Following agitation for ten minutes on a sieve shaker (Gilson), the fraction by mass of material remaining after each sieve was passed was calculated as the difference in final and initial mass of the sieve, and was plotted against sieve opening size to obtain a particle size distribution. Determination of the intrinsic permeability for hydrophobic biopolymer-coated sand products and industrial/play sand placed in bulk was made empirically therefrom using the particle size

distribution for each. Such a method was the only option available due to the large mass (and volume) required for permeameter testing and the small volume actually available.

As described by (*175*), intrinsic permeability may be correlated with a characteristic particle size as shown in Equation 3.7, or an entire distribution of particle sizes as shown in Equation 3.8. In Equation 3.7, d is a characteristic particle diameter in centimeters and k is the intrinsic permeability in square centimeters. In Equation 3.8, k is the intrinsic permeability in square centimeters, E is approximately five, and B is a shape factor equal to six for spherical particles and 7.7 for highly angular ones. In the present study, B is taken as the average of 6 and 7.7, or 6.85. Additionally, P is the percent by mass of the material between two particle sizes, $\eta_{b,d}$ is the bulk porosity of the material, and d_m is the geometric mean of the two particle sizes corresponding to P in centimeters.

$$k = 6.54(10^{-4})d^2$$

Equation 3.7: Characteristic Intrinsic Permeability

$$k = \frac{1}{E}\left[\frac{\left(1-\eta_{b,d}\right)^2}{\eta_{b,d}^3}\left(\frac{B}{100}\sum\frac{P}{d_m}\right)^2\right]^{-1}$$

Equation 3.8: Fair-Hatch Intrinsic Permeability

As may be inferred from the above relationships, Equation 3.7 is most valid for materials of very uniform particle size. However, by defining a uniform particle size

approximately equal to d_{90}, the sieve opening in which 90 percent by mass of the material is retained, Equation 3.7 may be used for materials of varied particle diameters. Equation 3.8, for comparison, takes into account much more information, such as the entire distribution of particle sizes, as well as the shape and bulk porosity of the particles.

Darcy hydraulic conductivity of water through the hydrophobic biopolymer-coated sand products and industrial/play sand placed in bulk was calculated from the intrinsic permeability of each by Equation 3.9, where U represents the Darcy Hydraulic Conductivity in meters per second, k equals the intrinsic permeability of the material in square meters, μ_w is the dynamic viscosity of water in newtons-seconds per square meter, ρ_w is the density of water in kilograms per cubic meter, and g is the acceleration of gravity in meters per second squared.

$$U = k\frac{\rho_w g}{\mu_w}$$

Equation 3.9: Darcy Hydraulic Conductivity

3.4 Batch Kinetics and Equilibrium Sorption Tests of Selected Hydrophobic Biopolymers, Hydrophobic Biopolymer-Coated Sand Products, and Other Amendments

Experiments were designed to produce systems comprised of a solid phase initially devoid of PAHs and an aqueous phase having initial concentrations of selected

PAHs just below their respective half-solubilities, which, after reaching physiochemical equilibrium, have PAHs present in the aqueous phase at concentrations just above their respective conservative minimum detection limits. Equation 3.10 was used to determine the approximate vessel/system volume required for each of several biomaterials to exclusively comprise a given mass of solid inside such a system containing the PAHs naphthalene, phenanthrene, and pyrene. Such biomaterials included tomato peel cutin, cellulolytic enzyme lignin, keratin azure, purified keratin azure, [0%, 15.4%, and 87%] coated sand products, and other capping materials. In Equation 3.10, V_{vessel} is the vessel volume in liters, M_{solids} is the solids mass in kilograms, C_{init} is the initial aqueous concentration of a given PAH in milligrams per liter, C_{fin} is the equilibrium (or final) aqueous concentration the PAH in milligrams per liter, and W_s is the equilibrium (or final) solids concentration of the PAH in milligrams per kilogram.

$$W_s = \frac{(C_{init} - C_{fin})V_{vessel}}{M_{solids}}$$

Equation 3.10: Batch Test Design

Also expressed as the mass of the compound of interest per mass of solids, W_s was represented in terms of a final aqueous PAH concentration by either a linear or Freundlich isotherm model. Respectfully, these models are presented by Equation 3.11 and 3.12, where K_D is the linear partitioning coefficient in liters per kilogram, K_f is a Freundlich coefficient in milligrams$^{(1-n)}$ per kilogram-liter^{-n}, and n is a dimensionless constant. Of course, Equations 3.11 and 3.12 necessarily assume the PAH is not in

competition with other PAHs. By substituting the linear and/or Freundlich relationship for W_s, Equation 3.10 may be solved for its roots to determine batch test design parameters, using linear and/or Freundlich isotherm parameters estimated from literature (*40, 15*).

$$W_s = K_D C_{fin}$$

Equation 3.11: Linear Isotherm Model

$$W_s = K_f C_{fin}^n$$

Equation 3.12: Freundlich Isotherm Model

Following the design of the batch tests, initial aqueous solutions were prepared by first dissolving approximately 1.3 grams of NaN_3 to two liters in a volumetric flask with deionized water to yield 0.01 molar NaN_3. The resulting solution was then placed on a magnetic stir plate and spiked with an appropriate volume of naphthalene, phenanthrene, and pyrene stock solutions under continuous stirring to obtain the desired target initial concentrations. After spiking, the volumetric flask was then filled to minimal head space with deionized water, stopped using a glass stopper, sealed with parafilm, and covered in aluminum foil. Initial solutions were allowed to continue stirring for three to four hours until all PAHs were dissolved. In order to account for the increased volume of solution prepared to minimize head space in the flask, the volume of spike solutions added was increased slightly.

Table 3.2 presents target concentrations for naphthalene, phenanthrene and pyrene, along with the amount of spike solutions used to prepare initial solutions for each batch of systems. The volumes of spike solutions used for the preparation of initial solutions were slightly lower than those presented in Table 3.2 only for the two materials containing 75 percent apatite. This was due to the fact that allowance was not made in those tests for the extra volume of initial solution added to minimize the head space in the two liter volumetric flask.

Table 3.2: Preparation of Initial Solutions

Batch Test No.	Volume 8,000 parts per million Naph in 99.9% (w/v) ACN (microliters)	Volume 5,000 parts per million Phen in 99.9% (w/v) ACN (microliters)	Volume 1,000 parts per million Pyrene in 99.9% (w/v) ACN (microliters)	Target Initial Concentrations (parts per billion)		
				Naphtha-lene	Phenan-threne	Pyrene
1	6.4	12	55	25	25	25
2	14	23	78	50	50	35
3	28	44	99	100	100	45
4	55	88	121	200	200	55
5	137	220	143	500	500	65

Five batch tests, or five point isotherms, were used for all materials with an exception to the conventional amendments containing zeolite, which used four-point isotherms. In the case four point isotherms were obtained, the volumes of spike solutions, and subsequently the target initial concentrations, were the same as for the first four

points used on the five point isotherms. In each batch of systems, a mass of solid materials were weighed out and placed in each of X glass amber bottles which were designated as samples, while no solid materials were added to an additional X bottles which were designated as blanks. Teflon tape was used around the threads of the vessels to assure that there were minimal mass losses due to leaking. The vessels were then carefully filled to zero head space with the initial sample solution prepared previously, capped with Teflon-covered caps, and allowed to tumble for a number of days.

Prior to performance of batch equilibrium sorption testing, kinetics of sorption was measured. In kinetics tests, X equaled five. Each one of the five sets, each containing one sample (solids-containing) vessel and one blank (contains no solids) vessel, were used to measure the equilibrium partitioning coefficient for naphthalene, phenanthrene, and pyrene onto tomato peel cutin, cellulolytic enzyme lignin, keratin azure, and 0% coated sand product after a given tumbling time. Accordingly, the five tumbling times were two, four, seven, 14, and 21 days, yielding a five-point kinetics curve. Batch equilibrium testing was then performed using a conservative tumbling time as estimated by the kinetics testing, using an X value of three. Triplicates of each sample and blank vessel were taken for kinetics batches for a total of three measurements per vessel. However, one measurement was taken from each of the sample and blank vessels in equilibrium batches, yielding three independent repeats per vessel. Table 3.3 presents vessel volumes at zero head space, target masses of solids added to each sample vessel, and the tumbling times used for each vessel.

Table 3.3: Vessel Volumes, Solids Masses, and Tumbling Times

Solid Tested	Vessel Volume at Zero Head Space (milliliters)	Target Solid Mass (milligrams)	Tumbling Time (days)
Tomato Peel Cutin	65	25	14
Cellulolytic Enzyme Lignin	67	15	14
Keratin Azure	67	25	14
Purified Keratin Azure	67	25	14
0% Coated Sand Product	67	25	14
15.4% Coated Sand Product	67	25	14
87% Coated Sand Product	67	25	14
75% apatite and 25% organoclay	257	100	7
75% apatite, 20% organoclay, 2.5% guar gum, and 2.5% xanthan gum	257	100	7
25% (w/w) organoclay (CETCO PM-199), 25% (w/w) zeolite (Clinoptilotilte), 25% (w/w) NC apatite, and 25% (w/w) acid-washed sand	257	70	7
25% (w/w) organoclay (CETCO PM-199), 50% (w/w) zeolite (Clinoptilotilte), and 25% (w/w) acid-washed sand	257	70	7
25% (w/w) organoclay (CETCO PM-199) and 75% (w/w) zeolite (Clinoptilotilte)	257	70	7
50% (w/w) organoclay (CETCO PM-199) and 50% (w/w) zeolite (Clinoptilotilte)	257	70	7

Samples of the initial solution were taken from the two liter volumetric flask before and after filling the bottles and analyzed via High Performance Liquid Chromatography (HPLC). Such sampling allowed determination of any losses of HOC mass during the filling of the vessels. Following tumbling, samples were taken from the tumbler and allowed to sit for 30 minutes prior to being sampled. Such sampling allowed the determination of any losses in the blanks with respect to HOC masses during the tumbling period, as well as equilibrium HOC concentrations in the sample vessels. In the case natural settling was insufficient to settle all particles, samples were centrifuged for 20 minutes at 3,000 rounds per minute. Following settling of the solid particles, samples were taken from the supernatant of each bottle and analyzed via HPLC. Equilibrium solids concentration, W_s, was plotted against equilibrium aqueous concentration, C_{fin} for each solid tested. Linear and Freundlich model parameters were taken from the best-fit solutions of Equations 3.11 and 3.12, respectively to the plotted W_s and C_{fin} data.

Samples were analyzed using a Waters 2795 Separations Module equipped with a Luna (Phenomenex) 5u C18(2) 100A column (250x4.6 millimeters, five micron). Instrument methods used a flow of one milliliter per minute, a carrier solution composition of 15% (v/v) deionized water: 85% (v/v) acetonitrile (acetonitrile from EMD, 99.9% w/v, HPLC grade), and a column temperature of 40 degrees Celsius. Ultraviolet and fluorescence signals of the separated output were obtained using a Waters 996 Photodiode Array Detector and a Waters 2475 Multi λ Fluorescence Detector, respectively. Ultraviolet signals were taken at a wavelength of 254 nanometers.

Fluorescence detector excitation wavelengths used were 250 nanometers from 0 minutes to 5.3 minutes, 244 nanometers from 5.3 minutes to 6.5 minutes, and 295 nanometers from 6.5 minutes to 10.0 minutes (the total run time of the method). Emission wavelengths used were 340 nanometers from 0.0 minutes to 5.3 minutes, 360 nanometers from 5.3 minutes to 6.5 minutes, and 390 nanometers from 6.5 minutes to 10.0 minutes. The approximate retention times for naphthalene, phenanthrene, and pyrene using the above methods were 4.7, 5.9, and 7.2, minutes, respectively.

3.5 FEASIBILITY ANALYSIS OF HYDROPHOBIC BIOPOLYMERS AND HYDROPHOBIC BIOPOLYMER-COATED SAND PRODUCTS

Following their preparation, physiochemical characterization, and measurement of sorption capacity for HOCs, each of the hydrophobic biopolymers were evaluated in terms of their ability to form economical, nontoxic, environmentally stable, and sorptive coatings on sand grains. A hydrophobic biopolymer was then chosen for continued study which had the largest feasibility factor, F, which is described by Equation 3.13. In Equation 3.13, F is a dimensionless feasibility factor used to define feasibility in the present study, w_i is a weight factor corresponding to the i^{th} term between zero and one, and RV_i is a rating value corresponding to the i^{th} term. Equation 3.13 was used to populate a decision matrix as presented in Table 3.4.

$$F = \sum_{i=1}^{3} w_i RV_i$$

Equation 3.13: Feasibility Factor

Table 3.4: Decision Matrix

Hydrophobic Biopolymer	Weighted and Normalized Sorption Capacity, w_1RV_1 (-)	Weighted and Normalized Reagent Cost, w_2RV_2 (-)	Weighted Environmental Stability and Toxicity Factor, w_3RV_3 (-)	Feasibility Factor, F (-)
Tomato Peel Cutin				
Cellulolytic Enzyme Lignin				
Keratin Azure				
Purified Keratin Azure				

Table 3.4 graphically presents weighted components which sum to F for each of the hydrophobic biopolymers studied. These weighted rating terms may be described as the weighted sorption capacity of a given biopolymer normalized to the sorption capacity of a typical activated carbon (w_1RV_1), the weighted material cost of bulk carbonate sand normalized to the chemical cost of a given biopolymer (w_2RV_2), and a weighted environmental stability and toxicity factor for a given biopolymer (w_3RV_3).

Relationships presenting the formulation of RV_1 and RV_2 in particular are presented in Equation 3.14 and Equation 3.15, respectively, where K_D is the equilibrium linear partitioning coefficient of the prepared hydrophobic biopolymer in liters per kilogram, $K_{D,AC}$ is the equilibrium linear partitioning coefficient of the activated carbon in liters per kilogram, $\rho_{b,d}$ is the dry bulk density of the hydrophobic biopolymer in kilograms per cubic meter, $\rho_{b,d,sand}$ is the dry bulk density of carbonate sand in kilograms per cubic meter, and UC_{sand} is the cost (USD) per kilogram of bulk carbonate sand. In the summation term, r equals the number of reagents (reducing agents, hydrolysis agents, acid, etc.) required to prepare and isolate the hydrophobic biopolymer, f_j is the mass of reagent required per mass of prepared hydrophobic biopolymer in kilograms per kilogram corresponding to the j^{th} reagent, and UC_j is the cost (USD) per mass of the reagent corresponding to the j^{th} reagent. Obviously, f_j may be appropriately determined by several of equally valid methods, depending on the particular case:

- *Stoichiometry*- The number of sites in a source material reactive to a given reagent is exactly the same type and number of sites reactive on the prepared hydrophobic biopolymer to the given reagent. Therefore stoichiometry of known reactions may be used to determine the number of moles, and subsequently the mass, of reagent required to facilitate the formation of reaction products which include a given mass of the prepared hydrophobic biopolymer.
- *Over- or Under-Estimate With Respect to Stoichiometry*- The number of total sites and/or number of site types in a source material reactive to a given reagent may be greater or less than the number of total sites and/or number of site types

reactive to the given reagent in the prepared hydrophobic biopolymer, respectively. This could be due to mass-transfer limitations of the reagent to the source material sites, for example, or a large number of undesired reactions within the source material which must necessarily take place to complete the desired reactions. In addition to the mass of reagent required to react with the number and type(s) of sites present in the prepared hydrophobic biopolymer, however, the mass of reagent required to account for the difference in the number and types of sites present in the source material is known. Accordingly, the mass of reagent required per mass of prepared hydrophobic biopolymer remains to be a function of the reactive fraction in the prepared hydrophobic biopolymer. This may be the case described by the estimation of potassium hydroxide mass required to hydrolyze oxygen-containing groups and release materials which are not exclusively comprised of cutin. In addition, it may also be the case described by the estimation of enzyme mass required to cleave lignin-cellulose bonds and release a material containing polar components in addition to cellulolytic enzyme lignin.

- *Estimate Without Respect to Stoichiometry*- The undesired reactions within the source material may be taking place between an unknown number of site types and/or total sites. In addition, mass transfer limitations may be too complex to be fully characterized. Accordingly, the mass of reagent required per mass of prepared hydrophobic biopolymer does not remain to be a function of the reactive fraction in the prepared hydrophobic biopolymer.

$$RV_1 = \frac{\log (K_D)}{\log (K_{D,AC})}$$

Equation 3.14: Normalized Sorption Capacity

$$RV_2 = \frac{\rho_{b,d,sand} UC_{sand}}{\rho_{b,d} \sum_{j=1}^{r} f_j UC_j}$$

Equation 3.15: Normalized Chemical Cost

Values for UC_j may be estimated from indicative bulk chemical costs (*176*) and indicative bulk chemical distributor costs, depending on the geographic area. For the purposes of the present study, sorption capacity rating values were normalized to the sorption capacity of activated carbon, and chemical cost was inversely normalized to the bulk material cost of carbonate sand. This was due to activated carbon and carbonate sand comprising, respectfully, the approximate highest sorption capacity and lowest material cost in industry. Normalization to the highest sorption capacity and the lowest chemical cost observed out of all the biopolymers was not performed. While proving somewhat useful in determining relative chemical costs and sorption capacities between the particular biopolymers studied, such a method does not acceptably represent the impact of the overall magnitude of chemical cost or sorption capacity in relation to typical industry values.

Equation 3.15 is also not a function of the amount of solvents needed for dissolutions, purifications, and extractions, for example, because solvents are assumed to be 100 percent recycleable in the present study. Extractions performed in industrial-sized soxhlet reactors, for example, would not require an amount of extraction solvent(s) as a function of mass of extractable source material, or subsequently, the number of extractions of source materials required. Any solvents containing solutes may also be recovered from rotoevaporators in near theoretical efficiencies if multiple condensers are used in series. Only reagents were considered in the comparative cost of hydrophobic biopolymer preparations, which are defined in the present study as the exhaustible chemicals or biological agents required.

Noticeably, neither the cost nor the current commercial availability of the required waste source materials were considered in the present study as well, in order to simplify the calculation of RV_2. Such omissions do not necessitate the assumption that the cost of waste biomaterials containing the desired hydrophobic biopolymers should be approximately zero, however, although the relatively negligible cost of samples of spruce chips and tomatoes for the present study supports that assumption. In fact, large bulk quantities of these waste biomaterials may actually have a significant overall project cost. The necessary assumption, rather, is that, on a per-unit basis, the bulk source-material cost may be insignificant in relation to the cost of chemicals required to process them into usable forms. A potentially challenge to the validity of insignificant material costs would be keratin azure, which is marketed for academic use and has a very high cost (Sigma-

Aldrich, $115 USD per five grams, March 2010). Due to its necessary modifications, the cost of keratin azure happened to remain proportionally small in comparison to the cost of high-purity research chemicals use in its various modifications. However, in any case, prices for materials and chemicals for academic use are obviously not representative of the potential cost (or intrinsic value) of bulk (undyed) sheep's wool and less-pure bulk chemicals which may be substituted for keratin's use in a capping environment. Rationale for the negligible material cost assumption and no consideration of the commercial availability of source biomaterials may also be based on the premise that a large supply of waste products are available which contain the required biomaterials. Upon existence of a small demand in the presence of a large supply, source biomaterials may be marketed and competitively priced. The lack of a currently available market for anything other than keratin azure is irrelevant with respect to the availability of sources.

In addition to the aforementioned items, carbonate sand placed in bulk has a zero cost associated with chemicals used for its preparation from the material purchased. Its use as a standard of normalization to chemical costs may not immediately seem obvious. An argument supporting the validation of carbonate sand as a normalization standard may be supported by the fact that the bulk material cost of carbonate sand is approximately less than or equal to that of any bulk waste biomaterials used in the isolation and preparation of the hydrophobic biopolymers studied. Moreover, the bulk material cost of hydrophobic biopolymers removed from such waste materials, along with the bulk material cost of sand products amended with the same hydrophobic biopolymers, are

necessarily higher than the bulk material cost of carbonate sand due to the additional cost of chemicals required for their isolation and preparation.

Following the preparation of hydrophobic biopolymer-coated sand products, a similar decision matrix procedure may be used to analyze the effect of varying sand content on F. In such a case, "hydrophobic biopolymer-coated sand product" would replace "hydrophobic biopolymer" in the above relationships. The bulk density, $\rho_{b,d}$ would be for the bulk hydrophobic-biopolymer coated sand product, and f_j would equal the mass of reagent required per mass of hydrophobic biopolymer-coated sand product. Estimation of f_j may be made based on the first case described or stoichiometry. In other words, the mass of ammonium thioglycolate required may be determined from exactly a known mass of cystine groups in the source material, unpurified keratin azure, and prepare a given mass of hydrophobic biopolymer product. A parameter representing the mass of prepared hydrophobic biopolymer per mass of hydrophobic biopolymer-coated sand product is not required in the denominator of Equation 3.15 due to it already being inherent in f_j. In the estimation of UC_j, the cost per mass of thioglycolic acid may be used as the cost per mass of ammonium thioglycolate. Ammonium is just used as a cation because of the additional aid in the swelling of the biopolymer matrix.

In order to most accurately determine the most feasible of the hydrophobic biopolymers, however, for continued study as coatings on sand grains, consideration must be made in the feasibility analysis of those hydrophobic biopolymers to include the

estimated cost of reagents required to produce coated sand products from the same. An example of the significance of this issue may be described by the relative feasibility of tomato peel cutin and keratin azure. In relation to other hydrophobic biopolymers, keratin azure is obviously at an advantage for being chosen for future study in the present method, due to its relatively nonexistent cost requirements for isolation and very small cost requirements for purification. However, it requires significant cost in order to render it suitable for coating sand grains. Tomato peel cutin, on the other hand, requires significant initial preparation costs, but can be used to coat sand grains without any additional cost. This is due to the low melting point of cutin and ability to natural-cross link (after cooling). Therefore, it is conceivable that the most feasible hydrophobic biopolymer to prepare and use in bulk may not be the most feasible hydrophobic biopolymer to use in the preparation of hydrophobic biopolymer-coated sand products. Although such a shortcoming in the aforementioned method is significant, it was not investigated in the present study due to only one of the hydrophobic biopolymers studied being chosen to coat sand products. In other words, methods were not developed for coating sand particles using tomato peel cutin and cellulolytic enzyme lignin, thus, the mass of reagents required was not predetermined for use in feasibility calculations.

3.6 FINITE DIFFERENCE SIMULATION OF THE TRANSPORT OF NAPHTHALENE THROUGH A THIN-LAYER CAP COMPRISED OF HYDROPHOBIC BIOPOLYMER-COATED SAND PRODUCTS

In the present study, a finite difference solution was achieved for the linear one-dimensional transport equation, without reaction, through a sorbing porous media. The numerical solution was then compared to an existing analytical solution for a given set of transport parameters in order to determine the numerical error of the model. Such a solution was used to simulate the fate and transport of naphthalene though a thin cap comprised of sand only, hydrophobic biopolymers only, and hydrophobic biopolymer-coated sand products. Such simulations could also be used in laboratory column simulation of contaminant fate and transport through and within cap hydrophobic biopolymers and hydrophobic biopolymer-coated sand products. During column studies, sorption parameters are verified and contaminant breakthrough curves are determined by passing an aqueous solution containing the dissolved contaminant through a length of capping material in a column. Dispersion coefficients are estimated by first conducting a tracer test on the column. Figure 3.1 illustrates an example column setup in which the effluent is not recirculated after leaving the column.

3.6.1 Formulation

Consider a cylindrical column of finite domain such as the one illustrated in Figure 3.1. Performing a mass balance for contaminant A (not the water) on a differential

element in a finite region yields Equation 3.16, where parameters used in the formulation are described in Table 3.5.

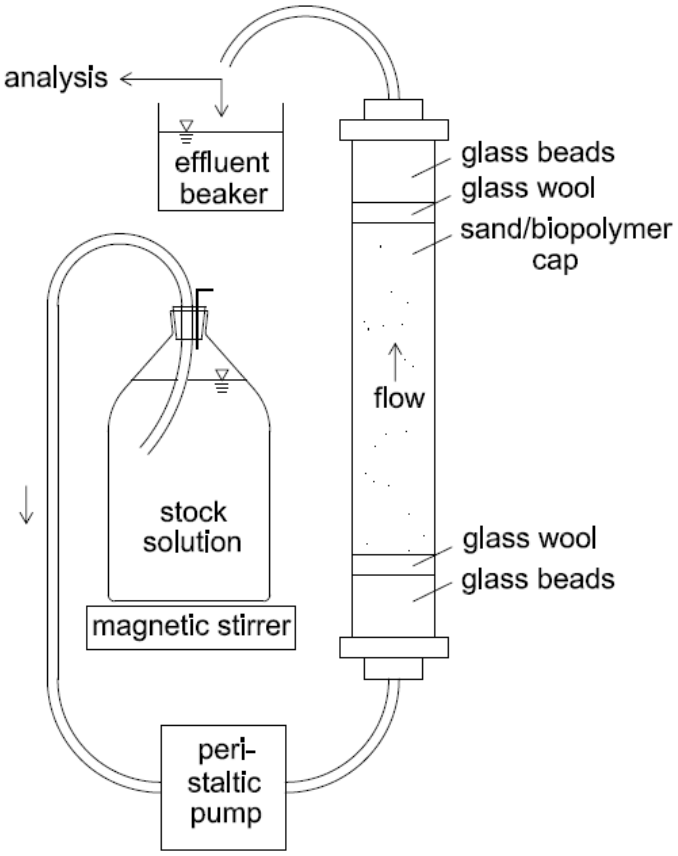

Figure 3.1: Column Apparatus

The following assumptions are made for developing the specific form of the transport equation:

- Only a single contaminant is present in the system. If multiple contaminants are present, they must be at low enough concentrations to assume no competition for sorption sites

- No other reaction takes place in the system other than sorption to solids
- Sorption media is saturated with no air space
- Sorption to black carbon may be considered negligible for the residence times the model will be used for. Therefore, only sorption to natural organic carbon is considered
- The contaminant in the water phase achieves local equilibrium with the media and dissolved organic matter
- The effective dispersion coefficient is constant in both space and time

$$\left\{\begin{matrix} rate\ of\ accumulation \\ of\ contaminant\ A\ per \\ unit\ of\ total\ volume \end{matrix}\right\} = \left\{\begin{matrix} net\ rate\ of\ flow\ (in-out) \\ of\ contaminant\ A\ by \\ advection \end{matrix}\right\} + \left\{\begin{matrix} net\ rate\ of\ flow\ (in-out) \\ of\ contaminant\ A\ by \\ dispersion \end{matrix}\right\} \pm \left\{\begin{matrix} rate\ of\ generation\ or \\ consumption\ of \\ contaminant\ A\ by \\ reaction \end{matrix}\right\}$$

$$\frac{\partial}{\partial t}\left[\left(\eta_{b,d}C_{A,W} + \rho_{b,d}W_S + \rho_{DOC}W_{DOC}\right)\right] = -\left(\frac{U}{86400}\right)\frac{\partial C_{A,W}}{\partial \mathrm{z}} + \left(D_{\mathrm{disp}}\right)\frac{\partial^2 C_{A,W}}{\partial z^2}$$

Equation 3.16: Mass Balance

Table 3.5: Variable Descriptions

Parameter	Description	Units
$\eta_{b,d}$	water-filled porosity in the control volume, or total volume of water-filled voids divided by the total volume	liters water per liters total volume
$C_{A,W}$	concentration of A in the water	milligrams A per liter water
$\rho_{b,d}$	dry bulk density of the media in the control volume	kilogram dry media per liter total volume
W_S	concentration of A on the media	milligrams A per kilogram dry media
W_{DOC}	concentration of A on Dissolved Organic Colloids (DOC)	milligrams A per kilogram dry colloids
ρ_{DOC}	concentration of DOC in the control volume	kilogram dry colloids per liter total volume
U	Darcy velocity	centimeters per day
D_{disp}	dispersion coefficient	square centimeters per second

Specific formulation of each of the above parameters may be found in (*177-180*). All length scales are in centimeters. ρ_{DOC} may be obtained by multiplying C_{DOC}, or the concentration of DOC in water in kilograms dry colloids per liter water, by the water-filled porosity, $\eta_{b,d}$. The Darcy velocity, U is obtained by multiplying the interstitial velocity by the water-filled porosity, $\eta_{b,d}$. The dispersion coefficient, D_{disp} in square centimeters per second, is given by Equation 3.17, where $D_{A,W}$ is the molecular diffusion coefficient of contaminant A through the water in square centimeters per second, $D_{Brownian}$ is the Brownian diffusion coefficient for the colloids in water in square centimeters per

second, K_{DOC} is the linear overall DOC-water partitioning coefficient for contaminant A in liters water per kilogram dry colloids, and α_D is the dispersivity in centimeters. The dispersivity may be approximated by Equation 3.18, where L is the length of the column in meters. The diffusion coefficient of contaminant A through water, $D_{A,W}$, may be estimated by Equation 3.19, where $D_{B,W}$ and MW_B is the diffusion coefficient and molecular weight of a reference compound in water, respectively, and $D_{A,W}$ and MW_A is the diffusion coefficient and molecular weight of contaminant A, respectively. An appropriate reference compound to use would be ethanol, with a molecular weight of 42 grams per mole and diffusivity in water of approximately 10^{-5} square centimeters per second.

$$D_{disp} = D_{A,W}\eta_{b,d}^{\frac{4}{3}} + D_{Brownian}\rho_{DOC}K_{DOC} + \alpha_D\left(\frac{U}{86400}\right)$$

Equation 3.17: Dispersion Coefficient (*177-180*)

$$\alpha_D = 0.017\left[\left(\frac{L}{100}\right)^{1.5}\right]100$$

Equation 3.18: Dispersivity (*177-180*)

$$\frac{D_{A,W}}{D_{B,W}} = \left(\frac{MW_B}{MW_A}\right)^{0.6}$$

Equation 3.19: Diffusion Coefficient (*177-180*)

K_{DOC} is given by Equation 3.20. The Brownian diffusivity may be estimated by Equation 3.21, where k_B is the Boltzmann constant (1.3805E-06 (grams*square centimeters) per (square seconds*Kelvin)), r_C is the colloid radius in centimeters, μ_W is the dynamic viscosity of water (0.01 grams per (centimeter*second)), and T is the absolute water temperature in Kelvin.

$$logK_{DOC} = logK_{OW} - 0.58$$

Equation 3.20: Overall DOC-Water Partitioning Coefficient (Linear) (*177-180*)

$$D_{Brownian} = \frac{k_B T}{6\pi r_C \mu_W}$$

Equation 3.21: Brownian Diffusivity (*177-180*)

K_{OW} is the octanol-water partitioning coefficient in (liters water per kilogram octanol), which may be related to K_{OC} by the Karickhoff relationship (described by Equation 3.22).

$$logK_{OC} = logK_{OW} - 0.21$$

Equation 3.22: Karickhoff Relationship (*177-180*)

In the case of linear sorption of contaminant A to the media, the accumulation term may be represented by a dimensionless retardation factor, R_f, multiplied by the time

rate of change of contaminant A in the water phase. The simplified mass balance equation then becomes Equation 3.23, where R_f is the retardation factor given by Equation 3.24, and K_D is the linear media-water partitioning coefficient given by Equation 3.25 in (liters water per kilogram dry media).

$$R_f \frac{\partial C_{A,W}}{\partial t} = -\left(\frac{U}{86400}\right)\frac{\partial C_{A,W}}{\partial z} + \left(D_{disp}\right)\frac{\partial^2 C_{A,W}}{\partial z^2}$$

Equation 3.23: Simplified Mass Balance

$$R_f = \eta_{b,d} + \rho_{b,d} K_D + \rho_{DOC} K_{DOC}$$

Equation 3.24: Retardation Factor

$$K_D = f_{OC} K_{OC}$$

Equation 3.25: Overall Media-Water Partitioning Coefficient (Linear)

The fraction of organic carbon in the media is denoted by f_{OC}. In the case where the type of organic carbon present within the media is more efficient or less efficient than natural organic matter at sorbing PAHs, the K_{OC} value in Equation 3.25 may be the material-specific K_{OC}, or the measured overall K_D may be used as-is when the appropriate experimental data exists.

For the purposes of simplifying the above expressions for computational purposes, the governing transport equation may be non-dimensionalized as shown by Equation 3.26, where τ is the dimensionless time given by Equation 3.27, ζ is the dimensionless distance given by Equation 3.28, u is the dimensionless concentration given by Equation 3.29, and Pe is the dimensionless Peclet number given by Equation 3.30.

$$\frac{\partial u}{\partial \tau} = -\mathrm{Pe}\frac{\partial \mathrm{u}}{\partial \zeta} + \frac{\partial^2 \mathrm{u}}{\partial \zeta^2}$$

Equation 3.26: Non-Dimensionalized Transport Equation

$$\tau = \frac{D_{disp,eff}\, t}{R_{f,eff} L^2}$$

Equation 3.27: Dimensionless Time

$$\zeta = \frac{\mathrm{z}}{\mathrm{L}}$$

Equation 3.28: Dimensionless Distance

$$u = \frac{C_{A,W}}{C_{A,W}(0)}$$

Equation 3.29: Dimensionless Concentration

$$Pe = \frac{U_{eff} L}{D_{disp,eff}}$$

Equation 3.30: Peclet Number

In these expressions, $C_{A,W}(0)$ is the concentration of contaminant A at z equals zero in milligrams A per liter water, U_{eff} is the effective Darcy velocity given by Equation 3.31 in centimeters per second, $D_{disp,eff}$ is the effective dispersion coefficient given by Equation 3.32 in square centimeters per second, and $R_{f,eff}$ is the dimensionless effective retardation factor given by Equation 3.33.

$$U_{eff} = \frac{\left(\frac{U}{86400}\right)}{\eta_{b,d}}$$

Equation 3.31: Effective Darcy Velocity

$$D_{disp,eff} = \frac{D_{disp}}{\eta_{b,d}}$$

Equation 3.32: Effective Dispersion Coefficient

$$R_{f,eff} = \frac{R_f}{\eta_{b,d}}$$

Equation 3.33: Effective Retardation Factor

3.6.2 Numerical Scheme

The Peclet number, as defined by Equation 3.30 is expected to vary between the orders of 10^{-1} and 10^{2} for the range of Darcy velocities typically found in non-tidal environments. In the case where Pe is less than two, upwind schemes are over-diffusive and central differencing schemes are preferred. However, when Pe is greater than two, central differencing schemes become unstable and the over-diffusiveness of upwind schemes becomes insignificant due to the dominating convective term.

Spalding (*181*) developed a scheme which is identical to a central differencing scheme for local Peclet number in the range Pe greater than negative two and less than two. The scheme then reduces to an upwind differencing scheme when local Pe is outside of that range, where the diffusive term is set to zero. The result is a three-line approximation of the left-hand-side coefficients in the linear set. Shortcomings associated with this scheme include the cost of computing exponentials, departure from the exact solution when Pe equals plus or minus two, and the inability to handle the diffusive term when the absolute value of Pe is greater than two. A similar power-law scheme improves on this hybrid method and is described by Patankar (*182*). The power law scheme does not eliminate the diffusive term at any value of local Pe, does not require computation of exponentials, and makes use of a more accurate four-line approximation of the left-hand-side coefficients (which apply in the local Peclet number ranges less than negative ten,

greater than negative ten and less than zero, greater than zero and less than ten, and greater than ten.

For the purposes of this model, the power law scheme is more complex in the unsteady case than what is necessary. In light of the considerations discussed above, the convective term shall be discretized using a three-point second-order upwind scheme, while the diffusive term shall be discretized using a three-point second-order central-differencing scheme. The Crank-Nicolson scheme shall be used for time discretization.

In the case of linear sorption, the discretized transport equation then becomes Equation 3.34, using uniform spacing in both space and time and assuming the flow is always positive in the direction of z (*183, 184*). In Equation 3.34 and the equations which follow describing the discretization of the transport equation, i represents the current node index and n represents the current time step index. It should be noted that the index n should not be confused with the variable n (Freundlich n).

$$\frac{u_i^{n+1} - u_i^n}{\Delta\tau} = \frac{1}{2}\left\{-Pe\left[\frac{u_{i-2} - 4u_{i-1} + 3u_i}{2\Delta\zeta}\right] + \left[\frac{u_{i+1} - 2u_i + u_{i-1}}{(\Delta\zeta)^2}\right]\right\}^n + \frac{1}{2}\left\{-Pe\left[\frac{u_{i-2} - 4u_{i-1} + 3u_i}{2\Delta\zeta}\right] + \left[\frac{u_{i+1} - 2u_i + u_{i-1}}{(\Delta\zeta)^2}\right]\right\}^{n+1}$$

Equation 3.34: Discretized Transport Equation

The assumption that flow is always positive in the direction of z is only valid for non-tidal environments or environments in which flow remains constant in one direction. Letting $CO1 = \frac{\Delta\tau Pe}{4\Delta\zeta}$ and $CO2 = \frac{\Delta\tau}{2(\Delta\zeta)^2}$, the above equation reduces to Equation 3.35.

$$(CO1)u_{i-2}^{n+1} + (-4CO1 - CO2)u_{i-1}^{n+1} + (1 + 3CO1 + 2CO2)u_i^{n+1} + (-CO2)u_{i+1}^{n+1} = (-CO1)u_{i-2}^{n} + (4CO1 + CO2)u_{i-1}^{n} + (1 - 3CO1 - 2CO2)u_i^{n} + (CO2)u_{i+1}^{n}$$

Equation 3.35: Reduced and Discretized Transport Equation

The resulting tetradiagonal linear set Ax equals b may be solved by first decomposing the coefficient matrix, A, into LU, where L and U are lower and upper triangular matrices, respectively. Following decomposition, forward substitution may be carried out to solve Ly equals b and backward substitution may be carried out to solve Ux equals y. An appropriate LU solver to be used in C++ is presented in Algorithm A: LU solver, and was adapted from (*185*), where N is the number of unknowns, p is the lower bandwidth of the linear set (coefficient matrix), and q is the upper bandwidth.

In order to avoid confusion, it should be noted that L and U as they are used in Algorithm A are not variables, but matrices representing coefficients in the linear set of equations. They should not be confused with the variables L and U, which in this document represent the length of the column and Darcy velocity, respectively.

```
//Decomposition of A into L and U. The entry a[i][j] is
//overwritten by l[i][j] if i>j and by u[i][j] otherwise
for(k=0; k<=N-2; k++)
{
     for(i=k+1; i<=min(k+p,N-1); i++)
          a[i][k]=a[i][k]/a[k][k];
     for(i=k+1; i<=min(k+p,N-1); i++)
          for(j=k+1; j<=min(k+q,N-1); j++)
               a[i][j]=a[i][j]-(a[i][k]*a[k][j]);
}

//Forward substitution to solve Ly=b. The entry b[i] is
//overwritten by y[i].
for(i=0; i<=N-1; i++)
{
     sum=0;
     for(j=max(0,i-p); j<=i-1; j++)
     {
          sum=sum+(a[i][j]*b[j]);
     }
     b[i]=b[i]-sum;
}
```

Algorithm A: LU Solver (continued on next page)

```
//Backward substitution to solve Ux=y. The entry y[i] is
//overwritten by x[i].
for(i=N-1; i>=0; i--)
{
      sum=0;
      for(j=i+1; j<=min(i+q,N-1); j++)
      {
            sum=sum+(a[i][j]*b[j]);
      }
      b[i]=(b[i]-sum)/a[i][i];
}
```

Algorithm A: LU Solver (continued)

3.6.3 Implementation of Initial and Boundary Conditions

A Dirichlet boundary condition of u equals u(0) is applied at x equals zero for all t greater than zero. A Neumann boundary condition of $\frac{\partial u}{\partial \zeta}$ equals zero is applied at x equals L for all t greater than zero. As an initial condition, u equals zero for all 0<x<L. Alternatively, a dimensionless mass flux, $J_A = U_{eff}u - D_{disp,eff}\frac{\partial u}{\partial \zeta}$ may be specified as a Dirichlet boundary condition at x equals zero for all t greater than zero.

In order to preserve second order accuracy as much as possible, a first order upwind differencing scheme scheme is not employed at node i equals two. Instead, u at

the second node is approximated using a central difference approximation for both the convective and diffusive terms. In this case, the system becomes Equation 3.36.

$$\frac{u_i^{n+1}-u_i^n}{\Delta\tau}=\frac{1}{2}\left\{-Pe\left[\frac{u_{i+1}-u_{i-1}}{2\Delta\zeta}\right]+\left[\frac{u_{i+1}-2u_i+u_{i-1}}{(\Delta\zeta)^2}\right]\right\}^n + \frac{1}{2}\left\{-Pe\left[\frac{u_{i+1}-u_{i-1}}{2\Delta\zeta}\right]+\left[\frac{u_{i+1}-2u_i+u_{i-1}}{(\Delta\zeta)^2}\right]\right\}^{n+1}$$

Equation 3.36: Discretized Transport Equation for the Second Node

Again, letting $CO1=\frac{\Delta\tau Pe}{4\Delta\zeta}$ and $CO2=\frac{\Delta\tau}{2(\Delta\zeta)^2}$, the above equation reduces to Equation 3.37.

$$(-CO1-CO2)u_{i-1}^{n+1}+(1+2CO2)u_i^{n+1}+(CO1-CO2)u_{i+1}^{n+1}= (CO1+\mathrm{CO2})u_{i-1}^n+(1-2CO2)u_i^n+(-CO1+CO2)u_{i+1}^n$$

Equation 3.37: Reduced and Discretized Transport Equation for the Second Node

At the last node, a second-order central differencing scheme is applied to approximate the Neumann boundary condition as shown in Equation 3.38.

$$\frac{\partial u}{\partial\zeta}=\frac{u_{i+1}-u_{i-1}}{2\Delta\zeta}=0$$

Equation 3.38: Neumann Boundary Condition

The above expression may be reduced to u_{i+1} equals u_{i-1}. Substituting this into Equation 3.37 yields Equation 3.39, which was used as the system for the last node:

$$(-2CO2)u_{i-1}^{n+1} + (1 + 2CO2)u_i^{n+1} = (2CO2)u_{i-1}^{n} + (1 - 2CO2)u_i^{n}$$

Equation 3.39: Reduced and Discretized Transport Equation for the Last Node

3.6.4 Exact Solution

Exact solutions for the governing transport equation given by Equation 3.40 exist on both a finite and semi-infinite domain (*186*). In this case, R is the effective retardation factor, D is the effective dispersion coefficient, and v is the effective velocity.

$$R\frac{\partial C}{\partial t} = D\frac{\partial^2 C}{\partial x} - v\frac{\partial C}{\partial x}$$

Equation 3.40: One-Dimensional Transport Equation

An exact solution for the semi-infinite domain is given by Equation 3.41: Analytical Solution for a Semi-Infinite Domain:

Initial Condition:

$$C(x, 0) = C_i$$

Boundary Conditions:

$$C(0,t) = \begin{Bmatrix} C_0 & 0 < t < t_0 \\ 0 & t > t_0 \end{Bmatrix}$$

$$\frac{\partial C}{\partial x}(\infty, t) = 0$$

Solution:

$$C(0,t) = \begin{Bmatrix} C_i + (C_0 - C_i)A(x,t) & 0 < t < t_0 \\ C_i + (C_0 - C_i)A(x,t) - C_0 A(x, t - t_0) & t > t_0 \end{Bmatrix}$$

, where

$$A(x,t) = \frac{1}{2} erfc\left[\frac{Rx - vt}{2(DRt)^{\frac{1}{2}}}\right] + \frac{1}{2} exp\left(\frac{vx}{D}\right) erfc\left[\frac{Rx + vt}{2(DRt)^{\frac{1}{2}}}\right]$$

Equation 3.41: Analytical Solution for a Semi-Infinite Domain (*186*)

An exact solution for the finite domain is given by Equation 3.42:

Initial Condition:

$$C(x,0) = C_i$$

Boundary Conditions:

$$C(0,t) = \begin{matrix} C_0 & 0 < t < t_0 \\ 0 & t > t_0 \end{matrix}$$

$$\frac{\partial C}{\partial x}(L,t) = 0$$

Solution:

$$C(0,t) = \begin{matrix} C_i + (C_0 - C_i)A(x,t) & 0 < t < t_0 \\ C_i + (C_0 - C_i)A(x,t) - C_0 A(x,t-t_0) & t > t_0 \end{matrix}$$

, where

$$A(x,t) = 1 - \sum_{m=1}^{\infty} \frac{2\beta_m sin\left(\frac{\beta_m x}{L}\right) exp\left[\frac{vx}{2D} - \frac{v^2 t}{4DR} - \frac{\beta_m^2 Dt}{L^2 R}\right]}{\left[\beta_m^2 + \left(\frac{vL}{2D}\right)^2 + \frac{vL}{2D}\right]}$$

Equation 3.42: Analytical Solution for a Finite Domain (*186*)

, and where the eigenvalues, β_m, are the positive roots of Equation 3.43:

$$\beta_m cot(\beta_m) + \frac{vL}{2D} = 0$$

Equation 3.43: Eigenvalues for Finite Domain Solution

An approximate solution of a form similar to the solution on a semi-infinite domain is also given by Equation 3.44.

$$A(x,t) = \frac{1}{2} erfc\left[\frac{Rx - vt}{2(DRt)^{\frac{1}{2}}}\right] + \frac{1}{2} exp\left(\frac{vx}{D}\right) erfc\left[\frac{Rx + vt}{2(DRt)^{\frac{1}{2}}}\right] + \frac{1}{2}\left[2 + \frac{v(2L - x)}{D} + \frac{v^2 t}{DR}\right] exp\left(\frac{vL}{D}\right) erfc\left[\frac{R(2L - x) + vt}{2(DRt)^{\frac{1}{2}}}\right] - \left(\frac{v^2 t}{\pi DR}\right)^2 exp\left[\frac{vL}{D} - \frac{R}{4Dt}\left(2L - x + \frac{vt}{R}\right)^2\right]$$

Equation 3.44: Approximate Solution for a Semi-Infinite Domain

Note that these analytical solutions are for the constant concentration Dirichlet boundary condition at z equals zero. If a constant flux Dirichlet boundary condition is specified, a much different solution is needed for both the finite and semi-infinite domain. Those solutions are also presented in (*186*).

3.6.5 Fourier and Matrix Stability Analysis

In the case of linear sorption, the relationship for absolute error, ε at node i is the same as the relationship for u, as shown in Equation 3.45.

$$\frac{\varepsilon_i^{n+1}-\varepsilon_i^n}{\Delta\tau}=\frac{1}{2}\left\{-Pe\left[\frac{\varepsilon_{i-2}-4\varepsilon_{i-1}+3\varepsilon_i}{2\Delta\zeta}\right]+\left[\frac{\varepsilon_{i+1}-2\varepsilon_i+\varepsilon_{i-1}}{(\Delta\zeta)^2}\right]\right\}^n + \frac{1}{2}\left\{-Pe\left[\frac{\varepsilon_{i-2}-4\varepsilon_{i-1}+3\varepsilon_i}{2\Delta\zeta}\right]+\left[\frac{\varepsilon_{i+1}-2\varepsilon_i+\varepsilon_{i-1}}{(\Delta\zeta)^2}\right]\right\}^{n+1}$$

Equation 3.45: Absolute Error

Letting $\varepsilon_i^n=\gamma^{a\tau}e^{ih\zeta}$, the above expression is expanded to Equation 3.46. Dividing by $\gamma^{a\tau}e^{ih\zeta}$, Equation 3.46 reduces to Equation 3.47. Furthermore, substituting in Euler's Formula and trigonometric identities, and letting $CO1=\frac{\Delta\tau Pe}{4\Delta\zeta}$ and $CO2=\frac{\Delta\tau}{2(\Delta\zeta)^2}$, Equation 3.47 reduces to Equation 3.48.

$$\begin{aligned}\frac{\gamma^{a(\tau+\Delta\tau)}e^{ih\zeta}-\gamma^{a\tau}e^{ih\zeta}}{\Delta\tau} &= \frac{1}{2}\left\{-Pe\left[\frac{\gamma^{a\tau}e^{ih(\zeta-2\Delta\zeta)}-4\gamma^{a\tau}e^{ih(\zeta-\Delta\zeta)}+3\gamma^{a\tau}e^{ih\zeta}}{2\Delta\zeta}\right]\right.\\ &\left.+\left[\frac{\gamma^{a\tau}e^{ih(\zeta+\Delta\zeta)}-2\gamma^{a\tau}e^{ih\zeta}+\gamma^{a\tau}e^{ih(\zeta-\Delta\zeta)}}{(\Delta\zeta)^2}\right]\right\}\\ &+\frac{1}{2}\left\{-Pe\left[\frac{\gamma^{a(\tau+\Delta\tau)}e^{ih(\zeta-2\Delta\zeta)}-4\gamma^{a(\tau+\Delta\tau)}e^{ih(\zeta-\Delta\zeta)}+3\gamma^{a(\tau+\Delta\tau)}e^{ih\zeta}}{2\Delta\zeta}\right]\right.\\ &\left.+\left[\frac{\gamma^{a(\tau+\Delta\tau)}e^{ih(\zeta+\Delta\zeta)}-2\gamma^{a(\tau+\Delta\tau)}e^{ih\zeta}+\gamma^{a(\tau+\Delta\tau)}e^{ih(\zeta-\Delta\zeta)}}{(\Delta\zeta)^2}\right]\right\}\end{aligned}$$

Equation 3.46: Expanded Absolute Error

Equation 3.48 may be split into an equation for the real terms and an equation for the complex terms. The equation for the real terms is given by Equation 3.49.

$$\frac{\gamma^{a\Delta\tau}-1}{\Delta\tau}=\frac{1}{2}\left\{-Pe\left[\frac{e^{ih(-2\Delta\zeta)}-4e^{ih(-\Delta\zeta)}+3}{2\Delta\zeta}\right]+\left[\frac{e^{ih(\Delta\zeta)}-2+e^{ih(-\Delta\zeta)}}{(\Delta\zeta)^2}\right]\right\}$$
$$+\frac{1}{2}\gamma^{a\Delta\tau}\left\{-Pe\left[\frac{e^{ih(-2\Delta\zeta)}-4e^{ih(-\Delta\zeta)}+3}{2\Delta\zeta}\right]+\left[\frac{e^{ih(\Delta\zeta)}-2+e^{ih(-\Delta\zeta)}}{(\Delta\zeta)^2}\right]\right\}$$

Equation 3.47: Reduced Absolute Error

$$\gamma^{a\Delta\tau}-1=\{-CO1[\cos(2h\Delta\zeta)-isin(2h\Delta\zeta)-4\cos(h\Delta\zeta)+4isin(h\Delta\zeta)+3]$$
$$+CO2[2cos(h\Delta\zeta)-2]\}$$
$$+\{-CO1\gamma^{a\Delta\tau}[\cos(2h\Delta\zeta)-isin(2h\Delta\zeta)-4\cos(h\Delta\zeta)+4isin(h\Delta\zeta)$$
$$+3]+CO2[2cos(h\Delta\zeta)-2]\}$$

Equation 3.48: Substituted and Reduced Absolute Error

$$\frac{\gamma^{a\Delta\tau}-1}{\gamma^{a\Delta\tau}+1}=\{-CO1[\cos(2h\Delta\zeta)-4\cos(h\Delta\zeta)+3]+CO2[2cos(h\Delta\zeta)-2]\}$$

Equation 3.49: Real Absolute Error

For error to be bounded as τ approaches infinity, Equation 3.50 must be satisfied. Substituting Equation 3.50 into Equation 3.49, the equation that must be satisfied for stability is given by Equation 3.51.

The equation for the complex terms is given by Equation 3.52, which states that stability requirements are always satisfied. Thus, the complex term equation poses no additional stability requirements.

$$\frac{\varepsilon_i^{n+1} = \gamma^{a(\tau+\Delta\tau)} e^{ih\zeta}}{\varepsilon_i^n = \gamma^{a\tau} e^{ih\zeta}} = \gamma^{a\Delta\tau} \leq 1$$

(or)

$$\frac{\gamma^{a\Delta\tau} - 1}{\gamma^{a\Delta\tau} + 1} \leq 0$$

Equation 3.50: Bounded Error Requirement

$$\{-CO1[\cos(2h\Delta\zeta) - 4\cos(h\Delta\zeta) + 3] + CO2[2cos(h\Delta\zeta) - 2]\} \leq 0$$

(or)

$$-CO1\cos(2h\Delta\zeta) + (4\,\mathrm{CO1} + 2\mathrm{CO2})\cos(h\Delta\zeta) \leq 3CO1 + 2CO2$$

Equation 3.51: Real Stability

$$0 = (\gamma^{a\Delta\tau} + 1)[-isin(2h\Delta\zeta) + 4isin(h\Delta\zeta) + 3]$$

(or)

$$\gamma^{a\Delta\tau} = \frac{-[-sin(2h\Delta\zeta) + 4sin(h\Delta\zeta) + 3]}{[-sin(2h\Delta\zeta) + 4sin(h\Delta\zeta) + 3]} = -1$$

Equation 3.52: Nonreal Absolute Error

Chapter 4: Results and Discussion

The experimental results, as well as a discussion of their significance, are provided for each of the methods and experiments described in the previous chapter.

4.1 Isolation and Preparation of Selected Hydrophobic Biopolymers

Presented below are results of the preparation and isolation of cutin from tomato peels (CUT), cellulolytic enzyme lignin (CEL) from spruce wood chips, keratin azure (KER) from dyed sheep's wool, and purified keratin azure (KER PUR).

4.1.1 Tomato Peel Cutin

In the first extraction of tomato peels in methanol, the suspension obtained was dark amber and produced a significant mass of residue. During a second extraction, the solution turned a light yellow color and the amount of residue was significantly lower. A total of four more extractions were then performed, for a total of six extractions, with no further significant change in suspension color or residue mass upon filtration. The rate of recovery of the final tomato peel cutin inside the rotoevaporator during the last 25 milliliters of solvent was very slow without a rapid stream of air passing over the sample. Due to this issue, the last remaining 25 milliliters of trichloromethane solution containing

the trichloromethane-soluble tomato peel cutin were concentrated to dryness in a drying oven set at 60 degrees Celsius. The cutin obtained was liquid at 60 degrees, and upon cooling to room temperature, turned a dark butterscotch color. Figure 4.1 illustrates the appearance of tomato peel cutin following preparation and before evaporation of moisture in a drying oven. The consistency and texture of the tomato peel cutin upon cooling was not quite waxy. Rather, it seemed to exhibit a larger degree of toughness, and oftentimes slight brittleness which increased after removal of moisture in a drying oven at 105 degrees Celsius. This could have been due to a very small amount of deionized water residual in the initially obtained cutin, which, after repeated drying, eventually left the pores. This residual was not enough to conceivably affect accurate weighing of the cutin samples. Since batch tests were carried out in an aqueous environment, water residual would also not affect sorption capacity values obtained and therefore the change in color was not considered a significant issue in the present study. Approximately 1.9 grams of tomato peel cutin were obtained following the trichloromethane extraction of the first batch of hydrolyzed residue (first reaction with KOH). A second hydrolysis reaction did not produce any more significant mass of residue, or subsequently, cutin.

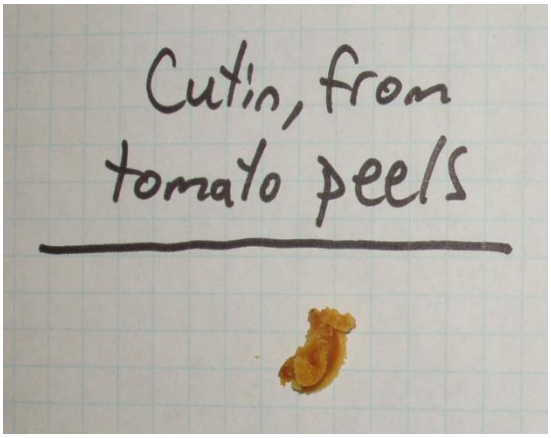

Figure 4.1: Tomato Peel Cutin

4.1.2 Cellulolytic Enzyme Lignin

Enzyme treatment yielded an insoluble fraction with the consistency, strength, color, and texture of clumped sawdust. In an initial attempt at soxhlet extraction of the treated wood meal, an extraction solvent consisting of 100 percent concentrated dioxane was unsuccessful in dissolving cellulolytic enzyme lignin. A second and third extraction of a second and third batch of the treated wool meal, respectively, was much more successful, using either a soxhlet apparatus and volumetric flask on a non-heated stir plate. Extraction solutions obtained after separation from the wood meal were a translucent, light yellow color in each successful batch extraction. However, additional precipitates often formed in the boiling flasks when a soxhlet apparatus was used for extraction. In such cases, the precipitates were separated from the bulk solution phase by filtration using 45 micrometer glass-fiber microfilters. Each batch of treated wood meal

was extracted twice, however, solutions obtained from second extractions were never concentrated enough to yield significant mass of resinous material after rotoevaporation.

Concentration to dryness of the extraction solutions obtained following the successful extractions was carried out under a rapid stream of air, slight vacuum, 55 degrees Celsius, and a rotovap rotational speed of 45 rounds per minute. Such a method yielded a highly concentrated, dark brown material with a resinous consistency that hardened somewhat at room temperature. The resinous material presumably contained residual solvents resistant to evaporation and cellulolytic enzyme lignin. Solution-State Nuclear Magnetic Resonance (SS-NMR) spectroscopic analysis of the resinous material revealed that there was a large fraction of oxygenated carbon groups present, which was presumed to be from residual dioxane. The sorption capacity of the resinous material for naphthalene, phenanthrene, and pyrene was also several orders of magnitude below expected values.

The SS-NMR and sorption test results of the resinous material obtained is a strong indication that a purification step is absolutely necessary to obtain a usable cellulolytic lignin of known purity. Following purification with deionized water and petroleum ether, the cellulolytic enzyme lignin obtained was very fine, powdery, and had a light-tan color which did not change significantly following removal of moisture in an oven at 105 degrees Celsius. Figure 4.2 illustrates the appearance of the cellulolytic enzyme lignin following preparation. The first successful batch extraction used approximately 18 grams

of treated wood meal and yielded over 100 milligrams of cellulolytic enzyme lignin after purification. The second batch extraction used approximately twice the mass of treated wood meal, however, the yield was not able to be determined because of partial accidental loss of resinous material during the purification step.

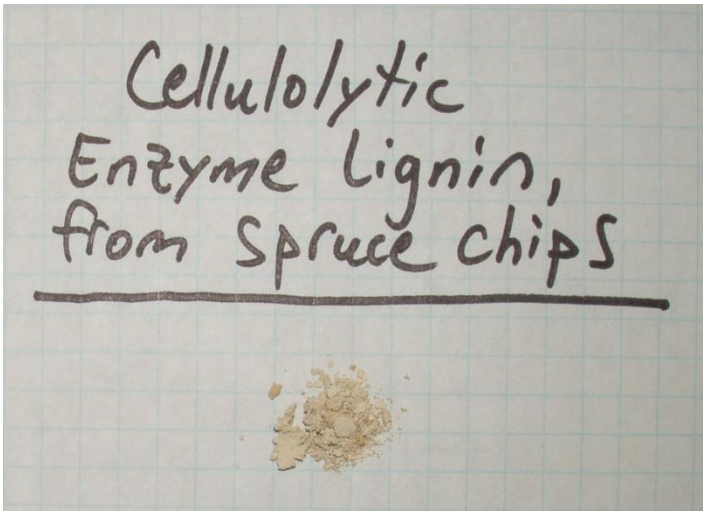

Figure 4.2: Cellulolytic Enzyme Lignin

4.1.3 Keratin Azure and Purifed Keratin Azure

A first, second, and third extraction of keratin azure in the acidified, aqueous pyridine solution yielded filtrates of a dark purple color, a slight burghandy color, and of no visible color, respectively. A lighter blue color of the purified keratin azure fibers was barely noticeable, and is shown in Figure: 4.3.

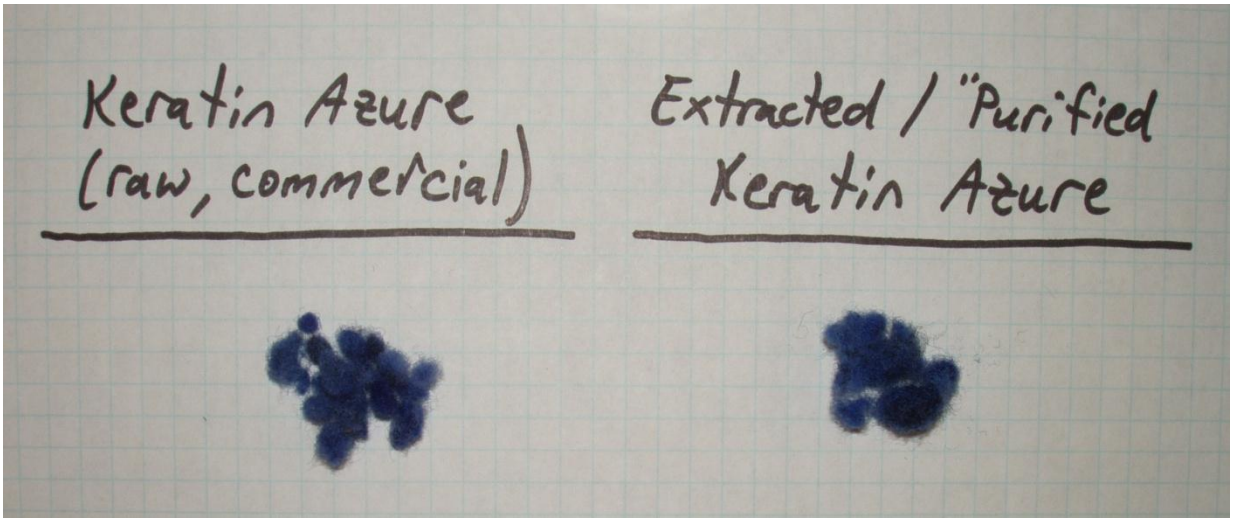

Figure: 4.3: Keratin Azure and Purified Keratin Azure

4.2 CONSTRUCTION OF HYDROPHOBIC BIOPOLYMER-COATED SAND PRODUCTS

Following the first few minutes of reaction with the alkaline ammonium thioglycolate solution, the keratin azure fibers were already noticeably degraded and starting to flocculate together, forming semi-solid masses of degraded fibers. In a first reduction batch, the fibers were removed at six hours, rinsed, and resuspended in a 100 percent aqueous solution as described in the previous section for homogenization using a food processor. This step was required because of the unsuccessful homogenization of the fibers with a mortar and pestle at two hours. The temperature of the reducing solution was also allowed to come to equilibrium and remain at 60 degrees Celsius prior to the onset of reaction. This immediate heating caused very fast reaction kinetics in the first two hours of reaction, causing the copious release of ammonia and hydrogen sulfide gas.

The excess hydrogen sulfide and ammonia were safely removed from the gas phase inside the glovebox over the course of several additional hours. After six hours, the natural decrease in reaction kinetics over time had reduced the rate of gas production and the overall concentrations of dangerous gases were easily held constant by the sequestration methods. The filtrate from the reduction solution was dark amber with a hint of blue after two hours. After six hours, there was a stronger hint of blue; however, the solution was dominantly dark brown. After six hours, the fibers lost all hint of blue and turned a dark brown color. This color change could be due to dye being significantly removed to the polar phase or otherwise chemically modified so as to change color. After 18 hours, the filtrate was very light amber with a slight hint of blue.

In a second reduction batch, the fibers were removed at two hours for homogenization using a food processor. The temperature of the reducing solution was also not allowed to increase above ambient temperature for one hour following the onset of reaction. This delayed heating caused reaction kinetics to slow remarkably in the first two hours, resulting in no significant hydrogen sulfide or ammonia gas concentrations inside the glovebox over the background levels at any time during reaction. The earlier homogenization also caused a more rapid release or reaction with dye molecules. Dry yield of reduced, beta-enriched keratin product after gravimetric settling and gravity filtration was not recorded after either the first or second batches because the retentate could not dry in the glovebox.

Minimal heat was released during the addition of formic acid to the reduced keratin product after being removed from the glovebox. The slurry after acidification was verified to be at a pH of approximately two using litmus paper. Immediately following their addition to sand, the approximately zero percent, approximately 15 percent, and approximately 85 percent coated sand product slurries were characterized as described in Table 4.1. The characteristics after 24 and 48 hours in the fume hood were approximately similar, and are presented in Table 4.2. The characteristics after 24 and 48 hours in the drying oven, or 72 and 96 total hours outside of the glovebox, were also approximately similar, and are presented in Table 4.3.

Table 4.1: Slurries at Time Zero

Parameter	Petri Dish Contents at Time Zero		
	No. 1 (~0% sand)	No. 2 (~15% sand)	No. 3 (~85% sand)
Consistency	Free-flowing, liquid-like, low viscosity	Gritty, liquid-like, low viscosity	Gritty, clumpy, particles "glued" together
Color	Dark brown	Dark brown	Dark Brown
Texture	Smooth	Slightly rough	Very rough

The slurry containing the highest mass fractions of sand dried the quickest, and upon grinding in a mortar and pestle, produced uniformly sized particles with a similar size as the sand used. The approximately 15 percent slurry, upon grinding, yielded

Table 4.2: Slurries at 24 and 48 Hours

Parameter	Petri Dish Contents After 24 and 48 Hours in Fume Hood		
	No. 1 (~0% sand)	No. 2 (~15% sand)	No. 3 (~85% sand)
Consistency	Moderately soft, gum-like	Moderately hard, gum-like with harder particles of grit	Very hard, very gritty, feels and looks like sand particles glued together
Color	Dark brown	Dark brown	Brown
Texture	Smooth, goopey	Smooth, goopey with particles of rough grit	Very rough

Table 4.3: Slurries at 72 and 96 Hours

Parameter	Petri Dish Contents After 24 Hours in Drying Oven		
	No. 1 (~0% sand)	No. 2 (~15% sand)	No. 3 (~85% sand)
Consistency	Hard, very tough, grinds into relatively uniformly sized granules slightly larger than sand particles	Hard, very tough, grinds into relatively uniformly sized granules slightly larger than sand particles	Hard, brittle, grinds into relatively uniformly sized granules approximately the same size as sand particles
Color	Brown	Brown	Brown with contrasting sand-colored particles
Texture	Smooth	Gritty	Rough

particle sizes closer to the approximately zero percent coated sand product. After purification by boiling in water, a fraction of the sand particles and dried keratin product

had separated in the approximately 85 percent coated sand product, suggesting high mass fractions of sand may not be able to provide for a stable coating on sand particles using the methods in the present study. Also during boiling, a strong ammonia and hydrogen sulfide smell was detected, further suggesting that the purification step is absolutely necessary to remove toxic residual solvents from the final products. Filtrates from purification were colored light salmon after the first boiling. After the final products were returned to fresh deionized water for subsequent boilings, no color was noticeable.

Figure 4.4 illustrates the appearance of the hydrophobic biopolymer-coated sand products following their preparation. The final dry mass of beta-enriched keratin obtained from the two 4.0-5.0 gram batches of keratin azure was just over five grams. Such a percent yield may be indicative of roughly 50 percent of the original mass of keratin azure being removed to a polar phase during reduction, which presumably is mostly α-keratin. The remaining keratin product is still dominantly α-keratin, but contains a much higher percentage of beta keratin and much fewer dye molecules. Table 4.4 includes the mass of sand added to each petri dish, the final total mass of coated sand products in each petri dish, and subsequently the mass fraction of sand for each of the three hydrophobic biopolymer-coated sand products contained in the petri dishes using reduced and beta-enriched keratin from two reaction batches.

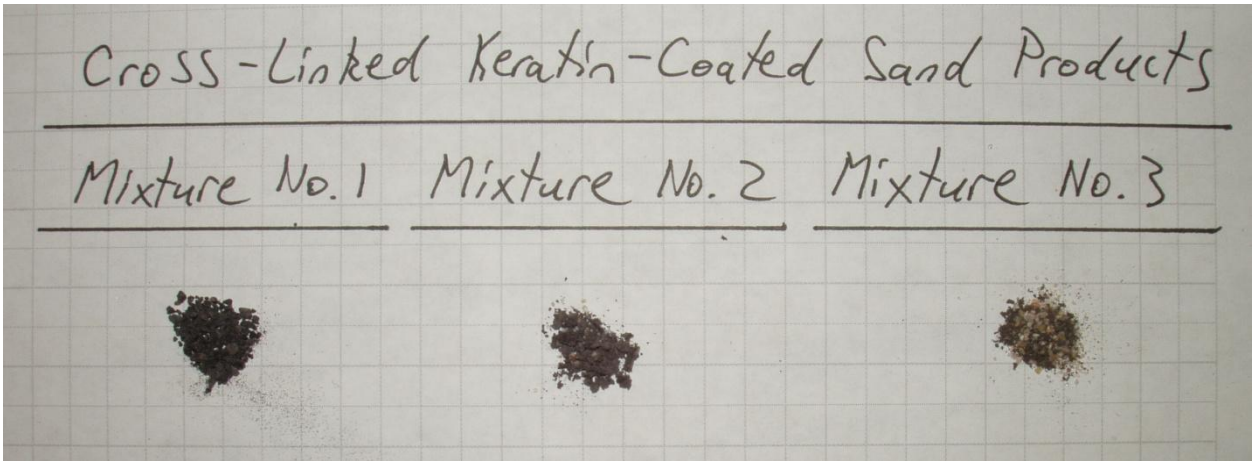

Figure 4.4: Hydrophobic Biopolymer-Coated Sand Products

Table 4.4: Yield of Beta-Enriched Keratin Product

Petri Dish No.	Target Mass Fraction of Sand (gram per gram)	Total mass of Sand (grams)	Total Mass of Dried, Coated Sand Product (grams)	Actual Mass Fraction of Sand (gram per gram)
1	0	0	2.28	0.00
2	0.15	0.43	2.8	0.154
3	0.85	2.88	3.31	0.870

4.3 PHYSICAL AND CHEMICAL CHARACTERIZATION OF SELECTED HYDROPHOBIC BIOPOLYMERS AND HYDROPHOBIC BIOPOLYMER-COATED SAND PRODUCTS

Chemical and physical analysis results of hydrophobic biopolymers and hydrophobic biopolymer-coated sand products isolated and prepared for use in the present study are presented and discussed below.

4.3.1 Solution-State ^{1}H and ^{13}C Nuclear Magnetic Resonance

Quantitative ^{1}H spectra and qualitative ^{13}C spectra obtained from SS-NMR tests are presented in Figure 4.5, Figure 4.6, Figure 4.7, and Figure 4.8. Signal peaks within the ^{1}H spectra were associated with specific carbon types for tomato peel cutin and cellulolytic enzyme lignin as included in Table 4.5 and Table 4.6, respectively.

Noticeably, the spectra for cutin have very little "noise" when compared to the spectra for cellulolytic enzyme lignin, which may be attributed to the very high molecular weight of cellulolytic enzyme lignin obtained for use in the present study (*62*). Cutin isolated using methods adapted from (*40*) are mostly monomeric or oligomeric, thus, the diversity of carbon groups is relatively low. Cellulolytic enzyme lignin, on the other hand, has a much wider array of carbon types present and is already polymeric in the form isolated with the methods used in the present study. Due to such additional complexity in the cellulolytic enzyme lignin spectra, association of proton signals with specific carbon groups could only be estimated for the tomato peel cutin. The ^{13}C spectra for cellulolytic enzyme lignin has much better separation between groups of peaks than the ^{1}H spectra for cellulolytic enzyme lignin, suggesting the importance of obtaining quantitative ^{13}C NMR spectra for detailed chemical analysis. Accordingly, Table 4.6 is kept much more general than in Table 4.5.

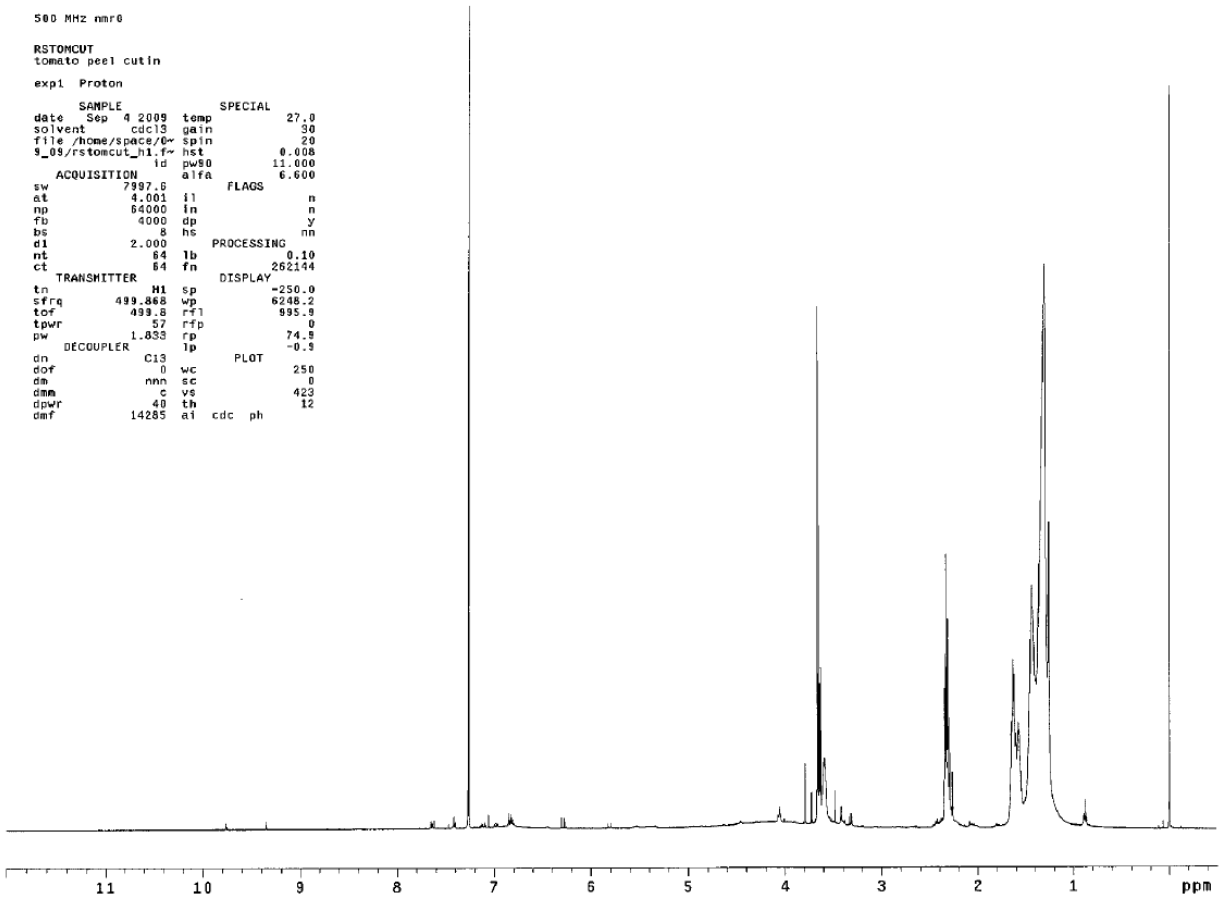

Figure 4.5: ^{1}H Spectra of Tomato Peel Cutin

Carbon type associations for tomato peel cutin may be simplified even further as defined in Table 3.1 by comparing the ^{1}H spectra with the ^{13}C spectra, and are presented

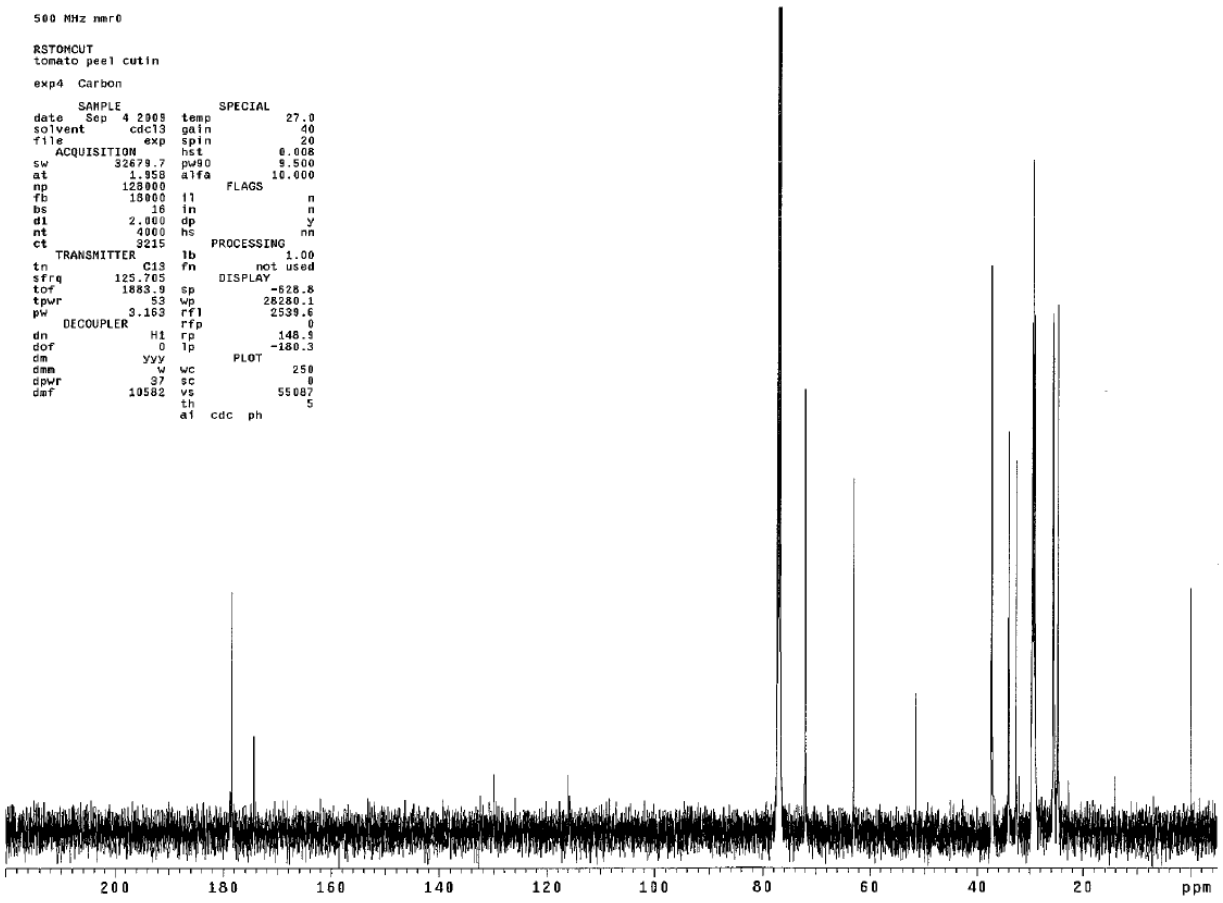

Figure 4.6: ^{13}C Spectra of Tomato Peel Cutin

in Table 4.7. In general, the approximate proportions of key chemical groups or carbon type associations matched those of unpurified cutin obtained by (*29, 22, 18*)

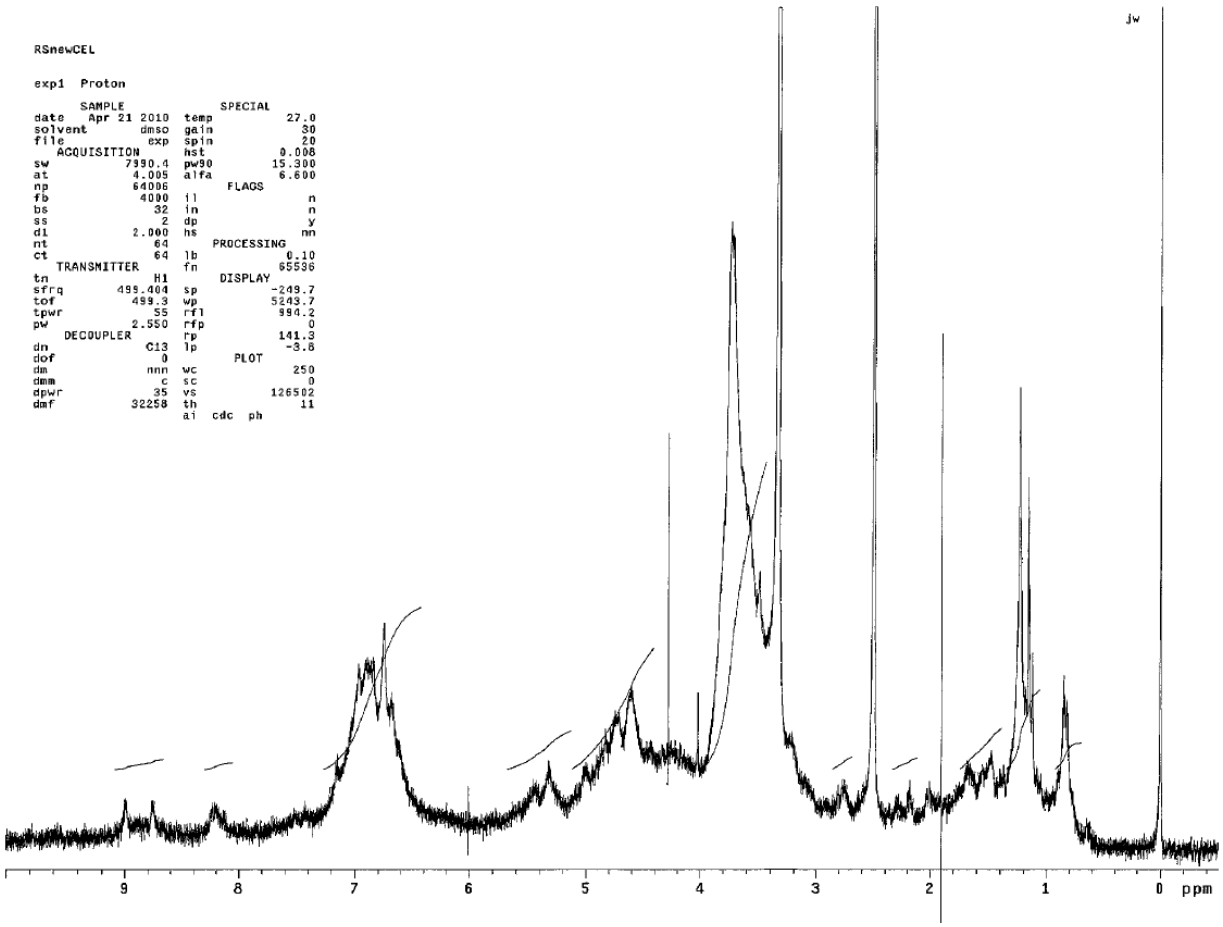

Figure 4.7: ^{1}H Spectra of Cellulolytic Enzyme Lignin

reasonably well, and matched a highly purified cutin fraction obtained by (*28*) very well, suggesting that tomato peel cutin isolated for use in the present study is of very high

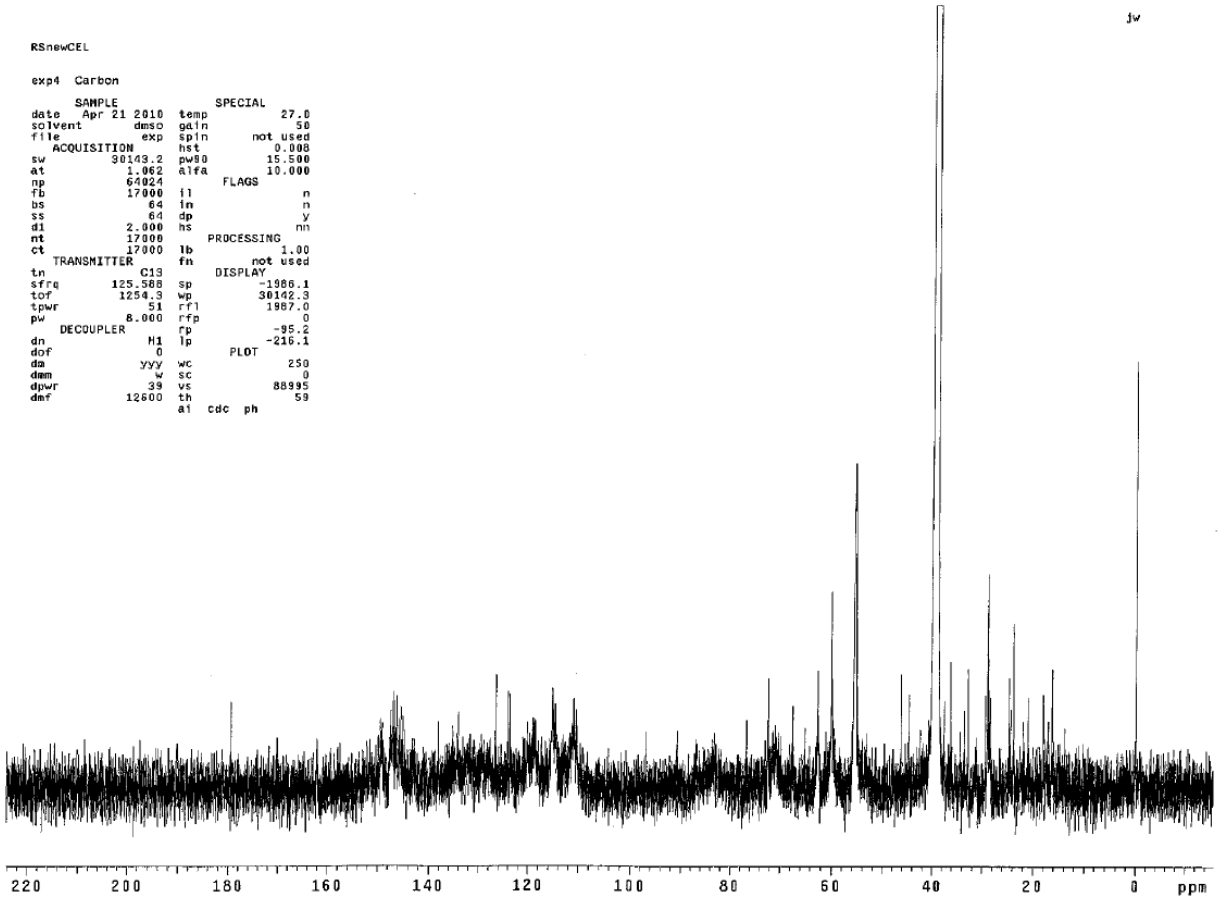

Figure 4.8: ^{13}C Spectra of Cellulolytic Enzyme Lignin

purity. The amorphous paraffinic-C region, accounting for roughly 67 percent of the protons in the tomato peel cutin isolated in the present study, is also roughly twice that

Table 4.5: ^{1}H Spectra Integration Results for Tomato Peel Cutin (continued on next page)

Peak No.	ppm (δ)	Frequency (Hz)	Height	Area	% of Protons	Carbon Group Association
1	-0.007	-3.356	5.2	N/A	N/A	TMS and Deuterium standards
2	0	0	144			
3	0.006	3.234	5.2			
4	0.866	432.793	3	0.76	0.712	Carbohydrates (C-CH_3)
5	0.88	439.87	5.8			
6	0.893	446.582	2.9			
7	1.229	614.257	9	71.75	67.182	Saturated (non polar) rubbery, amorphous paraffinic C (polymethylene C)
8	1.243	621.274	16.2			
9	1.254	627.07	59.7			
10	1.3	650.013	109.7			
11	1.361	680.155	42.9			
12	1.389	694.433	29.3			
13	1.396	697.606	29			
14	1.43	714.751	47.4			
15	1.443	721.219	39.9			
16	1.538	768.995	7.8	13.97	13.081	Saturated glassy, crystalline paraffinic C (polymethylene C)
17	1.552	775.585	14.2			
18	1.56	779.673	19.4			
19	1.565	782.236	19.4			
20	1.573	786.446	20.7			
21	1.588	793.768	16.8			
22	1.601	800.175	18.7			
23	1.614	807.009	30.1			
24	1.629	814.209	33			
25	1.643	821.165	21			

Table 4.5: ^{1}H Spectra Integration Results for Tomato Peel Cutin (continued)

Peak No.	ppm (δ)	Frequency (Hz)	Height	Area	% of Protons	Carbon Group Association
26	2.264	1131.619	17	8.31	7.781	Esters (H-C-COOR), carbohydrates (O=C-O-CH_3), carbonyls from esters, nitrogen-containing groups, and Aromatic-C-H
27	2.276	1137.72	6.6			
28	2.287	1143.395	22.5			
29	2.303	1151.022	33			
30	2.306	1152.73	23.7			
31	2.318	1158.771	62.3			
32	2.333	1166.337	81.4			
33	2.348	1173.781	41.8			
34	3.315	1656.974	4.6	0.4	0.375	
35	3.412	1705.421	7	0.45	0.421	
36	3.415	1707.129	5.8			
37	3.417	1708.228	6.6			
38	3.485	1741.97	11.6	0.25	0.234	
39	3.59	1794.628	21.2	3.62	3.390	
40	3.629	1813.787	30.3	3.73	3.493	Ester (RCOO-C-H) and ether linkages, carbohydrates (-O-CH_3 and H2-H6), and nitrogen-containing groups
41	3.631	1814.946	48			
42	3.642	1820.438	55.6			
43	3.644	1821.536	90.1			
44	3.655	1827.15	30.7			
45	3.657	1828.126	46.2			
46	3.667	1832.885	154.8	2.01	1.882	
47	3.724	1861.441	10.9	0.26	0.243	
48	3.79	1894.39	19.6	0.29	0.272	
49	4.049	2024.173	4.5	1	0.936	
50	4.063	2030.702	6.6			

Table 4.6: ^{1}H Spectra Integration Results for Cellulolytic Enzyme Lignin (continued on next page)

Peak No.	ppm (δ)	Frequency (Hz)	Height	Area	% of Protons	Carbon Group Association
1	0.82	409.42	28.2	3.84	3.202	Carbohydrates (C-CH_3)
2	0.852	425.51	33.3			
3	1.124	561.09	38.1	11.67	9.732	Hydroxyl-C, Saturated (non polar) rubbery, amorphous paraffinic C, R_2NH
4	1.148	573.29	52.3			
5	1.161	579.63	74.8			
6	1.187	592.79	31			
7	1.234	616.45	93.5			
8	1.372	684.97	14.7	6.09	5.079	Hydroxyl-C, Saturated glassy, crystalline paraffinic C, R_2NH
9	1.477	737.4	17.7			
10	1.683	840.3	15.5			
11	1.858	927.84	8.6	N/A	N/A	R_2NH, Hydroxyl-C, and R_2C=CR-CH
12	1.904	951.01	11.6			
13	1.904	951.25	-105.7			
14	1.905	951.49	104.7			
15	2.007	1002.22	11.3			
16	2.181	1089.03	11.6	1.68	1.401	Methoxy, Hydroxyl-C, Aromatic-C-H, Undesignated Nitrogen-Containing Groups, and O=CH
17	2.278	1137.79	8.7			
18	2.5	1248.75	450	N/A	N/A	
19	2.771	1383.59	11.8	1.84	1.534	

associated with amorphous paraffinic-C in cutin obtained by (*28*) from tomato peels. The total paraffinic–C content is similar for cutin isolated in (*28*) and the present study,

Table 4.6: ^{1}H Spectra Integration Results for Cellulolytic Enzyme Lignin (continued)

Peak No.	ppm (δ)	Frequency (Hz)	Height	Area	% of Protons	Carbon Group Association
20	3.341	1668.65	937.4	N/A	N/A	Hydroxyl-C, Carbohydrates (O=C-O-CH_3, -O-CH_3, and H2-H6), Undesignated Nitrogen-Containing Groups, and Aromatic-C-H
21	3.49	1743.03	55.1	45.11	37.620	
22	3.744	1869.58	128			
23	4.021	2008.09	29.7	N/A	N/A	Hydroxyl-C and PhO-CH
24	4.283	2138.79	84			
25	4.287	2140.99	19.4			
26	4.603	2298.51	31.7	17.76	14.811	Hydroxyl-C, Undesignated Nitrogen-Containing Groups, Vinyllic-C, and Phenolic-C
27	4.75	2371.91	26.1			
28	4.834	2414.1	22.3			
29	5.004	2498.95	15.3			
30	5.325	2659.16	15.6	5.72	4.770	(RCH=CHR), Carbohydrates (H-1 of alpha-gly), Vinyllic-C, and Phenolic-C
31	5.45	2721.59	11.7			
32	6.685	3338.52	29.8	23.71	19.773	Aromatic-C and Phenolic-C
33	6.752	3372.17	44.3			
34	6.843	3417.29	37.4			
35	6.974	3482.88	35.8			
36	7.149	3570.42	17.1			
37	7.423	3707.22	7.3	N/A	N/A	Phenolic-C
38	8.213	4101.77	7	1	0.834	
39	8.761	4375.36	7.4	1.49	1.243	Carboxyl-C
40	8.995	4491.92	7.8			

however. This suggests the difference may be attributed to the generally broader peaks in ^{1}H spectra with respect to ^{13}C spectra, making integration less accurate and analysis more

difficult. Alternatively, the crystalline paraffinic-C content may actually be substantially lower in the present study than in (*28*).

Table 4.7: Carbon Type Associations for Tomato Peel Cutin

Carbon Type	Percentage of Total Protons Likely Associated with Designated Carbon Group
Alkyl (Paraffinic)-C	80.975
Amorphous ("rubbery") Paraffinic-C	67.182
Crystalline ("glassy") Paraffinic-C	13.081
Substituted Alkyl-C (Alkyl-O, Alkyl-N, etc)	19.026
Aromatic-C	Non-Detect
Phenolic-C	Non-Detect
Carboxyl-C	Non-Detect
Carbonyl-C	Non-Detect
Total Polar-C	19.026
Aliphaticity	1.00
Aromaticity	0.00

Qualitatively, ^{13}C tomato peel cutin and cellulolytic enzyme lignin spectra matched ^{13}C tomato peel cutin and organosolv lignin spectra obtained by (*40*) and (*15*) very well, respectively. An exception to this correspondence, however, is associated with the chloroform and dimethyl sulfoxide peaks within the tomato peel cutin and cellulolytic enzyme spectra in the present study, respectively, which are not present in (*40*) or (15). These peaks may be explained by the fact that spectra from (*40*) and (*15*) were both obtained using solid-state NMR, unlike the solution-state NMR used in the present study.

Thus, (*40*) and (*15*) do not have peaks associated with the solvent in which the material is dissolved.

4.3.2 Elemental Analysis

Total Carbon and Total Nitrogen were determined for tomato peel cutin, cellulolytic enzyme lignin, and zero percent coated sand product. Fraction of organic carbon was calculated as defined by Equation 3.1 using total carbon as previously discussed. Fraction of nitrogen was then calculated from the total nitrogen and total sample mass in a similar manner as Equation 3.1 was used to calculate fraction of organic carbon. Table 4.8 presents the results obtained as calculated. Total carbon, and subsequently the fraction of organic carbon for keratin azure, purified keratin azure, 15.4 percent coated sand product, and 87 percent coated sand product may be approximated by the total carbon content of zero percent coated sand product as previously described in Chapter 3.

The fraction of organic carbon obtained for tomato peel cutin, cellulolytic enzyme lignin, and zero percent coated sand product are within the range of values one may expect from their respective compositions. The fraction of nitrogen, however, of keratin from sheep's wool as estimated from (*159*) is roughly twice that of the zero percent coated sand product. Such a result may be reduced to the conclusion that less nitrogen was added to the insoluble keratin fraction by solvents than was taken away from the

Table 4.8: Fraction Organic Carbon and Fraction Nitrogen

Hydrophobic Biopolymer or Hydrophobic Biopolymer-Coated Sand Product	Fraction of Organic Carbon, f_{OC} (-)	Fraction of Nitrogen, f_N (-)
Tomato Peel Cutin	0.694	Non-Detect
Cellulolytic Enzyme Lignin	0.622	Non-Detect
0% Coated Sand Product	0.495	0.071

strong alkaline reduction of the keratin azure. The smell of ammonia noted previously may not have been exclusively due to the volatilization of solvent during the reduction reaction. However, the assumption that the original nitrogen content of the keratin azure was roughly double that of zero percent coated sand product may only be confirmed by measuring the total nitrogen of keratin azure and purified keratin azure. Reduction was most likely not the cause of the nitrogen removal if in fact nitrogen removal occurred as it primarily reacts at the cystine linkage sites. Hydrolysis is presumably the cause of nitrogen removal, and may additionally improve sorption affinity for hydrophobic solutes.

4.3.3 Loss On Ignition

Organic matter content was measured for tomato peel cutin, cellulolytic enzyme lignin, purified keratin azure, and zero percent coated sand product by Loss-On-Ignition (LOI) and used to calculate the fraction of organic matter as defined by Equation 3.2.

Calculation results are presented in Table 4.9. In general, results support the assumption that total organic carbon may be approximated by total carbon, but do not validate it.

Table 4.9: Fraction Organic Matter

Hydrophobic Biopolymer or Hydrophobic Biopolymer-Coated Sand Product	Fraction of Organic Matter, f_{OM} (-)
Tomato peel cutin	0.993±0.004
Cellulolytic enzyme lignin	0.942±0.024
Purified keratin azure	0.967±0.007
0% coated sand product	0.971±0.023

4.3.4 Bulk porosity, Bulk Density, Specific Density, Particle Size Distribution, and Estimated Hydraulic Conductivity

Bulk density, specific density, specific weight, and bulk porosity were calculated for hydrophobic biopolymer-coated sand products and the industrial/play carbonate sand from which each was produced as defined by Equation 3.3, Equation 3.4, Equation 3.5, and Equation 3.6, respectively, using the methods previously described in Chapter 3. Table 4.10 presents such results.

In general, zero percent coated sand product had very similar physical characteristics to 15.4 percent coated sand product, and 87 percent coated sand product had very similar physical characteristics to industrial sand alone. The magnitudes of the specific and bulk densities generally increase with increasing sand content. There was a

Table 4.10: Physical Parameters

Material	Bulk Density, $\rho_{b,d}$ (grams per milliliter)	Specific Density, $\rho_{s,d}$ (grams per milliliter)	Specific Weight, γ_d (newtons per cubic meter)	Bulk Porosity, η (-)
0% Coated Sand Product	0.55	1.283	12590	0.571
15.4% Coated Sand Product	0.353	1.675	16430	0.789
87% Coated Sand Product	1.042	2.71	26590	0.615
Industrial Carbonate Sand	1.381	2.64	25900	0.476

slightly lesser degree of correlation to that trend for the bulk density than the specific density, which may indicate that grinding with a ceramic mortar and pestle may not be the best way to break up the cured/oxidized coated sand product into granules. The fact that there was also separation of sand particles from the coated sand product for the 87 percent mixture supports this even further.

Particle Size distributions were also obtained for each material, and are presented in Figure 4.9. As may be quickly inferred from the particle size distributions, the zero percent and 15.4 percent coated sand products had a more uniform, less graded particle size distribution in general when compared to the 87 percent coated sand product and

sand alone. There is also a general trend of decreasing characteristic particle size, d_{90}, with increasing sand content, which was expected. The characteristic particle size for the zero percent coated sand product had a very similar characteristic particle size to 15.4 percent coated sand product (~1.5 millimeters), and 87 percent coated sand product had a very similar characteristic particle size to industrial sand alone (~0.6 millimeters). An approximation of the intrinsic permeability and Darcy hydraulic conductivity was then calculated by Equation 3.7 and Equation 3.9, respectively, with the latter using properties for water. Table 4.11 presents the approximate characteristic particle size, intrinsic permeability, and Darcy hydraulic conductivity for each material. Darcy hydraulic conductivities are within the range of expected values for a material having sand-like particle size.

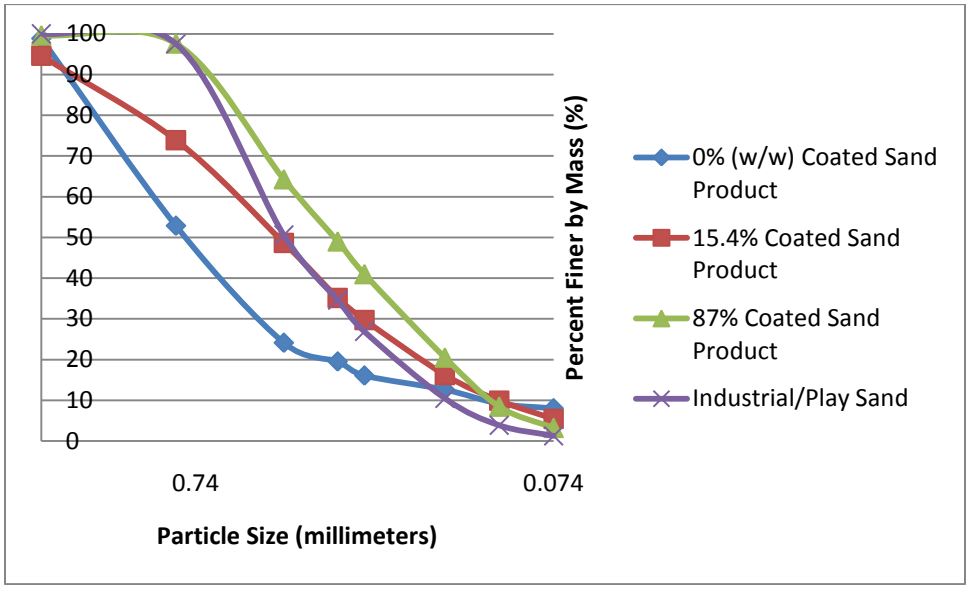

Figure 4.9: Coated Sand Product Particle Size Distribution

Table 4.11: Permeability and Hydraulic Conductivity

Material	Characteristic Particle Size, d_{90} (millimeters)	Intrinsic Permeability, k (square centimeters)	Darcy Hydraulic Conductivity, K (centimeters per second)
0% Coated Sand Product	1.5	1.47E-09	1.44E-08
15.4% Coated Sand Product	1.5	1.47E-09	1.44E-08
87% Coated Sand Product	0.6	2.35E-10	2.31E-09
Industrial Carbonate Sand	0.6	2.35E-10	2.31E-09

4.4 BATCH KINETICS AND EQUILIBRIUM SORPTION TESTS OF SELECTED HYDROPHOBIC BIOPOLYMERS, HYDROPHOBIC BIOPOLYMER- COATED SAND PRODUCTS, AND OTHER AMENDMENTS

Figure 4.10, Figure 4.11, Figure 4.12, and Figure 4.13 illustrate batch kinetics test results for the sorption of naphthalene, phenanthrene, and pyrene onto tomato peel cutin, cellulolytic enzyme lignin, keratin azure, and zero percent coated sand products, respectively. As may be inferred from Figure 4.10, 4.11, 4.12, and 4.13, equilibrium is achieved in under seven days for all materials. However, 14 days was chosen as the conservative time to equilibrium for performance of batch equilibrium studies.

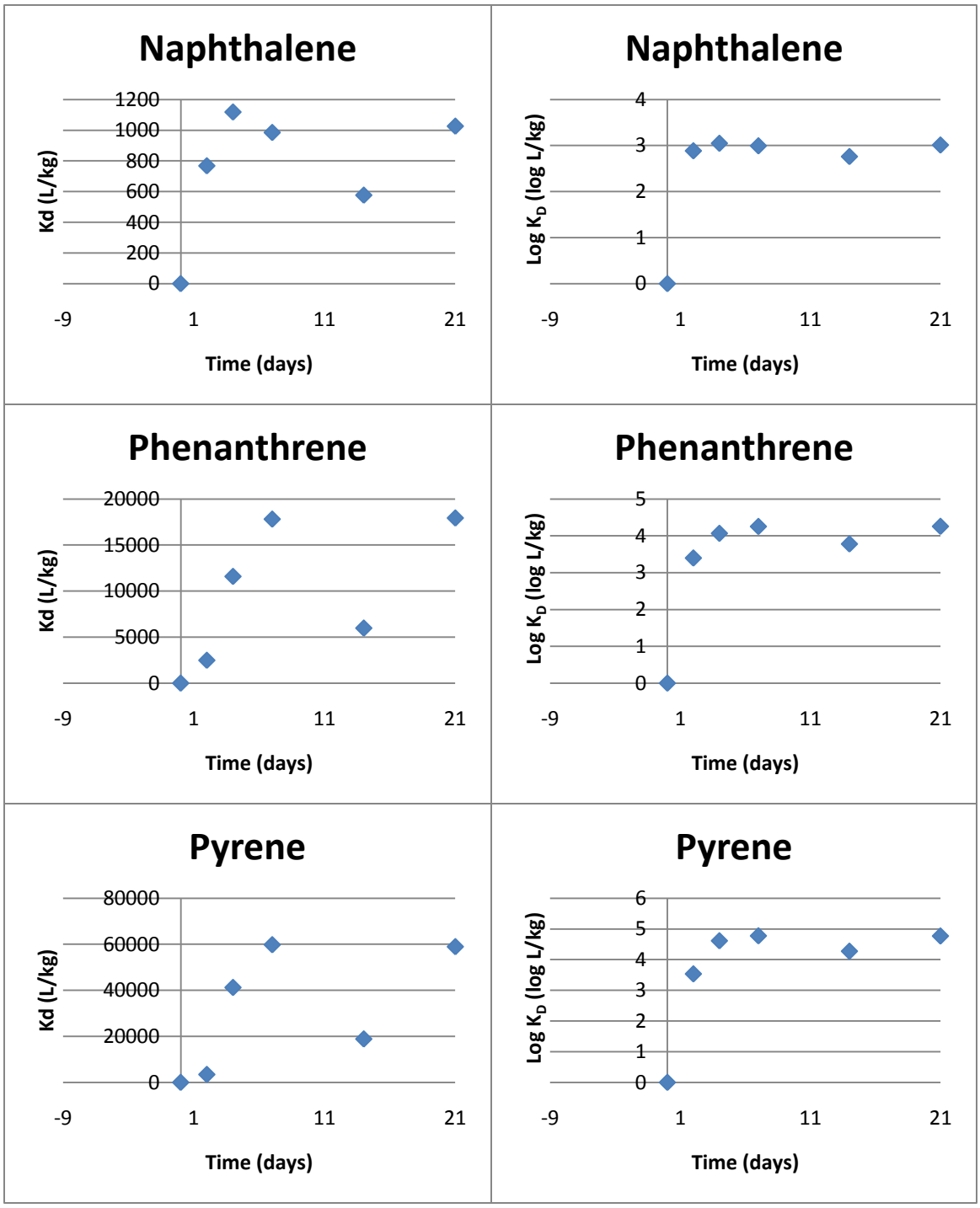

Figure 4.10: Kinetics of Sorption Onto Tomato Peel Cutin

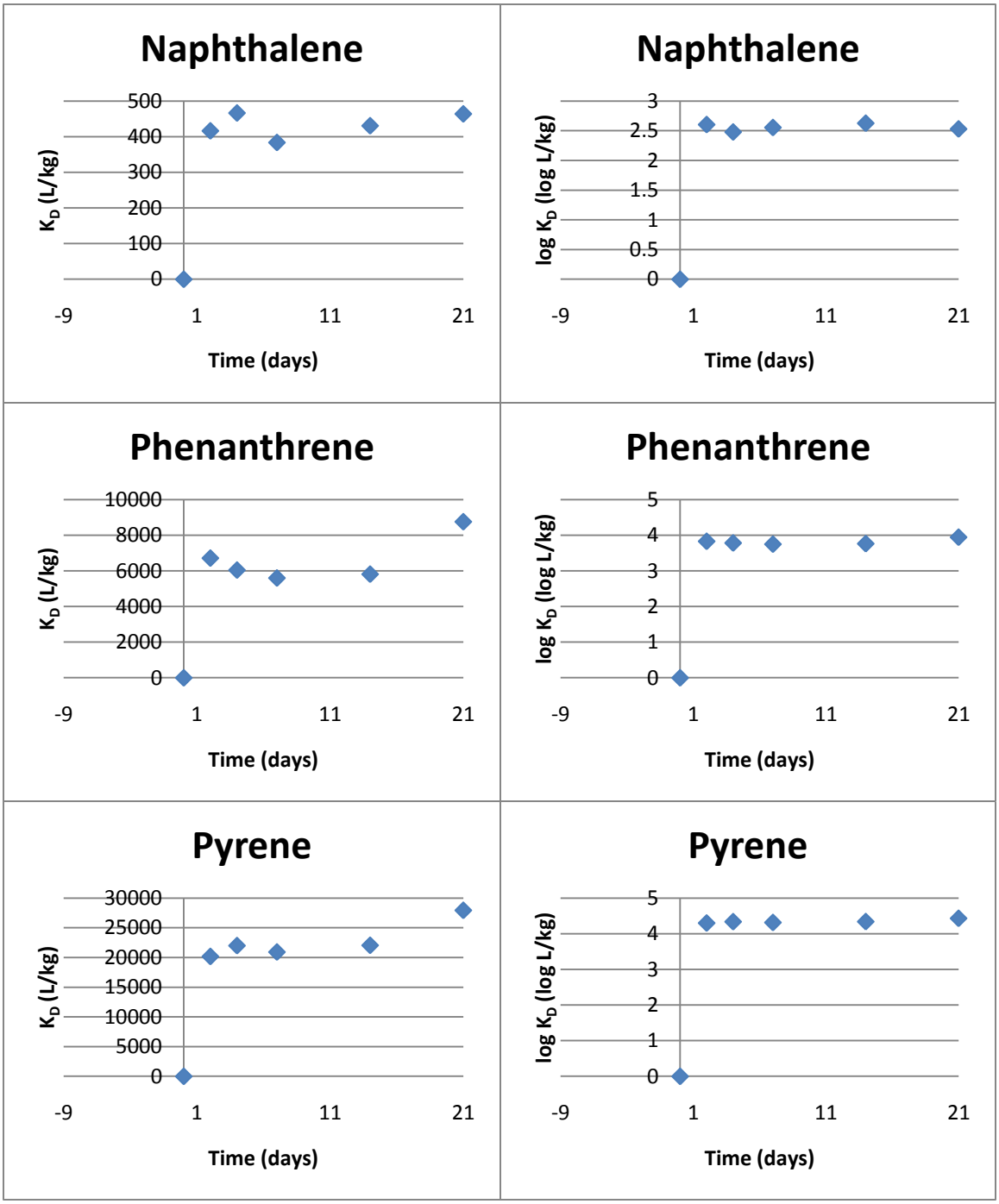

Figure 4.11: Kinetics of Sorption Onto Cellulolytic Enzyme Lignin

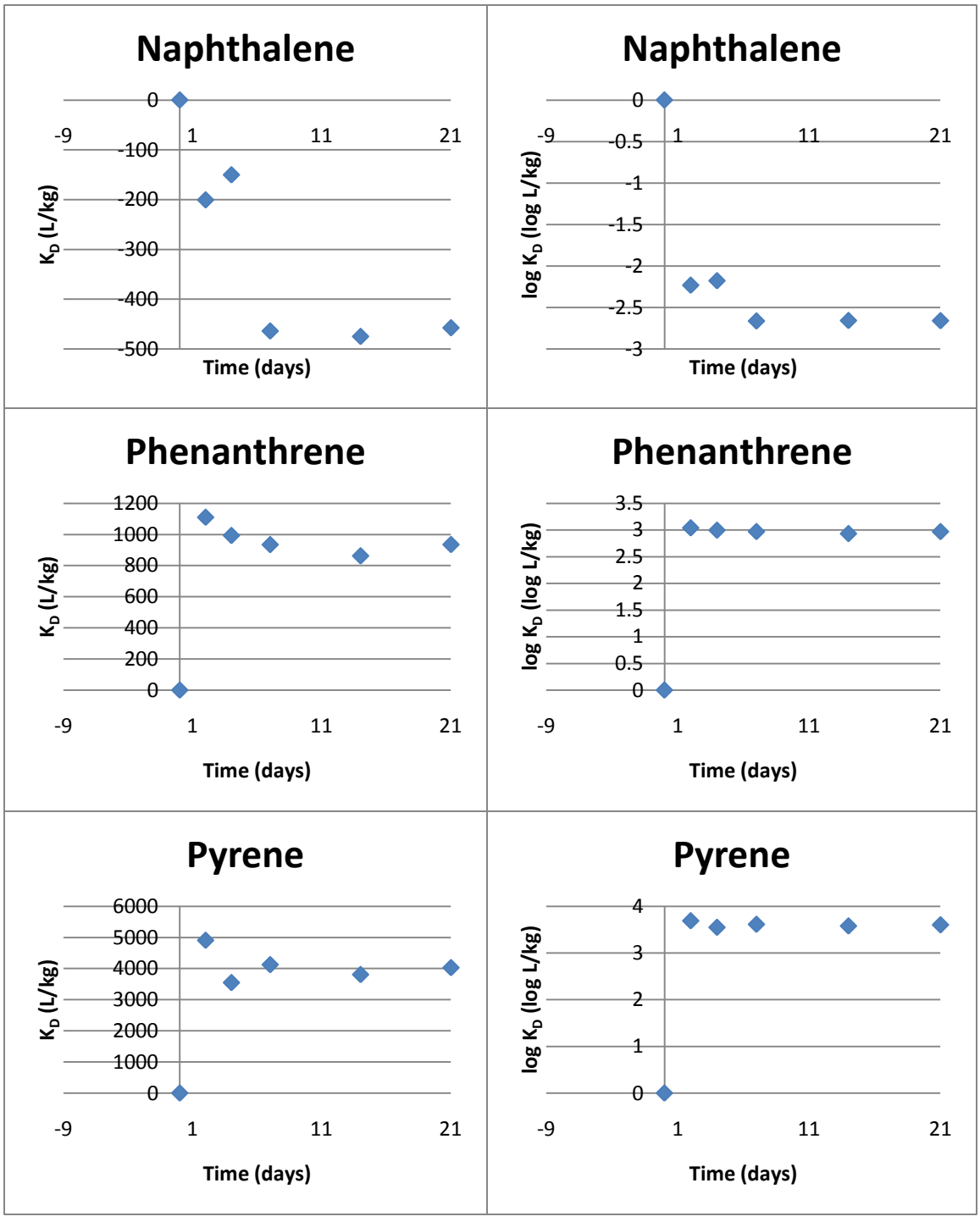

Figure 4.12: Kinetics of Sorption Onto Keratin Azure

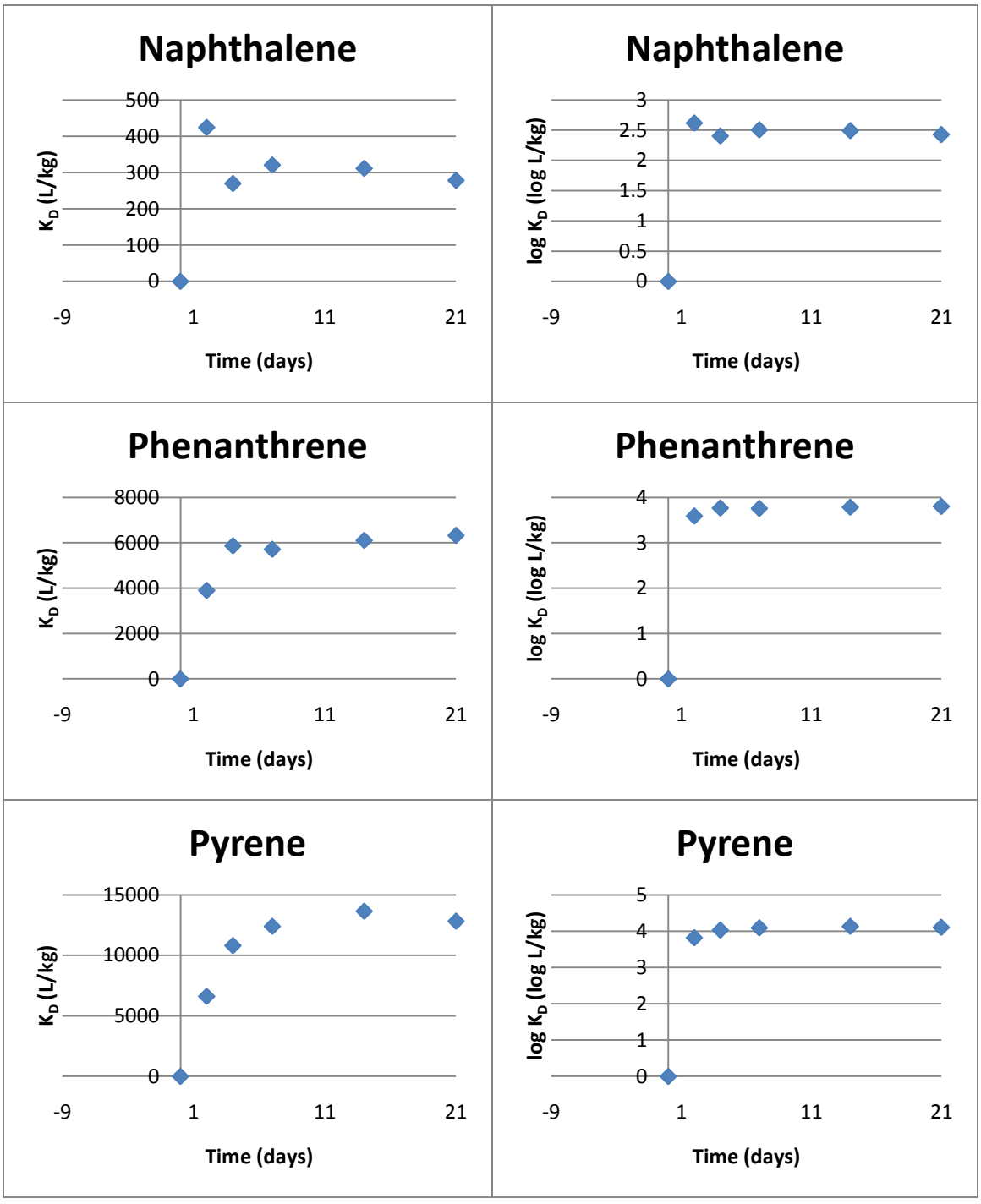

Figure 4.13: Kinetics of Sorption Onto 0% Coated Sand Product

Noticeably, a significant peak in the overall magnitude of the equilibrium partitioning coefficient, K_D, occurred for each of the HOCs onto keratin azure. In addition, occurrence of a peak was noticed for naphthalene only onto zero percent coated sand product. The cause of the peaks is unknown with the amount of available data. The overall magnitude of peak intensity for Naphthalene sorption onto both materials is roughly constant with respect to the ratio of the peak height to equilibrium values of K_D. Peaks in phenanthrene and pyrene sorption disappeared upon removal of a large fraction of the α-keratin fraction.

The peaks were not noticed in the sorption of HOCs onto cellulolytic enzyme lignin, although there did seem to be a larger degree of unsteadiness in the rate of sorption. The sudden and isolated decrease in K_D on day 14 for HOC sorption onto tomato peel cutin was attributed to an inconsistency in experimental methods isolated to that particular batch and not an actual decrease in sorption capacity. In addition to the peak effects and the irregularity in the cutin data, perhaps the most interesting result of the kinetics tests is the negative equilibrium partitioning coefficient for naphthalene sorption onto keratin azure (unpurified). Accompanying the net increase of naphthalene in sample bottles was also an increase in the signal peaks of compounds (presumably polyaromatic hydrocarbons) with molecular weights between naphthalene and phenanthrene, although those data are not shown in this document. Neither the naphthalene peak nor the peaks of the higher molecular weight unidentified compounds were noticed in the blanks, suggesting naphthalene and other non-specific aromatic

compounds were being released from the unpurified keratin azure. Such results confirm that the release of non-covalently linked anthraquinone dye molecules, which degrade into polyaromatic byproducts in the presence of ultraviolet light, may be significant, as previously discussed.

Figure 4.14, Figure 4.15, Figure 4.16, Figure 4.17, Figure 4.18, Figure 4.19, and Figure 4.20 illustrate batch equilibrium test results for the sorption of naphthalene, phenanthrene, and pyrene onto tomato peel cutin, cellulolytic enzyme lignin, keratin azure, purified keratin azure, and coated sand products, respectively. Table 4.12 and Table 4.13 present linear and Freundlich model parameters calculated for such results, respectively, along with their fraction of organic carbon- and octanol-water partitioning coefficient (K_{OW}, liters per kilogram)-normalized values. It should be noted that the R^2 in Table 4.12 and 4.13 represents the correlation coefficient of each respective set of batches and should not be confused with the variable R. Also, the values presented in Table 4.12 and 4.13 use physical parameters from (*187-190*) and are calculated as defined by Equations 3.11, 3.12, 3.23, and 3.25. K_{OC} values for coated sand products were assumed approximately equal to the fraction of organic carbon in the zero percent coated sand product multiplied by the mass fraction of prepared hydrophobic biopolymer in the coated sand product. This would assume that the mass of organic carbon in the carbonate sand (~0.1%) is negligible in relation to the mass of organic carbon in the prepared hydrophobic biopolymer.

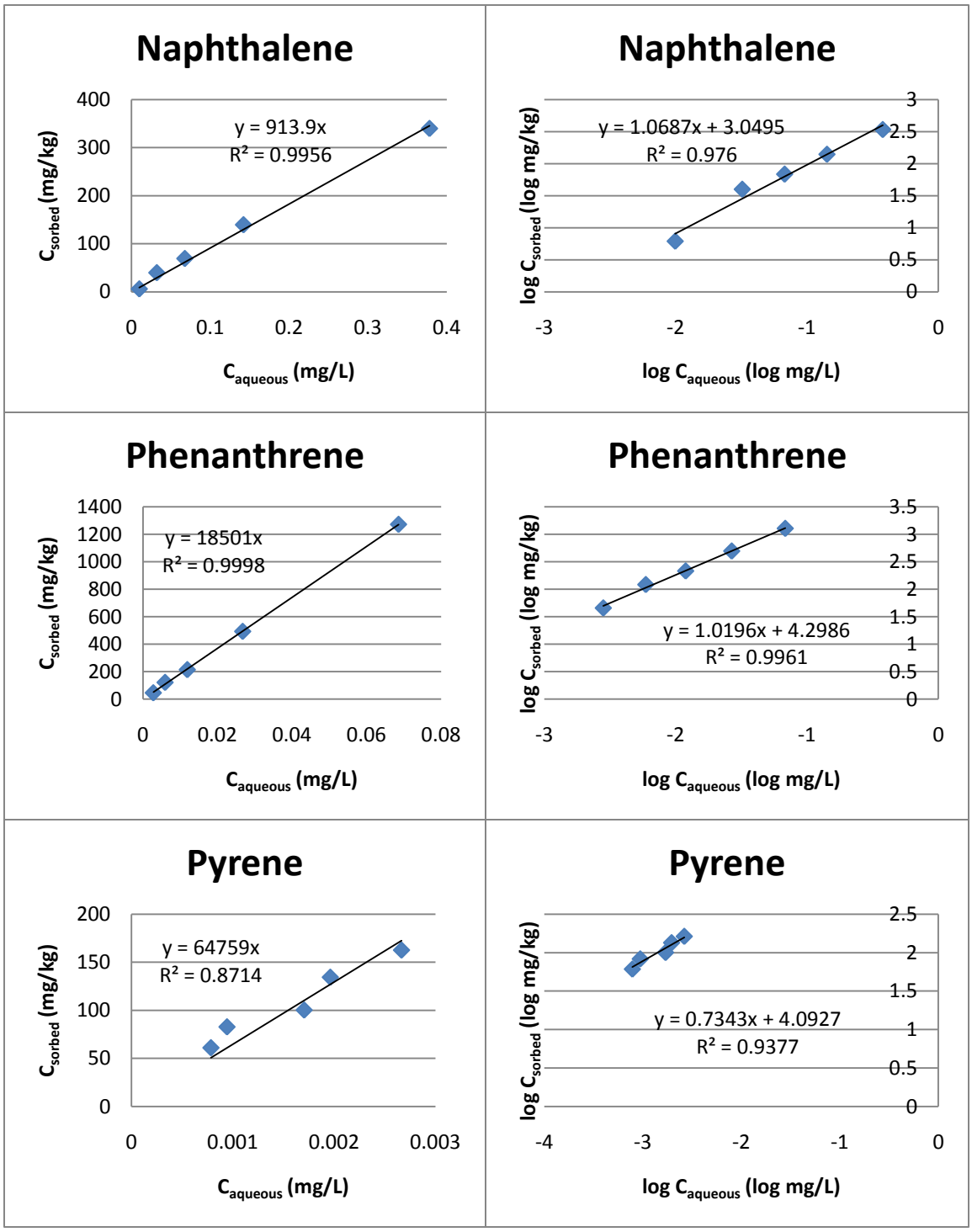

Figure 4.14: Equilibrium Sorption Onto Tomato Peel Cutin

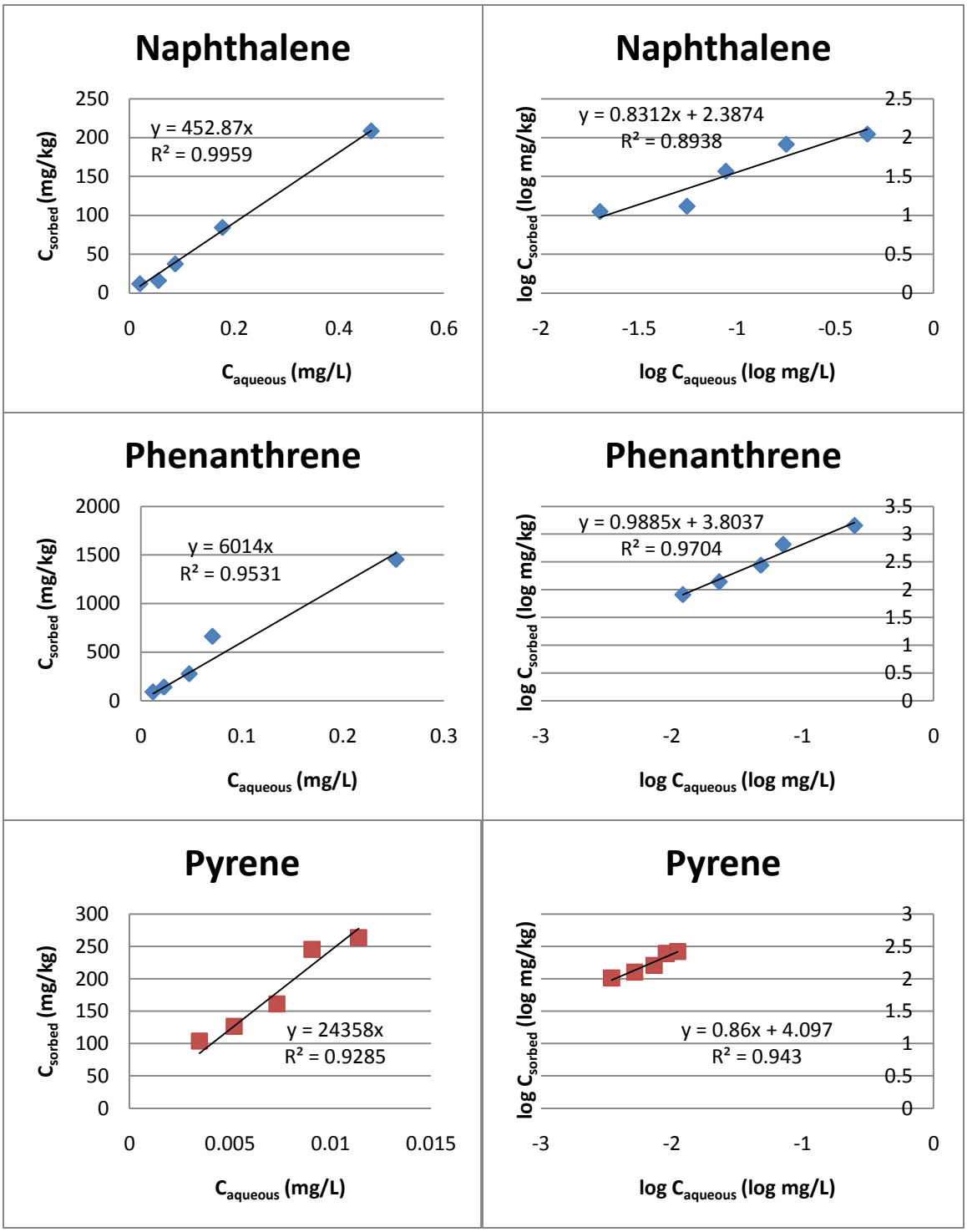

Figure 4.15: Equilibrium Sorption Onto Cellulolytic Enzyme Lignin

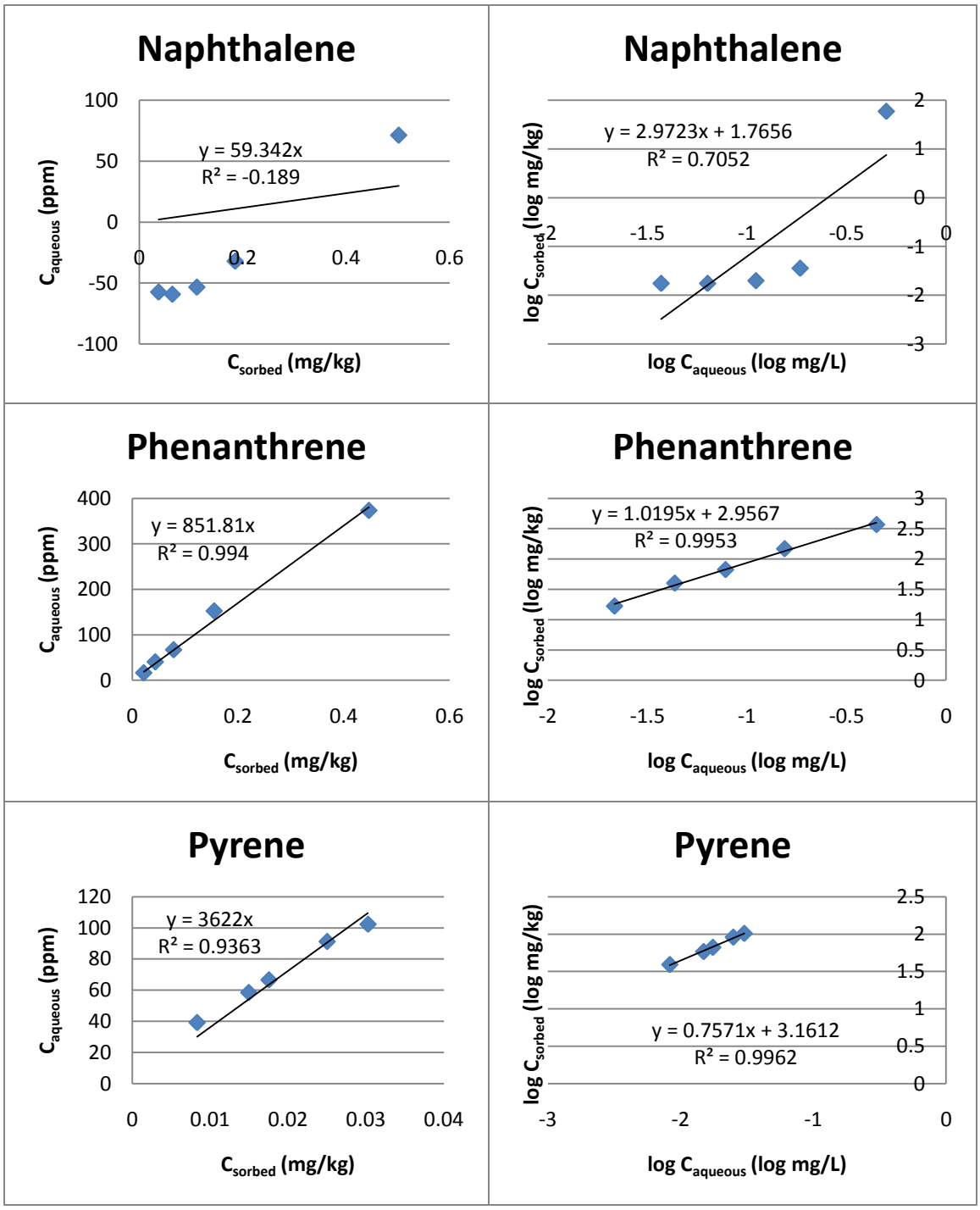

Figure 4.16: Equilibrium Sorption Onto Keratin Azure

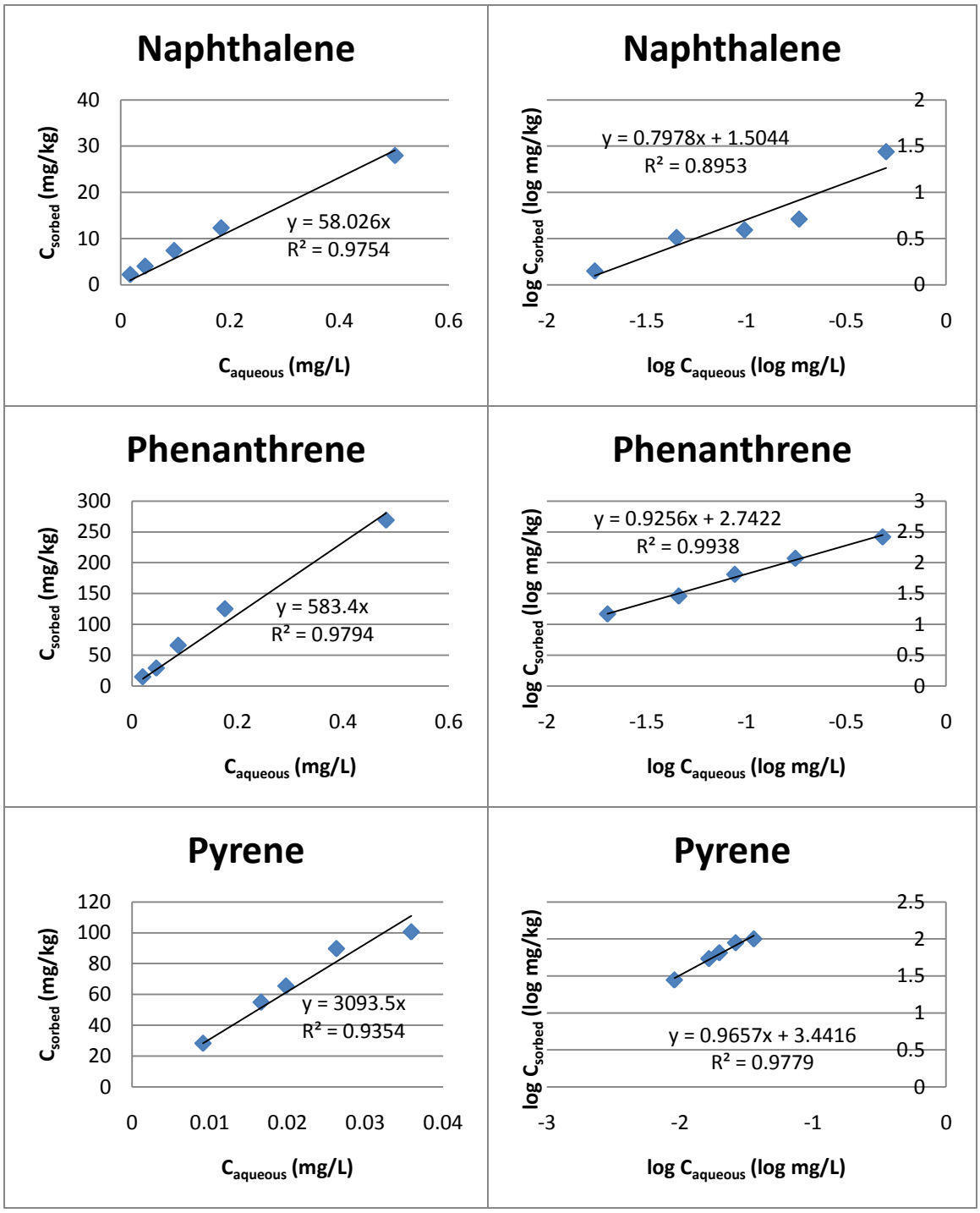

Figure 4.17: Equilibrium Sorption Onto Purified Keratin Azure

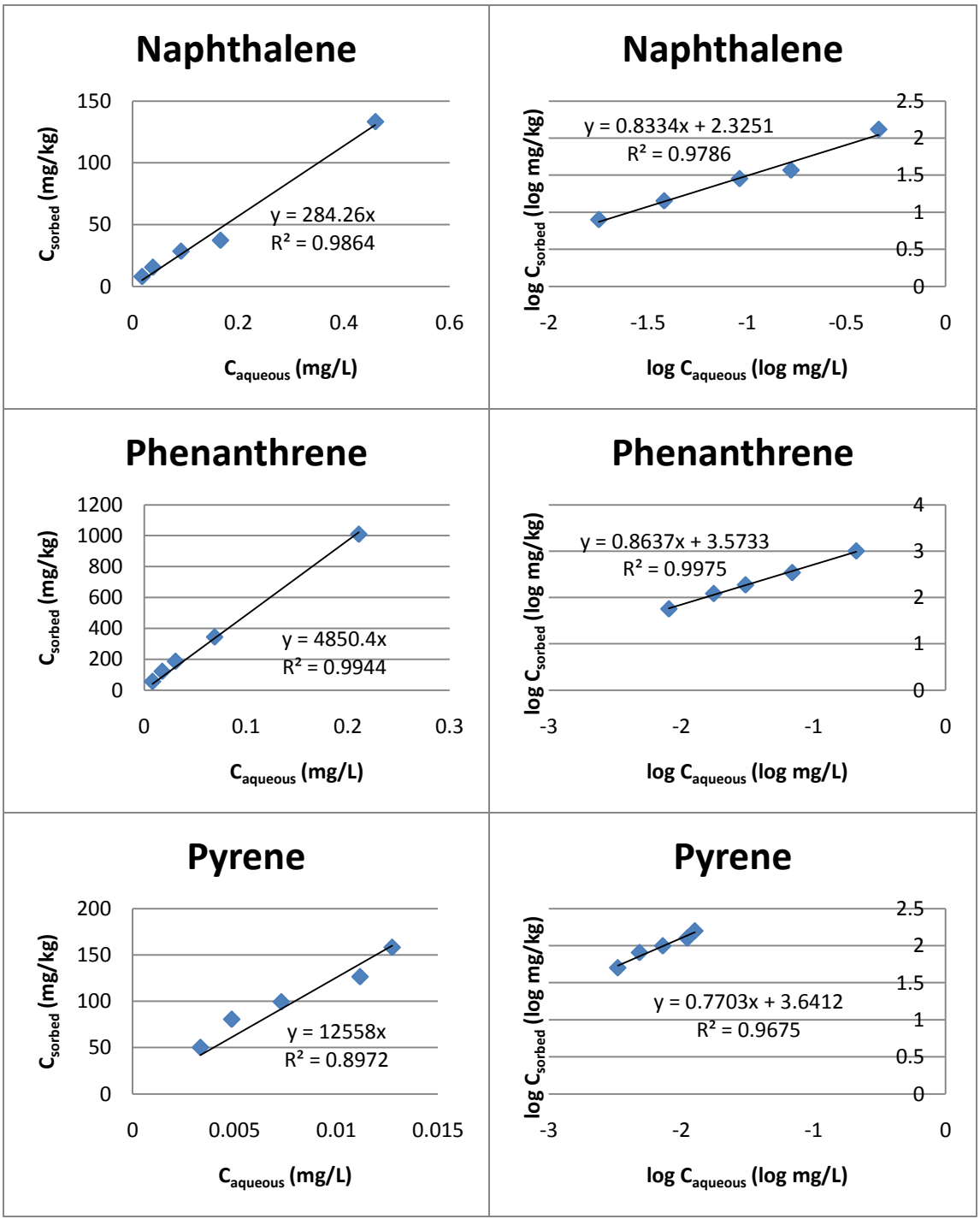

Figure 4.18: Equilibrium Sorption Onto 0% Coated Sand Product

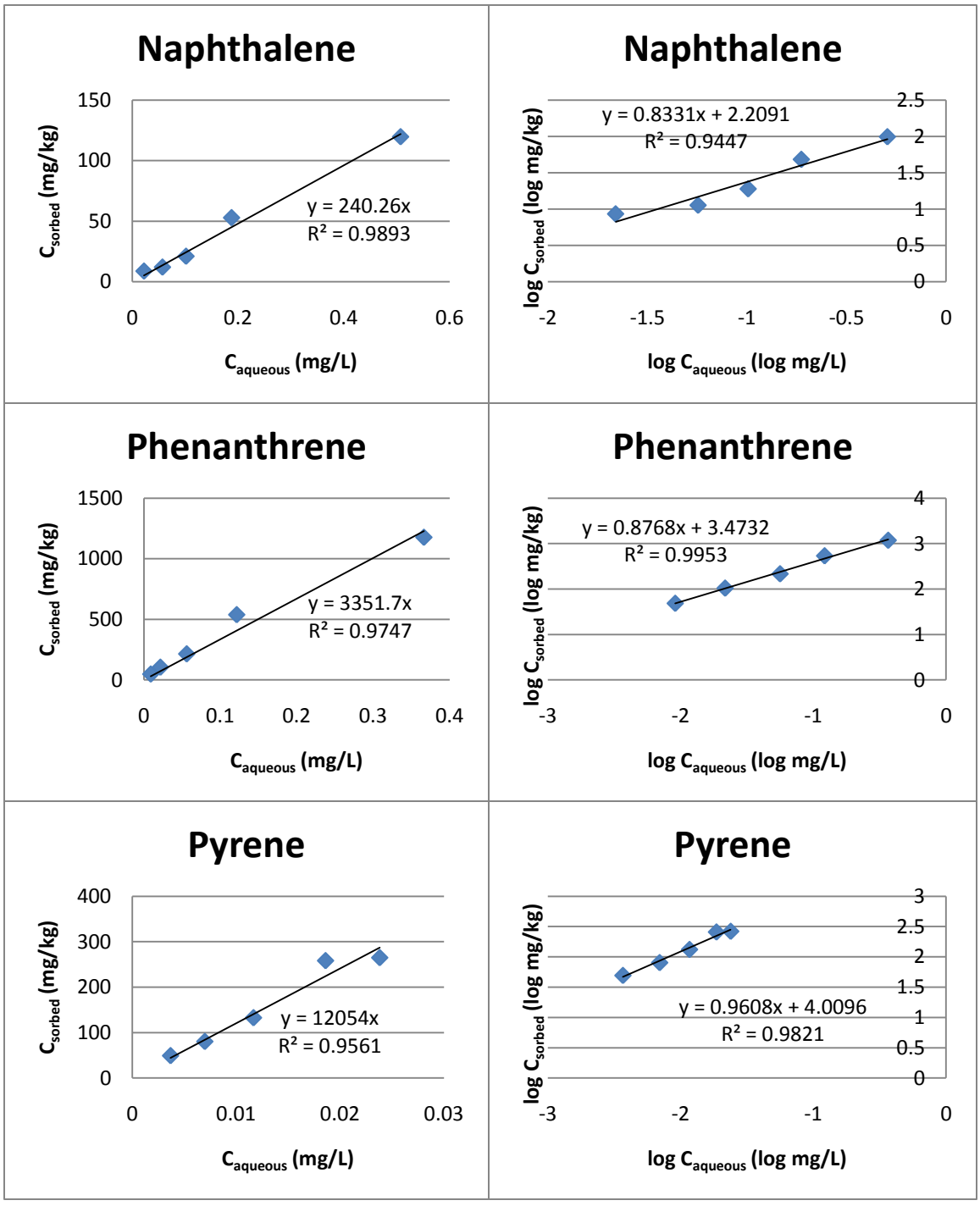

Figure 4.19: Equilibrium Sorption Onto 15.4% Coated Sand Product

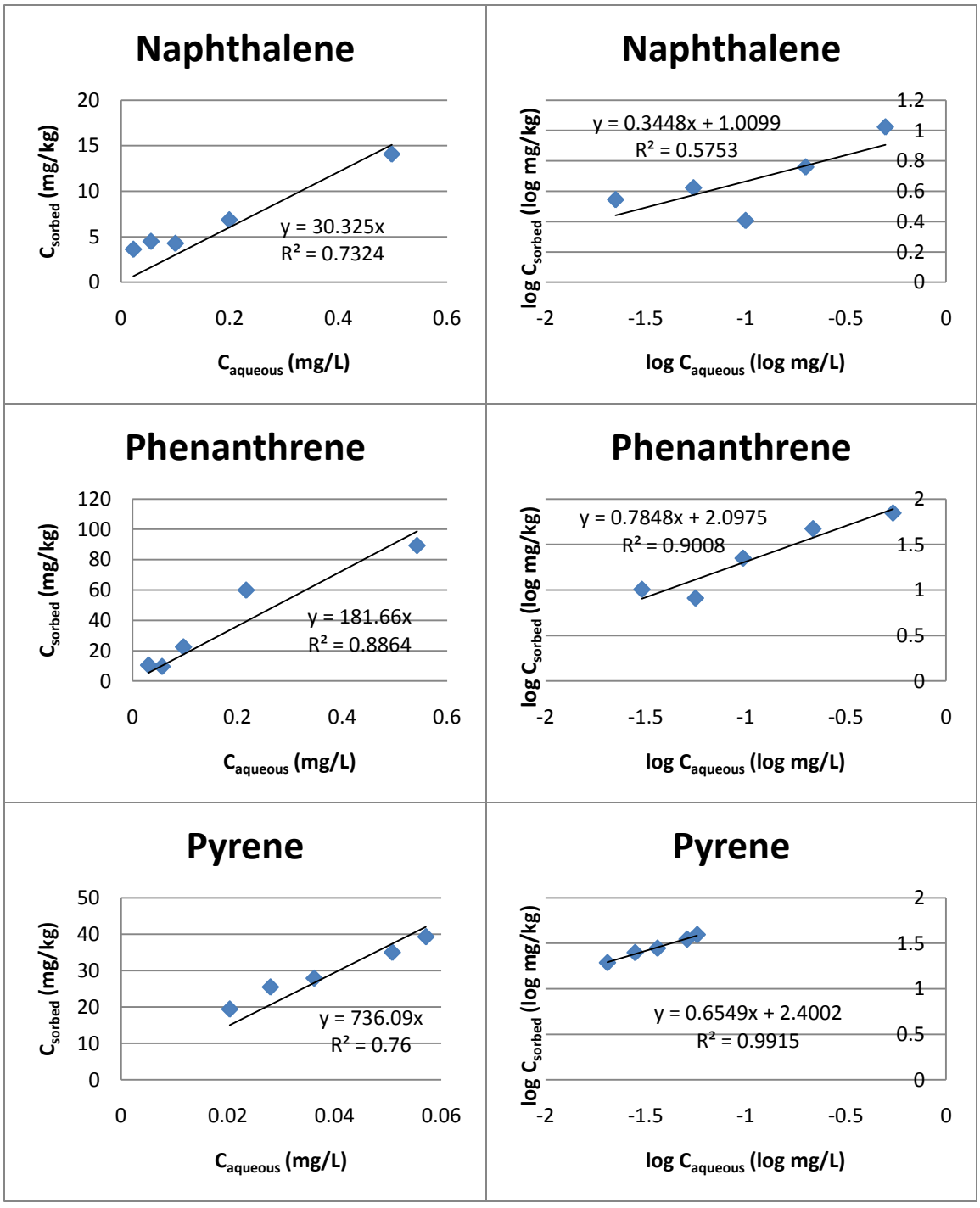

Figure 4.20: Equilibrium Sorption Onto 87% Coated Sand Product

Table 4.12: Linear Model Parameters

Compound of Interest	Hydrophobic Biopolymer or Hydrophobic Biopolymer-Coated Sand Product	K_D (liters per kilogram)	K_{OC} (liters per kilogram)	Linear R^2	$\frac{K_{OC}}{K_{OW}}$
Naphthalene	Tomato Peel Cutin	913.9	1317	0.995	0.775
	Cellulolytic Enzyme Lignin	452.8	728.0	0.995	0.429
	Keratin Azure	N/A	N/A	N/A	N/A
	Purified Keratin Azure	58.02	117.2	0.975	0.069
	0% Coated Sand Product	284.2	574.1	0.986	0.338
	15.4% Coated Sand Product	240.2	573.6	0.989	0.338
	87% Coated Sand Product	30.32	471.2	0.732	0.277
Phenanthrene	Tomato Peel Cutin	18500	26660	0.999	0.924
	Cellulolytic Enzyme Lignin	6014	9669	0.953	0.335
	Keratin Azure	851.8	1721	0.994	0.060
	Purified Keratin Azure	583.4	1179	0.979	0.041
	0% Coated Sand Product	4850	9798	0.994	0.340
	15.4% Coated Sand Product	3351	8002	0.974	0.277
	87% Coated Sand Product	181.6	2822	0.886	0.098
Pyrene	Tomato Peel Cutin	64760	93313	0.871	0.447
	Cellulolytic Enzyme Lignin	24360	39160	0.928	0.187
	Keratin Azure	3622	7317	0.936	0.035
	Purified Keratin Azure	3093	6249	0.935	0.030
	0% Coated Sand Product	12560	25370	0.897	0.121
	15.4% Coated Sand Product	12050	28780	0.956	0.138
	87% Coated Sand Product	736.0	11440	0.760	0.055

With comparison to K_{OC} values of sorption to natural organic matter found in (*187-190*), only cutin is more efficient than natural organic matter at sorbing all three PAHs (1.4-2.5 times greater K_{OC} values). Such strong affinity for HOCs is sharply contrasted to that of keratinous and cellulolytic enzyme lignin materials, which are much

Table 4.13: Freundlich Model Parameters

Compound of Interest	Hydrophobic Biopolymer or Hydrophobic Biopolymer-Coated Sand Product	log K_f (log milligrams$^{(1-n)}$ per kilogram-liter^{-n})	n (-)	Freundlich R^2
Naphthalene	Tomato Peel Cutin	3.049	1.068	0.976
	Cellulolytic Enzyme Lignin	2.387	0.831	0.893
	Keratin Azure	N/A	N/A	N/A
	Purified Keratin Azure	1.504	0.797	0.895
	0% Coated Sand Product	2.325	0.833	0.978
	15.4% Coated Sand Product	2.209	0.833	0.944
	87% Coated Sand Product	1.009	0.344	0.575
Phenanthrene	Tomato Peel Cutin	4.298	1.019	0.996
	Cellulolytic Enzyme Lignin	3.803	0.988	0.970
	Keratin Azure	2.956	1.019	0.995
	Purified Keratin Azure	2.742	0.925	0.993
	0% Coated Sand Product	3.573	0.863	0.997
	15.4% Coated Sand Product	3.473	0.876	0.995
	87% Coated Sand Product	2.097	0.784	0.900
Pyrene	Tomato Peel Cutin	4.092	0.734	0.937
	Cellulolytic Enzyme Lignin	4.097	0.860	0.943
	Keratin Azure	3.161	0.757	0.996
	Purified Keratin Azure	3.441	0.965	0.977
	0% Coated Sand Product	3.641	0.770	0.967
	15.4% Coated Sand Product	4.009	0.960	0.982
	87% Coated Sand Product	2.400	0.654	0.991

less efficient than natural organic matter. Cutin also shows no correlation of K_{OW}-normalized K_{OC} to hydrophobicity of sorbate, suggesting no influence of steric hindrance on sorption. Cellulolytic enzyme lignin, on the other hand, as well as each of the keratinous materials, shows a general trend of decreasing K_{OW}-normalized K_{OC} values with increasing hydrophobicity of the sorbate. Also in general, this trend is more pronounced with materials that do not contain sand. This trend suggests that more

hydrophobic compounds are possibly more sterically-hindered and will occupy less sorption sites than less sterically-hindered compounds of less hydrophobicity. The steric hindrance in the cellulolytic enzyme lignin was expected, due to the condensed, polyaromatic domains which presumably have a large occurrence of hole-filling sorption sites.

In general, the overall K_Ds for PAH sorption onto tomato peel cutin obtained for use in the present study were lower than those for PAH sorption onto highly purified cutin fraction obtained by (*28*) and higher than those for PAH sorption onto less purified cutin fractions obtained by (*18, 22, 29*). Naphthalene and phenanthrene both exhibited C-type (linear) sorption behavior onto the tomato peel cutin, which emphasizes that the dominant mechanism of sorption for these compounds is partitioning into rubbery aliphatic domains. Pyrene exhibited very strong specific interaction with the tomato peel cutin, as indicated by the relatively small Freundlich n value. This is most likely due to specific Van der Waals interactions on the undifferentiated surface (*18*). It is unlikely that the specific site binding is due to the alkyl-O moieties, as these are largely inaccessible to PAHs (*28*). Also, PAHs have no active hydrogen for hydrogen bonding. The aromatic content of the tomato peel cutin was below detection limits, and so π-π interactions are also not probable. K_{OC}/K_{OW} ratios were as expected for sorption of PAHs onto tomato peel cutin. Overall, sorption capacity of tomato peel cutin is roughly the same magnitude of typical organoclays with respect to PAHs, suggesting their strong potential for use as active capping amendments.

Sorption of PAHs onto cellulolytic enzyme lignin exhibited slight non-linearity in terms of Freundlich n values, although a high linear correlation was also observed. This may suggest specific sorption to condensed, poly-aromatic domains. However, statistical analysis is needed for validation of non-linearity. The mechanisms for specific sorption would likely be hole-filling and π-π interactions. K_{OC} values and the degree of non-linearity (Freundlich n) were very similar to those found by (*15*) for sorption of naphthalene, phenanthrene, and pyrene onto organosolv lignin. Sorption of PAHs onto keratinous materials was also non-linear in terms of Freundlich n values, while, once again, a high linear correlation was observed. The Freundlich n values have no obvious correlation between the alpha-keratin content or mass fraction of sand on the degree of nonlinearity (Freundlich n). In general, both K_{OC} and K_{OW}-normalized K_{OC} values decreased with increasing sand content, suggesting carbonate sand may reduce the availability of sorption sites to PAHs, with higher sorbates of higher hydrophobicity being affected the most as discussed previously. Sorption capacity increased with removal of a fraction of the α-keratin in the coated sand products, as expected. This increase may be due to the overall change in polarity of the coated sand products compared to the purified keratin azure. Interestingly enough, K_{OC} for sorption of PAHs onto keratin azure was higher than that for purified keratin azure, indicating that the dye molecules present afforded some affinity for hydrophobic solutes when reacted with wool. This is likely attributed to π-π bonding of the PAHs to the anthraquinone domains of the dye. Another possible explanation of the effects of dye molecules on sorption is

dispersive forces from the dye molecules. Once again, however, more data would need to be collected to confirm this. When non-covalently-linked, dye molecules may "gather" polar groups into charged "islands," opening accessibility of the hydrophobic regions to PAHs. When dye molecules are not present, the charges "spread out," blocking a larger area of hydrophobic regions to PAHs. At the very least, polarity may not play as large of factor in controlling PAH sorption onto dyed, α-dominant keratins as previously thought. Leaching of dye molecules was not significant at high concentrations for PAH sorption onto keratin azure. Extraction of the non-covalently linked dye molecules significantly reduced the leaching of dye molecules, and subsequently the production of naphthalene in the water phase, to the point of no observed effects.

Table 4.14 presents sorption results as shown above for hydrophobic biopolymer-coated sand products when normalized to the fraction of keratinous materials by mass. As may be inferred from Table 4.14, sorption capacity per unit mass of keratinous material roughly decreases with increasing sand content overall, further supporting the hypothesis that carbonate sand limits PAH accessibility to the sorption sites within keratin.

PAH sorption onto other amendments was mostly linear. Figure 4.21 presents equilibrium partition coefficients for PAH sorption onto a material containing 75 percent (w/w) apatite (North Carolina) and 25 percent (w/w) organoclay (PM-199, CETCO), as well as for a material containing 75 percent (w/w) apatite, 20 percent (w/w) organoclay, 2.5 percent (w/w) guar gum (Coyote Brand, Gum Technologies), and 2.5 percent (w/w)

Table 4.14: Keratin-Normalized Sorption Parameters

Compound of Interest	Hydrophobic Biopolymer or Hydrophobic Biopolymer-Coated Sand Product	Fraction Keratinous Materials, f_{ker}	$\frac{K_D}{f_{ker}}$ (liters per kilogram)	$\frac{K_F}{f_{ker}}$ (milligrams$^{(1-n)}$ per kilogram-liter^{-n})
Naphthalene	0% Coated Sand Product	1.00	284.20	211.35
	15.4% Coated Sand Product	0.85	282.59	190.36
	87% Coated Sand Product	0.13	233.23	78.53
Phenanthrene	0% Coated Sand Product	1.00	4850.00	3741.11
	15.4% Coated Sand Product	0.85	3942.35	3496.08
	87% Coated Sand Product	0.13	1396.92	961.74
Pyrene	0% Coated Sand Product	1.00	12558.00	4375.22
	15.4% Coated Sand Product	0.85	14181.18	12011.05
	87% Coated Sand Product	0.13	5661.54	1932.22

xanthan gum (CP Kelco). For the mixture without hydrophilic biopolymers, the resulting K_D values are less than what one would expect if 100 percent organoclay were used. However, the resulting K_D values are greater than what one would expect if 25 percent organoclay were used (0.25*100 percent organoclay sorption). For the mixture including hydrophilic biopolymers, the resulting K_D values are slightly lower than the K_D values for the mixture without, which was expected due to the hydrophilic nature of the biopolymers used. Such results emphasize the ineffectiveness of using hydrophilic biopolymers for HOC sorption.

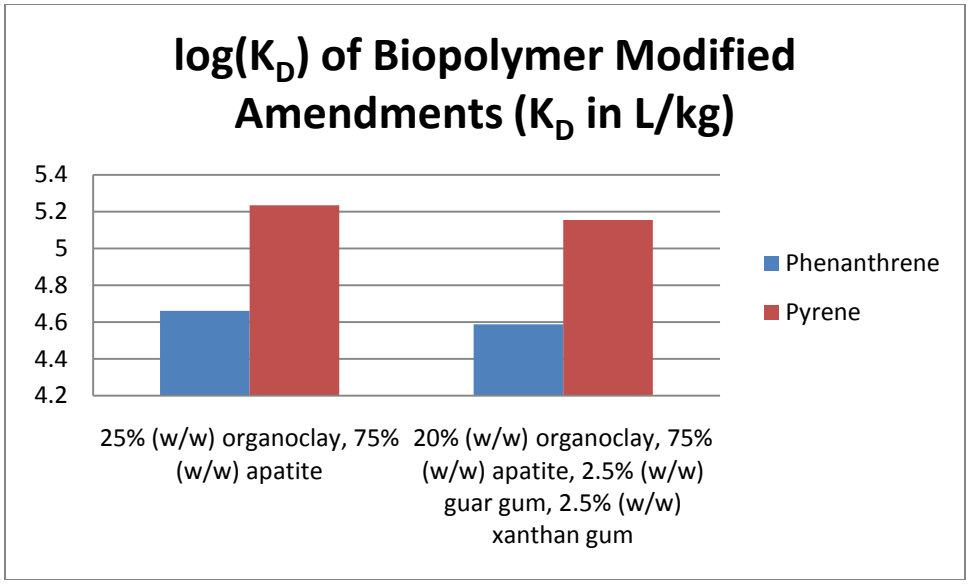

Figure 4.21: Other Amendments

Table 4.15 presents additional equilibrium partition coefficients for PAH sorption onto materials having the following compositions:

- 25 percent (w/w) organoclay (CETCO PM-199), 25 percent (w/w) zeolite (Clinoptilotilte), 25 percent (w/w) apatite (North Carolina), and 25 percent (w/w) acid-washed sand (Alfa Aesar, 100-350 mesh)
- 25 percent (w/w) organoclay, 50 percent (w/w) zeolite, and 25 percent (w/w) acid-washed sand
- 25 percent (w/w) organoclay, and 75 percent (w/w) zeolite
- 50 percent (w/w) organoclay and 50 percent (w/w) zeolite

Table 4.15: Other Amendments

Mixture	log K_D (log liters per kilogram)		
	Naphthalene	Phenanthrene	Pyrene
25% (w/w) organoclay, 25% (w/w) zeolite, 25% (w/w) apatite, 25% (w/w) sand	3.007705114	4.688864568	5.3083
25% (w/w) organoclay, 50% (w/w) zeolite, 25% (w/w) sand	2.984680302	4.671487569	5.2957
25% (w/w) organoclay, 75% (w/w) zeolite	3.004665233	4.680226699	5.3021
50% (w/w) organoclay, 50% (w/w) zeolite	3.372985606	4.97170251	5.4796

For Mixture No. 2, K_D values decrease with a decrease in apatite content and increase in zeolite content. Mixture No. three K_D values increase slightly from mixture No. 2 K_D values, which follows from the increase in zeolite content and decrease in acid-washed sand content. K_D values were highest in mixture No. 4, which had the highest mass fraction of organoclay. Magnitudes of K_D values were relatively close together for mixtures one through three, which was expected due to the constant organoclay mass fraction. Comparatively, tomato peel cutin would be competitive with respect to sorption capacity.

4.5 FEASIBILITY ANALYSIS OF HYDROPHOBIC BIOPOLYMERS AND HYDROPHOBIC BIOPOLYMER-COATED SAND PRODUCTS

Results of the feasibility analysis performed on the hydrophobic biopolymers following their preparation indicated that keratin azure would necessarily be the most likely to succeed at providing low-cost coatings on sand particles due to its zero chemical mass requirement for preparation. A qualitative argument was employed to validate such results due to several complications which did not allow use of the decision matrix method described previously in Chapter 3.

Such an argument begins with the highly variable, extremely complex, and sparsely understood chemistry of lignin-carbohydrate solids, as well as the lack of sufficiently quantitative studies on reactions involving lignin-carbohydrate matrices. In other words, the mass of cellulolytic enzyme required for the preparation of a given mass of cellulolytic enzyme lignin cannot be stoichiometrically predicted and generally must be grossly over-estimated. In addition, a very large mass of cellulolytic enzymes are required to yield only a very small amount of cellulolytic enzyme lignin. Coupled with the lack of a high sorption capacity to compensate and a very high cost per kilogram for cellulolytic enzymes ($150 per kilogram in USD, Yakult Pharmaceutical, Japan, March 2010), cellulolytic enzyme lignin was accordingly ruled out as a possible candidate for coating sand particles when cellulolytic enzymes are necessarily used.

Purified keratin azure, having a very similar sorption capacity and identical exhaustible reagent cost as keratin azure, is much less toxic than keratin azure. Therefore, keratin azure was also ruled out as a potential candidate for coating sand particles.

Analysis of the feasibility of prepared hydrophobic biopolymers was thus reduced to concerning only tomato peel cutin and purified keratin azure. Assuming that all methanol, trichloromethane, uncovalently-linked dye molecules, and/or any other highly toxic chemical residuals are significantly removed during purification of tomato peel cutin and purified keratin azure (drying at elevated temperature, washing, etc), each should have comparable RV_3 values. In the case where weighting factors are constant for all prepared hydrophobic biopolymers and the smallest in magnitude for the environmental stability and toxicity term, the feasibility factor for tomato peel cutin and purified keratin azure is most markedly varied by the sorption and chemical cost factors.

Equation 3.15 assumes the cost of reagent required to prepare a given mass of hydrophobic biopolymer is nonzero and greater than the cost per mass of bulk carbonate sand. Both assumptions are not valid for the case of purified keratin azure in bulk form. RV_2 for keratin azure would be undefined. However, even in the case where the chemical cost per mass of purified keratin azure was as high as bulk carbonate sand, the sorption capacity of tomato peel cutin would have to be greater than that of activated carbon in order to overcome the small cost of purified keratin azure in the case where RV_1 and RV_2 are equally weighted in the determination of the feasibility factor for each hydrophobic biopolymer. Such a sorption capacity was not achieved by the tomato peel cutin, and thus keratin azure was chosen for continued study.

Although purified keratin azure is technically most feasible, consideration of tomato peel cutin as a potential hydrophobic biopolymer for the coating of sand grains is not unjustified given the aforementioned difficulties. Tomato peel cutin has a very low melting point and, as mentioned previously, has naturally cross-linking abilities, requiring no reagents past its initial preparation. Keratin azure, by contrast, requires significant reagent material following preparation in order for it to be suitable for coating sand grains. Thus, while purified keratin azure may be most feasible when only the cost of reagent required to prepare the hydrophobic biopolymer is considered, tomato peel cutin may be the most feasible when both the cost of reagent required to prepare the hydrophobic biopolymer and the cost of reagent to render the hydrophobic biopolymer suitable for coating sand particles is considered.

Following the preparation of coated sand products using the purified keratin azure, a decision matrix was populated in order to determine relative industry feasibilities of the same as shown in Table 4.16. An analysis of the results is given following the rationale for decision matrix formulation. Table 4.17 presents assumed values used in the feasibility analysis of hydrophobic biopolymer-coated sand products which were considered constant, including $\rho_{b,d,sand}$, UC_{sand}, UC_j, $\log(K_{D,AC})$, w_1, w_2, and w_3. For the purposes of the present study, UC_j was assumed to be roughly constant in order of magnitude although it is technically variable depending on the reagent, and was subsequently factored out of the denominator in Equation 3.15, making RV_2 dependent upon one less variable. This was due to the lack of freely available data on bulk chemical

or enzyme prices for every reagent used in the present study. Accordingly, Table 4.18 lists the bulk prices for five "indicative" chemicals for the year 2006 (*176*).

Table 4.16: Feasibility Analysis

Hydrophobic Biopolymer	Weighted and Normalized Sorption Capacity, w_1RV_1 (-)	Weighted and Normalized Reagent Cost, w_2RV_2 (-)	Weighted Environmental Stability and Toxicity Factor, w_3RV_3 (-)	Feasibility Factor, F (-)
0% Coated Sand Product	0.24	71.74	0.1	72.08
15.4% Coated Sand Product	0.23	131.52	0.08	131.83
87% Coated Sand Product	0.15	265.07	0.01	265.2

Table 4.17: Constant Feasibility Parameters

Parameter	Value	Unit
$\rho_{b,d,sand}$	1381	kilograms per cubic meter bulk carbonate sand
UC_{sand}	0.01	$ (USD) per kilogram carbonate sand
UC_j	1.00	$ (USD) per kilogram prepared hydrophobic biopolymer
$\log(K_{D,AC})$	6.15	log(liters per kilogram)
w_1	0.4	-
w_2	0.4	-
w_3	0.2	-

An average of the five chemicals was used as the 1996 cost (USD) of a general reagent j per kilogram of hydrophobic biopolymer required, UC_j. Following adjustment

Table 4.18: ICIS Pricing

Chemical	Approximate Cost, $ USD, per kilogram
Methanol	0.50
Glacial Acetic Acid	1.10
Ammonium Hydroxide	0.60
Caustic Potash	0.55
Chloroform	0.88
Average	0.73

for an approximate 37% increase in the consumer price index from the year 1996 to the year 2009 (*191*), the constant value for the year 2009 UC_j as used in the present study was estimated at $1.00 (USD) per kilogram. One hundred times the K_{OC} for sorption of phenanthrene onto natural organic matter was used as $K_{D,AC}$ in liters per milligram.

During the alkaline reduction of the keratin, ammonium hydroxide is used in order to raise the pH to just below approximately ten. Although the ammonium ion performs many additional functions in aqueous keratin suspensions, namely, the swelling of the keratin fibers (increases mass transfer), it is not exhaustible and was thus not included in the feasibility analysis of the coated sand products. Only one non-exhaustible reagent was used in order to estimate the relative cost of chemicals, which was ammonium thioglycolate. The number of kilograms of ammonium thioglycolate required to prepare a kilogram of hydrophobic biopolymer-coated sand, f_l, was estimated from stoichiometry.

The reduction of cystine in purified keratin azure is a two-step displacement reaction, first between a mercaptan ion, RS-, on a sulfur atom of a cystine group (i), and second between a mercapton ion on a sulfur atom of a mixed disulfide (ii), as shown in Reaction 4.1 (*192*). The overall reaction is shown in (iii).

(i) Ker-S-S-Ker + RS-H ↔ Ker-S-S-R + Ker-S-H

\+ (ii) Ker-S-S-R + RS-H ↔ R-S-S-R + Ker-S-H

(iii) Ker-S-S-Ker + 2RS-H ↔ 2Ker-S-H + R-S-S-R

Reaction 4.1: Two-Step Reduction of Disulfide Bonds in Purified Keratin Azure (*192*)

In Reaction 4.1, Ker-S-S-Ker represents keratin-cystine-keratin, RS-H represents mercaptan, Ker-S-S-R represents mixed disulfide, Ker-S-H represents keratin-cysteine, and R-S-S-R represents disulfide. In the case the mercaptan is ammonium thioglycolate, R equals $CH_2COO\text{-}\ NH_4^+$. As may be inferred from Reaction 4.1, two moles of ammonium thioglycolate react with one mole of keratin-cystine-keratin to produce two moles keratin-cysteine.

In contrast, the oxidation of cysteine by atmospheric oxygen to reform cystine groups may be described by Reaction 4.2, where Ker-S-S-Ker* represents the reformed keratin-cystine-keratin group. By analysis of Equation 4.1 and 4.2, it is obvious that two moles of Ker-S-H are required to produce one mole of Ker-S-S-Ker*. This corresponds to one mole of Ker-S-S-Ker to produce one mole of Ker-S-S-Ker* and two moles of RS-H

to produce one mole of Ker-S-S-Ker*. Assuming the molecular weight of Ker-S-S-Ker equals approximately the molecular weight of Ker-S-S-Ker *, and also that the chemical formula of Ker-S-S-Ker is $2SC_2H_3NH_2COOH$ (molecular weight equals 240.34 grams per mole), 0.91 kilograms of ammonium thioglycolate are then required per kilogram of cystine in the prepared hydrophobic biopolymer. Considering the mass fraction of cystine in wool keratin is approximately 0.15 (*159*), such a requirement reduces to 0.14 kilograms of ammonium thioglycolate per kilogram of prepared hydrophobic biopolymer. The number of kilograms of ammonium thioglycolate required per kilogram of hydrophobic biopolymer-coated sand product, f_1, may then be obtained by multiplying 0.14 by the number of kilograms of prepared hydrophobic biopolymer per kilogram hydrophobic biopolymer-coated sand product.

$$4\text{Ker-S-H} + O_2 \leftrightarrow 2\text{Ker-S-S-Ker*} + 2\text{H2O}$$

Reaction 4.2: Oxidation of Cysteine by Atmospheric Oxygen

Table: 4.19 presents non-constant parameters used to calculate RV_1, RV_2, and RV_3, including f_1, for each of the hydrophobic biopolymer-coated sand products. The calculation of RV_1 was performed with respect to the sorption of phenanthrene. In addition, the calculation of RV_3 assumed that, since each of the coated sand products were coated with the same hydrophobic biopolymer, the relative toxicity would be a function of the mass fraction of the prepared hydrophobic biopolymer in the hydrophobic biopolymer-coated sand product as shown by Equation 4.1. In Equation 4.1, TR equals

the dimensionless toxicity rating of the prepared hydrophobic biopolymer between zero and one, and f_{bio} equals the number of kilograms of prepared hydrophobic biopolymer per kilogram of coated sand product. For the purposes of this study, TR was assumed to be roughly equal to 0.5. Although boiling of the coated sand products should remove all residual solvents, there is not sufficient data to conclude that all were in fact removed from the products prepared in this study. Timmons et al (*151*) describes human medical implants comprised of keratinous materials derived by alkaline reduction using ammonium thioglycolate followed by oxidation in air and purification via boiling in water. Thus, one may assume that boiling is sufficient for removal of toxicity from the final product. However, numerous toxic gases are released in the preparation process, which is why a partial degree of toxicity is inherent in the calculations.

Table: 4.19: Non-Constant Feasibility Parameters

Parameter	$\rho_{b,d}$ (kilograms per cubic meter)	log (K_D) log (liters per kilogram)	f_j (-)
0% Coated Sand Product	0.55	3.69	0.14
15.4% Coated Sand Product	0.35	3.53	0.12
87% Coated Sand Product	1.042	2.26	0.02

$$RV_3 = f_{bio}(TR)$$

Equation 4.1: Calculation of RV_3

As may be inferred from Table 4.16, w_2RV_2 is much greater than one. This was due to the fact that the cost of bulk carbonate sand per kilogram is higher than the estimated cost of ammonium thioglycolate per kilogram of coated sand product. Such results are unsatisfactory for the purposes of appropriately weighting each term in the calculation of the feasibility factor. A different standard of normalization is required at the very least. Another potential conclusion is that the bulk material cost may actually be significant to overall cost of the coated sand products and needs to also be considered. While it is less conceivable that the true cost of the coated sand products is less than carbonate sand, the feasibility factor calculated in Table 4.16 may still be used to compare relative costs of the coated sand products. According to the current values for F, the coated sand product with the highest sand content is the most feasible. However, such values obviously do not account for reduced sorption capacity.

In addition to the difficulties related to cost normalization, TR values are not without a degree of uncertainty with respect to the data that was collected in the present study. Wakida et al (*193*) has investigated the effects of strong degradation and/or modification of hair keratin in solvents which use ammonium as a base cation on total nitrogen content. Although not always observed, increases in total nitrogen content are

conceivable. Such change could also be due to residual solvents trapped or untrapped in the structure. With respect to the present study, the total nitrogen content of the zero percent coated sand product seems low, however, no total nitrogen was taken for comparison of purified keratin azure. The fraction of organic matter in purified keratin azure is in fact lower than that of zero percent coated sand product, although not by much, which may warrant possible support of the theory that the total nitrogen content of keratin was indeed reduced by modification. Manuszak et al (*194*) includes changes in the protein and lipid composition of keratin among the effects of interaction with mercaptans, as well as numerous sulfur-containing, amino, and fatty acid residual compounds that may or may not be completely removed by boiling in an aqueous solution. An interesting piece of data that might be analyzed in parallel to the total nitrogen content with respect to changes due to modification of the keratin is total sulfur content. Although not tested in this study, such information may prove useful in future studies to fully understand the effects of preparation methods on the dyed wool.

The calculations are also not without a few assumptions which need to be stated. A first is that during reaction, ammonium thioglycolate is always present in excess in the reducing solution with respect to the amount required to cleave the disulfide bonds present in any suspended keratin fibers. However, this excess is assumed inexhaustible, or able to be used in future reactions and was not included in the calculation of f_1. The pH of the reducing solution was also assumed to be approximately ten, and not over 10.4 (the pK_{SH} of the thiol groups). The excess thioglycolate and high pH (or high redox

potential) is required for the rate of reaction to proceed to relative completion within the allowed timeframe. If the rate is too low, the amount of prepared hydrophobic biopolymer produced per mass of ammonium thioglycolate, and thus the estimated cost of required reagent becomes inaccurate. A last assumption is that there is no resistant keratin fraction to reduction (not necessarily becoming soluble because thiols do not participate in hydrogen bonding), and diffusion of the thioglycolate into the fiber is fast and thorough.

4.6 Finite Difference Simulation of the Transport of Naphthalene through a Thin-Layer Cap Comprised of Hydrophobic Biopolymer-Coated Sand Products

Numerical solutions for a Darcy velocity of 100 centimeters per day were obtained for an industrial sand media (f_{OC} equals 0.01, η equals 0.2) using time step sizes $d\tau$ equals 0.0005, $d\tau$ equals 0.00005, and $d\tau$ equals 0.000005 for grid sizes $d\zeta$ equals 0.0033, $d\zeta$ equals 0.005, $d\zeta$ equals 0.01, $d\zeta$ equals 0.02, and $d\zeta$ equals 0.05. Sorption parameters used were for the PAH Naphthalene. The value of the K_D for sand was taken to be equal to $f_{OC}K_{OC}$, where K_{OC} is with respect to sorption to natural organic matter, not the coated sand products. Values for all other parameters used are presented in Appendix A: Finite Difference Model Code in C++. C++ code was written using guidance from Press et al (*195*). All runs were completed in under two minutes on an Intel Core™2 Duo T5200 processor (1.60 gigahertz). Results were compared to the analytical solution on a semi-infinite domain for simplicity. The exact solution on a finite domain is

recommended for future studies, but no comparison was made on the closeness of the finite and semi-infinite scale exact solutions in this project. Figure 4.22 presents numerical results and associated error at time τ equals 0.003 for the case with the least absolute error at dτ equals 0.00005 and dζ equals 0.0033.

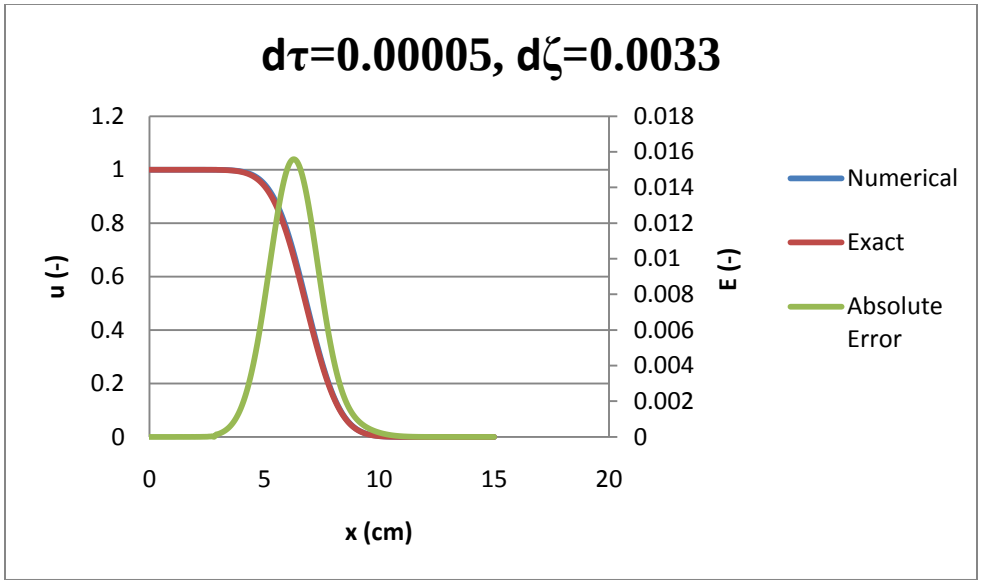

Figure 4.22: dτ=0.00005, dζ=0.0033

The dependence of the maximum absolute error upon the grid and time step sizes at time τ equals 0.003 are summarized in Figure 4.23 and Figure 4.24. The convergence of the absolute error as a function of dζ is presented in Figure 4.25.

The numerical results are satisfactory. The U equals 100 centimeters per day case was tried because the sharp front associated with the convection-dominated advection-

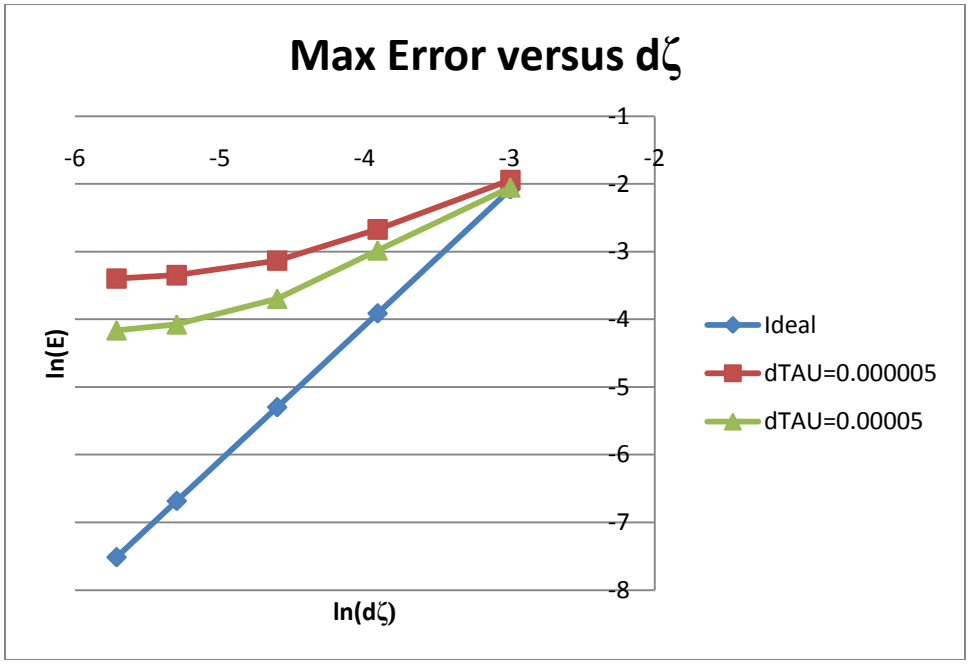

Figure 4.23: Maximum Error for the dτ=0.00005 and dτ=0.000005 Cases

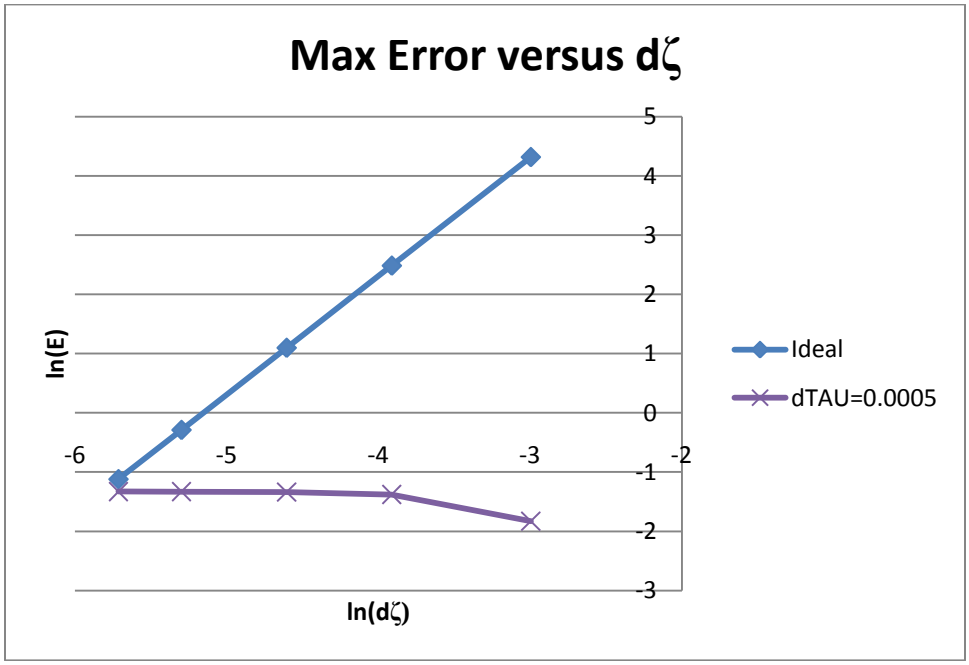

Figure 4.24: Maximum Error for the dτ=0.0005 Case

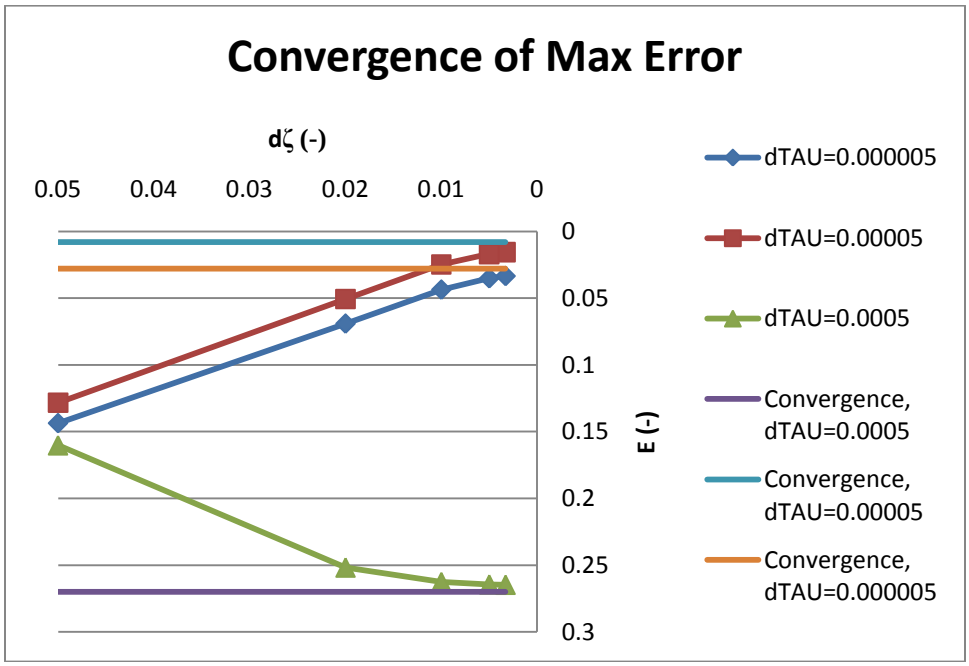

Figure 4.25: Error Convergence

diffusion curve is difficult to capture numerically and was expected to have the largest errors. Therefore, it is reasonable to conclude that the errors obtained in the results of this project are on the large end of error to be expected when running Darcy velocities typical in natural systems, since a Darcy velocity of 100 centimeters per day is quite large. Reducing dζ was most effective in reducing maximum error when dτ equals 0.00005 and dτ equals 0.000005. However, dζ equals 0.0033 was the finest grid size that could be handled before storage requirements of the coefficient matrix were too large for the computer. It is expected that finer grids would produce slightly lower absolute errors for the dτ equals 0.00005 and dτ equals 0.000005 cases, but as shown in Figure 4.25, the

error is starting to converge, so significantly better results are not expected with finer grid sizes.

Perhaps the most interesting result is that absolute error increased with decreasing $d\zeta$ for the $d\tau$ equals 0.0005 case. There seems to be an optimum time step size between $d\tau$ equals 0.0005 and $d\tau$ equals 0.000005. This is inferred from the divergence of absolute error with decreasing $d\zeta$ at $d\tau$ equals 0.0005 and the convergence of absolute error at $d\tau$ equals 0.000005 to a value higher than that at $d\tau$ equals 0.00005 for similar $d\zeta$s.

At $d\tau$ equals 0.000005 and large $d\zeta$, no oscillation occurred upstream of the front. However, significant overshooting frequently occured as $\frac{\partial u}{\partial \zeta}$ started to approach zero immediately downstream of the front. At these points, negative values of u were obtained. At $d\tau$ equals 0.0005, no overshooting occurred downstream of the front, but significant oscillation occurred upstream of the front. The front was also much less steep than for the other time steps.

Following the error analysis using industrial sand as media, the model was used to simulate the transport of naphthalene through a thin cap comprised of zero percent coated sand product, using a Darcy velocity of one centimeter per day instead of 100 centimeters per day, a grid size of $d\zeta$ equals 0.0033, and a time step size of $d\tau$ equals 0.00005. Such a Darcy velocity corresponded to a Peclet number of approximately 48 using the

parameters included in Appendix A. Results calculated the time to 10.00 percent breakthrough to be approximately 4.9 years and the time to 99.99% saturation to be approximately 13.2 years. When the K_D of the zero percent coated sand products is increased to that of tomato peel cutin, keeping all other parameters constant, the time to 10.00 percent breakthrough and 99.99 percent saturation becomes 153.1 years and 412.2 years, respectively, which further emphasizes the potential of cutin to serve as an amendment to sand in active capping materials. Figure 4.26 graphically illustrates the difference in the concentration profile of naphthalene through zero percent coated sand product and naphthalene through zero percent coated sand product using a sorption capacity of cutin at time 4.9 years.

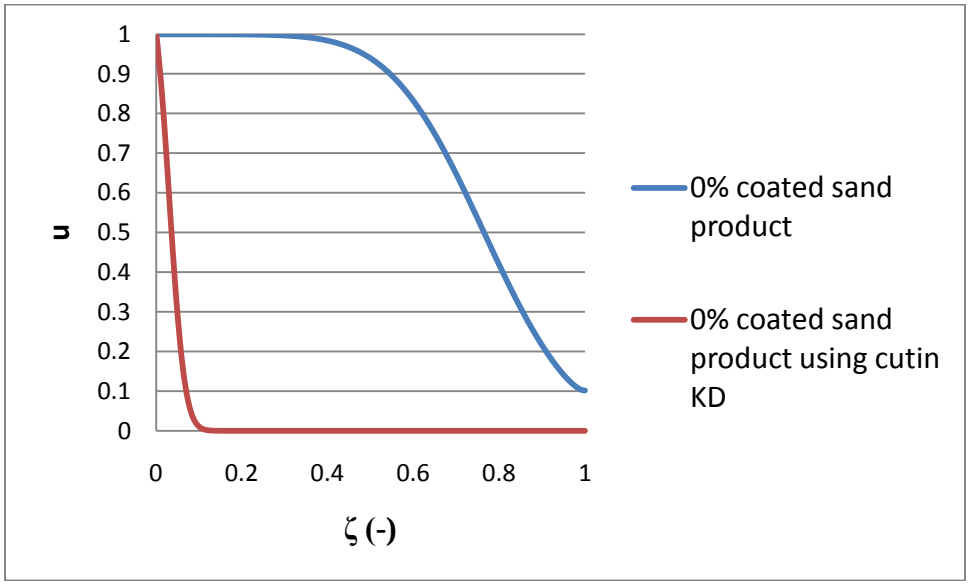

Figure 4.26: Concentration Profiles

Chapter 5: Conclusions and Future Work

Conclusions of the present study are presented in section 5.1, and recommendations for future research are given in section 5.2.

5.1 CONCLUSIONS

The present study was successful in amending sand grains with a sorptive hydrophobic biopolymer coating. Results of the study indicated that prepared hydrophobic biopolymers have the potential to reach competitive sorption capacities at costs comparable to conventional capping amendments. However, to more accurately determine the most feasible of the prepared hydrophobic biopolymers for providing a stable, sorptive coating on sand-grains, the costs must be reasonably estimated. These costs include those of the required bulk materials and non-exhaustible chemicals for both the preparation of the hydrophobic biopolymers and the construction of hydrophobic biopolymer-coated sand products. In addition to providing a more appropriate method for normalization of reagent cost in the determination of feasibility factors, such improvements could determine, for example, that tomato peel cutin is more feasible than keratin azure for coating sand particles. Cutin's low melting point makes inclusion of sand particles easy and very inexpensive. An expected difficulty may arise, however, in the ability of cutin to form rigid granular shapes after cooling and naturally cross-linking. As noted in Chapter 3, cutin becomes harder after repeated heating and cooling cycles at

105 degrees Celsius. Such methods may render a cutin-like product with a better ability to hold a granular form, although the structure of cutin may be modified slightly.

Results of the study also indicated that cellulolytic enzyme lignin is not a form of lignin that would be feasible to amend with sand grains in terms of cost per mass of prepared hydrophobic biopolymer, although it has a high sorption capacity in relation to more modified lignins. A more hydrophobic source of keratin, such as hen feathers, would prove useful to more fully understand the potential of keratin-based materials for sorbing HOCs. A further advantage of using a keratin source without pre-reacted dye molecules would be the elimination of the cost associated with extracting the non-covalently linked dye molecules.

Although coated sand products using modified keratin azure were stable at low concentrations of sand, the construction methods used in the present study were unable to maintain such stability at higher concentrations, as previously mentioned. The result was low uniformity of the coatings for higher concentrations of sand.

5.2 RECOMMENDATIONS FOR FUTURE RESEARCH

A more stable and uniform coating might be achieved using an electrostatic bead generator, such as the one produced by Nisco Engineering (Zurich, Switzerland) shown in Figure 5.1.

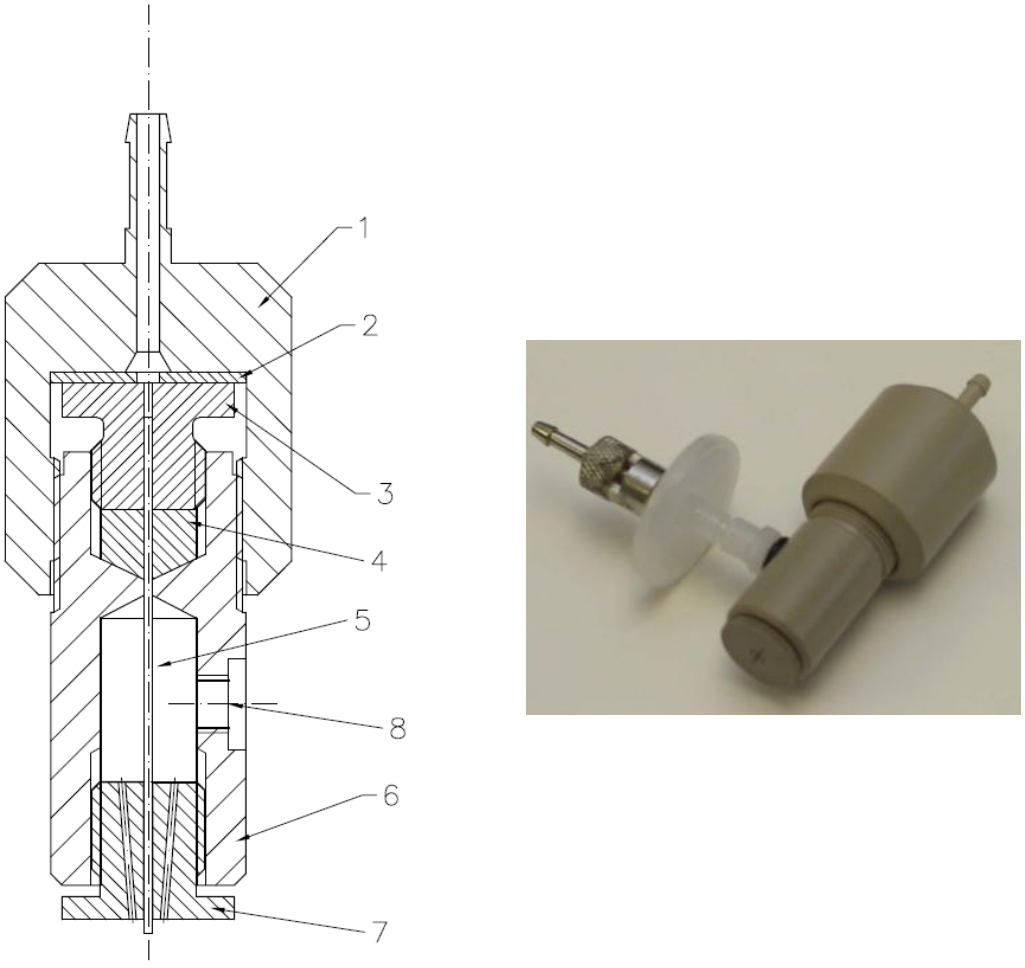

Figure 5.1: Nisco Electrostatic Bead Generator

An electrostatic bead generator applies an electrostatic potential between a conductive, hollow needle feeding a biomaterial solution and a gelling bath consisting of a cross-linking agent under continuous stirring. The biomaterial solution is added in drop-wise fashion to the gelling bath with the aid of the electrostatic potential and an

additional rapid stream of air. Capsules are allowed to cross-link for a time in the gelling bath or cross-linking solution before they are removed by filtration, washed, and stored. The size and shape of the beads formed is very uniform and can be varied by adjusting flow rate, voltage, and needle size. Homogeneity of the beads can also be varied by adjusting the concentration of the cross-linking solution and the cross-linking agent.

By introducing sand into the biomaterial, beads containing a homogeneous mixture of sand and biopolymer are formed. Studies performed by the manufacturer have confirmed their use for producing alginate beads for the immobilization of biological cells; however, efforts to utilize such technology in our laboratory have been unsuccessful. The problem was the difficulty in passing sand particles (100-350 mesh) safely through the needle without clogging, even at very low concentrations of sand. To pass a sand-biomaterial slurry, a large needle is required, which in turn may require large granule, or bead sizes. Larger bead sizes might cause mass transfer limitations with respect to the access of the cross-linking agent to the internal domains of the bead. If cross-linking is not rapid enough, the beads clump together and/or lose shape easily for large bead sizes. Mass transfer limitations may also exist with respect to the diffusion of HOCs into sorptive domains of the beads. In either case, further studies should incorporate such considerations.

Longevity and stability tests would also be necessary to assess the long-term fate of the amendment-biomaterial combinations under a wide variety of environmental

conditions. Stability is defined herein as the resistance of the capsules to deformation, dissolution, and/or leaching of amendments over time, while longevity is defined as the resistance of the capsules to biodegradation. A more thorough and quantitative toxicity evaluation of each of the prepared hydrophobic biopolymers and hydrophobic biopolymer-coated sand products would also make feasibility analysis more accurate. This evaluation could be achieved using chemical analysis techniques to assess in detail both the materials and solutions in contact with the materials. Incubation of indicative organisms may also be employed in the laboratory to determine dose-response relationships.

In addition to further chemical analysis for toxicity screening, analysis of the total sulfur, total hydrogen, and total oxygen may prove useful for the analysis of possible degradation of keratin under alkaline reduction and re-oxidation in ammonia-based solvents. Total hydrogen and total oxygen would also allow the calculation of a polarity index for each hydrophobic biopolymer and hydrophobic biopolymer-coated sand product for comparison to overall sorption capacities.

Fourier-Transform Infrared (FTIR) spectroscopy may also prove useful in assessing specific sorption mechanisms of HOCs to the hydrophobic biopolymers and hydrophobic biopolymer-coated sand products. Measurement of specific surface area and specific pore size distribution may provide insight into the mechanisms of HOC sorption to keratin products. It is appropriate to note, however, that the specific surface area

available in the keratin products for different gases such as nitrogen and carbon dioxide might be considerably different. Careful attention must be paid to the methods employed to obtain specific surface area results.

The modeling portion of the present study was intended to provide insight into contaminant transport through a column containing the hydrophobic biopolymer-coated sand products, and the simulations were sufficient to do so. However, further improvements in the model may be necessary to reduce errors. Economizing the coefficient matrix to solve finer grids would achieve this result. It would also be useful to obtain error results for diffusion-dominated cases, by investigating lower Darcy velocities such as 0.1, 1, and 10 centimeters per day.

It would also be useful to test other contaminants that have different sorption parameters, which would change the retardation coefficient. Wall effects can be incorporated into the two-dimensional axisymmetric transport equation under the same conditions for comparison to the one-dimensional results. For the purposes of having an analytical solution for comparison to numerical results, only the linear case was solved in the present study. Eventually, however, nonlinear sorption cases may need to be solved. In the case of Freundlich sorption to the media, sorption is non-competitive and the range of site binding energies present on the surface of the media is large (surface is more heterogeneous). W_S is not a function of $C_{A,W}$ to the power of one, and therefore a

retardation factor may not be factored out of the accumulation term. W_S is then given by Equation 3.12.

The resulting system would be nonlinear. To solve the nonlinear system, a Newton-Raphson iteration method could be employed. The Newton-Raphson method seeks to find the roots of the discretized transport equation, or more simply represented by Equation 5.1, where CO3, CO4, CO5, and CO6 are operational constants. In Equation 5.1, n equals the Freundlich parameter n and not the index of the current time step. The time step index, n, is replaced with an alternative index N only in Equation 5.1 and later in this section, Equation 5.2, which is not to be confused with the variable N.

$$f(C_{i-1}^{N+1}, C_i^{N+1}, (C^{\mathrm{n}})_i^{N+1}, C_{i+1}^{N+1}, C_{i+2}^{N+1}, C_{i-1}^{N}, C_i^{N}, (C^{\mathrm{n}})_i^{N}, C_{i+1}^{N}, C_{i+2}^{N}, CO3, \mathrm{CO4}, CO5, and\ CO6) = 0$$

Equation 5.1: Newton-Raphson Method

Expansion by Taylor's Formula gives a more useful version of Equation 5.1, which is presented in Equation 5.2, where K is an index representing the current iteration.

The resulting linear set may be solved using an LU decomposition scheme as previously described. Appendix B: Newton-Raphson Method presents an algorithm in C++ for linearizing a non-linear set, where MAX_ITER is the maximum number of iterations specified, and TOLERANCE is the maximum allowable absolute error.

$$[f(C_{i-1}^{N+1}, C_i^{N+1}, (C^{\mathrm{n}})_i^{N+1}, C_{i+1}^{N+1}, C_{i+2}^{N+1}, C_{i-1}^{N}, C_i^{N}, (C^{\mathrm{n}})_i^{N}, C_{i+1}^{N}, C_{i+2}^{N}, C, D, E, and\ F)]^{K+1}$$
$$= [f(C_{i-1}^{N+1}, C_i^{N+1}, (C^{\mathrm{n}})_i^{N+1}, C_{i+1}^{N+1}, C_{i+2}^{N+1}, C_{i-1}^{N}, C_i^{N}, (C^{\mathrm{n}})_i^{N}, C_{i+1}^{N}, C_{i+2}^{N}, C, D, E, and\ F)]^{K}$$
$$+ \sum_{j=i-1}^{i+2} \left\{ \left(C_j^{N+1,K+1} \right.\right.$$
$$\left.\left. - C_j^{n+1,K} \right) \frac{\partial [f(C_{i-1}^{N+1}, C_i^{N+1}, (C^{\mathrm{n}})_i^{N+1}, C_{i+1}^{N+1}, C_{i+2}^{N+1}, C_{i-1}^{N}, C_i^{N}, (C^{\mathrm{n}})_i^{N}, C_{i+1}^{N}, C_{i+2}^{N}, C, D, E, and\ F)]^{K}}{\partial (C_j^{N+1,K})} \right\}$$

Equation 5.2: Expanded Newton Raphson Method

Appendix A: Finite Difference Model Code in C++

```
//Copyright 2010 Ryan Z. Sitzes
//-------------------------------------------------------
//This program achieves a numerical solution for the 1-D
//transport equation with linear sorption to porous media
//and dissolved colloids through a column of finite
//dimension. A second-order (three-point) central
//difference approximation is used for the diffusive terms
//and a second-order (three-point) upwind difference
//approximation is used for the convective terms. A Crank-
//Nicolson method is used in time. An LU decomposition
//algorithm is used to solve the linear set.
//-------------------------------------------------------

#include<fstream>
#include<math.h>
using namespace std;

int main()
{

     //-----------------------------------------------------
     //GLOBAL VARIABLES
     //-----------------------------------------------------

     int                 n,
                         i,
                         j,
                         k;

     const int           N_ZETA=300,    //Number of space
                                        //steps in z-
                                        //direction
                         N=N_ZETA+1,    //Size of
                                        //coefficient
                                        //matrix and Right-
                                        //Hand-Side vector
                         N_TAU=1000,    //Number of time
                                        //steps
                         p=2,           //Lower bandwidth
                         q=1;           //Upper bandwidth
```

```
const double        L=15,           //Length of column
                                    //(cm)
                    dZETA=(1.0/300.0),
                                    //Space step length
                    dTAU=0.00005,   //Time step length
                    Pi=3.14159265,
                    k_B=(1.3805*(pow(10.0,-16.0))),
                                    //Boltzmann's
                                    //Constant
                                    //(g-cm^2/sec^2-K)
                    u_0=1.0,        //u at x=0, t>0

                    //--------------------------------
                    //INPUT >> ENVIRONMENTAL
                    //PROPERTIES
                    //--------------------------------
                    T=298,          //Absolute
                                    //temperature (K)
                    mu_W=0.01,      //Dynamic viscosity
                                    //of water(g/cm-
                                    //sec)(temperature
                                    //dependent)
                    U=100,          //Darcy velocity
                                    //(cm/day)

                    //--------------------------------
                    //INPUT >> MEDIA PROPERTIES
                    //--------------------------------
                    NU_b,d=0.2,     //Water-filled
                                    //porosity
                    RHO_b,d=2.65,   //Dry bulk density
                                    //of media (kg/L)


                    //--------------------------------
                    //INPUT >> COLLOID PROPERTIES AND
                    //CONSTANTS
                    //--------------------------------
                    RHO_DOC=(pow(10.0,-6.0)),
                                    //Concentration of
                                    //colloids (kg/L)
                    r_C=(5*(pow(10.0,-6.0))),
                                    //Radius of
```

```
                //colloids (cm)

//--------------------------------
//INPUT >> CONTAMINANT PROPERTIES
//--------------------------------
MW_A=128.2,     //Molecular weight
                //of A (g/mol)
K_OW=pow(10.0,3.23),
                //Octanol-water
                //partioning
                //coefficient
                //(L/kg)


//--------------------------------
//CALCULATED PARAMETERS
//--------------------------------
D_A_W=((pow(10.0,-5))*(pow((42.0/
MW_A) ,0.6))),
                //Molecular
                //diffusion
                //coefficient of A
                //in water
                //(cm^2/sec)
D_Brownian=(k_B*T)/(6*Pi*r_C*
mu_W),
                //Brownian
                //diffusion
                //coefficient of
                //colloids
                //(cm^2/sec)
K_D=(0.01* pow(10.0,2.97),),
                //Overall media-
                //water
                //partitioning
                //coefficient
                //(L/kg)
K_DOC=(K_OW*(pow(10.0,-0.58))),
                //DOC-water
                //partitioning
                //coefficient
                //(L/kg)
```

```
                        ALPHA_D=((0.017*(pow((L/100),1.5))
                        )* 100),
                                        //Dispersivity (cm)
                        R_f=(NU_b,d+(RHO_b,d*K_D)+
                        (RHO_DOC*K_DOC)),
                                        //Retardation
                                        //factor (-)
                        R_f_eff=(R_f/NU_b,d),
                                        //Effective
                                        //retardation
                                        //factor (-)
                        D_overall=((D_A_W*(pow(NU_b,d,
                        1.33)))+D_Brownian*RHO_DOC*
                        K_DOC)+((ALPHA_D*U)/86400)),
                                        //Diffusion
                                        //coefficient
                                        //(cm^2/sec)
                        D_eff=(D_overall/NU_b,d),
                                        //Effective
                                        //diffusion
                                        //coefficient
                                        //(cm^2/sec)
                        U_eff=((U/86400)/NU_b,d),
                                        //Effective Darcy
                                        //velocity (cm/s)
                        Pe=((U_eff*L)/D_eff),
                                        //Peclet Number (-)
                        CO1=(dTAU*Pe)/(4*dZETA),
                                        //Operational
                                        //constant
                        CO2=(dTAU)/(2*(dZETA*dZETA));
                                        //Operational
                                        //constant

double                  a[N][N],
                        b[N],
                        sum,
                        u_n[N],
                        u_n_plus_1[N];

ofstream myfile;
myfile.open("Column_Model_Linear_Sorption.csv");
```

```
//-----------------------------------------------------
//OUTPUT PARAMETERS
//-----------------------------------------------------

myfile << "L(cm)=" << "," << L << "\n";
myfile << "T(K)=" << "," << T << "\n";
myfile << "mu_W(g/cm-sec)=" << "," << mu_W << "\n";
myfile << "U(cm/day)=" << "," << U << "\n";
myfile << "U_eff(cm/s)=" << "," << U_eff << "\n";
myfile << "NU_b,d(-)=" << "," << ETA_W << "\n";
myfile << "RHO_b,d(kg/L)=" << "," << RHO_b << "\n";
myfile << "ALPHA_D(cm)=" << "," << ALPHA_D << "\n";
myfile << "k_B(g-cm^2/sec^2-K)=" << "," << k_B
       << "\n";
myfile << "RHO_DOC(kg/L)=" << "," << RHO_DOC << "\n";
myfile << "r_C(cm)=" << "," << r_C << "\n";
myfile << "D_Brownian(cm^2/sec)=" << "," << D_B
       << "\n";
myfile << "MW_A(g/mol)=" << "," << MW_A << "\n";
myfile << "D_A_W(cm^2/sec)=" << "," << D_A_W << "\n";
myfile << "K_OW(L/kg)=" << "," << K_OW << "\n";
myfile << "K_DOC(L/kg)=" << "," << K_DOC << "\n";
myfile << "K_D(L/kg)=" << "," << K_D << "\n";
myfile << "R_f(-)=" << "," << R_f << "\n";
myfile << "R_f_eff(-)=" << "," << R_f_eff << "\n";
myfile << "D_overall(cm^2/sec)=" << "," << D_overall
       << "\n";
myfile << "D_eff (cm^2/sec)=" << "," << D_eff << "\n";
myfile << "Pe(-)=" << "," << Pe << "\n";
myfile << "CO1(-)=" << "," << C << "\n";
myfile << "CO2(-)=" << "," << D << "\n";

//-----------------------------------------------------
//INITIAL CONDITION
//-----------------------------------------------------

for(i=0; i<=N_ZETA; i++)
{
     u_n[i]=0;
     myfile << u_n[i] << ",";
}
myfile << "\n";
```

```
//-----------------------------------------------------
//BEGIN TIME STEPS
//-----------------------------------------------------

for(n=1; n<=N_TAU; n++)
{
     //-------------------------------------------------
     //COEFFICIENT MATRIX
     //-------------------------------------------------

     //Set all elements initially to zero:
     for(i=0; i<=N_ZETA; i++)
     {
          for(j=0; j<=N_ZETA; j++)
          {
               a[i][j]=0;
          }
     }

     //Set the main diagonal element at k=0 to 1 for
     //the dirichlet boundary condition at ZETA=0:
     a[0][0]=1;

     //Set the k=1 elements on the superdiagonal, main
     //diagonal, and upper subdiagonal using a central
     //differencing scheme for both the diffusive
     //terms and convective terms:
     a[1][0]=(-CO1-CO2);
     a[1][1]=(1+(2*CO2));
     a[1][2]=(CO1-CO2);

     //Set k=2 through k=N_ZETA-1 elements using a
     //central differencing scheme for the diffusive
     //terms and an upwind scheme for the convective
     //terms:
     for(k=2; k<=(N_ZETA-1); k++)
     {
          a[k][k-2]=(CO1);
          a[k][k-1]=((-4*CO1)-CO2);
          a[k][k]=(1+(3*CO1)+(2*CO2));
          a[k][k+1]=(-CO2);
     }
```

```
//Set the upper subdiagonal and main diagonal
//element at k=Nz using a central differencing
//scheme for both the diffusive terms and
//convective terms and set
//u_n_plus_1[i+1]=u_n_plus_1[i-1] for the
//Neumann boundary condition:
a[N_ZETA][N_ZETA-1]=(-2*CO2);
a[N_ZETA][N_ZETA]=(1+(2*CO2));

//-----------------------------------------------
//RIGHT-HAND-SIDE VECTOR
//-----------------------------------------------

//Set the first element at k=0 to the Dirichlet
//boundary condition at ZETA=0:
b[0]=u_0;

//Set the second element at k=1 to the Right-
//Hand-Side corresponding to a central-difference
//approximation for both the convective and
//diffusive terms:
b[1]=((CO1+CO2)*u_n[0])+((1-(2*CO2))*u_n[1])+((-
CO1+CO2)*u_n[2]);

//Set elements at k=2 through k=N_ZETA-1 to the
//Right-Hand-Side corresponding to a central-
//difference approximation scheme for the
//diffusive terms and an upwind approximation
//scheme for the convective terms:
for(k=2; k<=(N_ZETA-1); k++)
{
     b[k]=(((-CO1)*u_n[k-
     2])+(((4*CO1)+CO2)*u_n[k-1])+((1-(3*CO1)-
     (2*CO2))*u_n[k])+((CO2)* u_n[k+1]));
}

//Set the second element at k=N_ZETA to the
//Right-Hand-Side corresponding to a central-
//difference approximation for both the
//convective and diffusive terms:
b[N_ZETA]=((2*CO2)*u_n[N_ZETA-1])+((1-
(2*CO2))*u_n[N_ZETA]);
```

```
//-----------------------------------------------
//SOLVE THE LINEAR SET VIA AN LU DECOMPOSITION
//ALGORITHM
//Adapted from: Golub, G.H. and Van Loan, G.F.
//Matrix Computations, 3rd Ed. (1996).
//-----------------------------------------------

//Decomposition of A into L and U. The entry
//a[i][j] is overwritten by l[i][j] if i>j and by
//u[i][j] otherwise
for(k=0; k<=N-2; k++)
{
     for(i=k+1; i<=min(k+p,N-1); i++)
          a[i][k]=a[i][k]/a[k][k];
     for(i=k+1; i<=min(k+p,N-1); i++)
          for(j=k+1; j<=min(k+q,N-1); j++)
               a[i][j]=a[i][j]-(a[i][k]*a[k][j]);
}

//Forward substitution to solve Ly=b. The entry
//b[i] is overwritten by y[i].
for(i=0; i<=N-1; i++)
{
     sum=0;
     for(j=max(0,i-p); j<=i-1; j++)
     {
          sum=sum+(a[i][j]*b[j]);
     }
     b[i]=b[i]-sum;
}

//Backward substitution to solve Ux=y. The entry
//y[i] is overwritten by x[i].
for(i=N-1; i>=0; i--)
{
     sum=0;
     for(j=i+1; j<=min(i+q,N-1); j++)
     {
          sum=sum+(a[i][j]*b[j]);
     }
     b[i]=(b[i]-sum)/a[i][i];
}
```

```
            //-----------------------------------------------
            //OUTPUT SOLUTION AT CURRENT TIME STEP AND RESET
            //u_n[k] TO u_n_plus_1[k]
            //-----------------------------------------------
            for(k=0; k<=N_ZETA; k++)
            {
                  u_n_plus_1[k]=b[k];
                  myfile << u_n_plus_1[k] << ",";
                  u_n[k]=u_n_plus_1[k];
            }
            myfile << "\n";
      }
      return 0;
}
```

Appendix B: Newton-Raphson Method

```
//Fill initial condition at t=n=0 and set equal to C_n[i]

//Begin time step loop
for(n=1; n<Nt+1; n++)
{
     //Set solution for the first iteration equal to the
     //solution at the previous time step (use previous
     //time step as an initial guess)
     for(i=0; i<Nx+1; i++)
     {
          C_n_plus_1_k[i]=C_n[i];
     }

     //Begin iteration loop
     for(k=0; k<MAX_ITER; k++)
     {
          //Fill coefficient matrix

          //Fill Right-Hand-Side (RHS)vector

          //Solve linear set using an appropriate matrix
          //solver

     //Reset solution at current time step and previous
     //iteration to the solution at the current time step
     //and current iteration
          for(i=0; i<Nx+1; i++)
          {
               C_n_plus_1_k[i]=C_n_plus_1_k_plus_1[i];
          }
     }
     //End iteration loop

     //Test for convergence and output solution
     for(i=0; i<Nx+1; i++)
     {
          if(abs(C_n_plus_1_k_plus_1[i]-C_n_plus_1_k[i])<=
               TOLERANCE)
          {
```

```
                myfile << C_n_plus_1_k_plus_1[i] << ",";
                u_n[i]=C_n_plus_1_k_plus_1[i];
           }
           else
           {
                myfile << "Error: System did not converge”
                       << "to within " << TOLERANCE
                       << " in " << MAX_ITER
                       << " iterations." << ",";
                break;
           }
      }
      myfile << "\n";
}
//End time step loop
```

Bibliography

1. *The Incidence and Severity of Sediment Contamination in Surface Waters of the United States, National Sediment Quality Survey: Second Edition*; EPA-823-R-04-007; United States Environmental Protection Agency, Office of Science and Technology, Standards and Health Protection Division: Washington, DC, 2004.

2. Reible, D.D. University of Texas at Austin, Austin, TX. Personal communication, April 2010.

3. Forrest, C. Evaluation of Biopolymer Coated Sands as Capping Materials. M.S. Thesis, University of Texas, Austin, TX, 2008.

4. Knox, Anna. *Innovative In-Situ Remediation of Contaminated Sediments for Simultaneous Control of Contamination and Erosion: Annual Report*; WSRC-RP-2007-00666; Savannah River National Laboratory, US Department of Energy: Savannah, Georgia, December 2007.

5. Huang, H. et al. Colloids and Surfaces. *Biointerfaces*. **2004**, 39, 31-37.

6. Krajewska, B. Application of Chitin- and Chitosan-Based Materials for Enzyme Immobilizations: a Review. *Enzyme and Microbial Technology*. **2004**, 35, 126-139.

7. Ngomsik, A. et al. Nickel Adsorption by Magnetic Alginate Microcapsules Containing an Extractant. *Water Research*. **2006**, 40, 1848-1856.

8. Ngah, W.S. et al. Removal of Copper(II) Ions from Aqueous Solution onto Chitosan and Cross-Linked Chitosan Beads. *Reactive and Functional Polymers*. **2002**, 50, 181-190.

9. Uzun, İ.; Güzel, F. Adsorption of Some Heavy Metal Ions from Aqueous Solution by Activated Carbon and Comparison of Percent Adsorption Results of Activated Carbon with those of Some Other Adsorbents. *Turk. J. Chem*. **2000**, 24, 291-297.

10. Minamisawa, M. et al. Adsorption Behavior of Heavy Metals on Biomaterials. *J. Agric. Food Chem*. **2004**, 52, 5606-5611.

11. Severtson, S.J.; Banerjee, S. Sorption of Chlorophenols to Wood Pulp. *Environ. Sci. Technol*. **1996**, *30*, 1961-1969.

12. Wang, X.; Xing, B. Sorption of Organic Contaminants by Biopolymer-Derived Chars. *Environ. Sci. Tech.* **2007**, *41*, 8342-8348.

13. Zhu, D.Q. et al. Evidence for π-π Electron Donor-Acceptor Interactions Between π-Donor Aromatic Compounds and π-Acceptor Sites in Soil Organic Matter Through pH Effects on Sorption. *Environ. Sci. Technol.* **2004**, *38*, 4361-4368.

14. Wang, X. et al. Competitive Sorption of Pyrene on Wood Chars. *Environ. Sci. Technol.* **2006**, *40*, 3267-3272.

15. Wang, X. et al. Sorption of Organic Contaminants by Biopolymers: Role of Polarity, Structure, and Domain Spatial Arrangement. *Chemosphere* **2007**, *66*, 1476-1484.

16. Wang, X.; Xing, B. Importance of Structural Makeup of Biopolymers for Organic Contaminant Sorption. *Environ. Sci. Technol.* **2007**, *41*, 10, 3559-3565.

17. Gunasekara, A.S.; Xing, B. Sorption and Desorption of Naphthalene by Soil Organic Matter: Importance of Aromatic and Aliphatic Components. *J. Environ. Qual.* **2003**, *32*, 240-246.

18. Chefetz, B. et al. Pyrene Sorption by Natural Organic Matter. *Environ. Sci. Technol.* **2000**, *34*, 2925-2930.

19. Chiou, C.T. et al. Partition Characteristics of Polycyclic Aromatic Hydrocarbons on Soils and Sediments. *Environ. Sci. Technol.* **1998**, *32*, 264-269.

20. Johnson, M. D. et al. A Distributed Reactivity Model for Sorption by Soils and Sediments. 13. Simulated Diagenesis of Natural Sediment Organic Matter and Its Impact on Sorption/Desorption Equilibria. *Environ. Sci. Technol.* **2001**, *35*, 1680-1687.

21. Xing, B. Sorption of Naphthalene and Phenanthrene by Soil Humic Acids. *Environ. Pollut.* **2001**, *111*, 303-309.

22. Salloum, M.J. et al. Phenanthrene Sorption by Aliphatic-Rich Natural Organic Matter. *Environ. Sci. Technol*. **2002**, *36*, 1953-1958.

23. Kang, S.; Xing, B. Phenanthrene Sorption to Sequentially Extracted Soil Humic Acids and Humins. *Environ. Sci. Technol.* **2005**, *39*, 134-140.

24. Chefetz, B. Sorption of Phenanthrene and Atrazine by Plant Cuticular Fractions. *Environ. Toxicol. Chem.* **2003**, *22*, 10, 2492-2498.

25. Chaplin, Martin. London South Bank University: Water Structure and Science. http://www.lsbu.ac.uk/water/ (accessed Aug 2008).

26. Burken, J. Missouri University of Science and Technology, Rolla, MO. Personal communication, October 18, 2007.

27. Jonker, M. Absorption of Polycyclic Aromatic Hydrocarbons to Cellulose. *Chemosphere* **2008**, *70*, 778-782.

28. Shechter, M.; Chefetz, B. Insights Into the Sorption Properties of Cutin and Cutan Biopolymers. *Environ. Sci. Technol.* **2008**, *42*, 1165-1171.

29. Chen, B. et al. Sorption of Polar and Nonpolar Aromatic Organic Contaminants by Plant Cuticular Materials: Role of Polarity and Accessibility. *Environ. Sci. Technol.* **2005**, *39*, 6138-6146.

30. Sachleben, J.R. et al. Solid-State NMR Characterization of Pyrene-Cuticular Matter Interactions. *Environ. Sci. Technol.* **2004**, *38*, 4369-4376.

31. Deshmukh, A.P. Sorption and Sequestration of Phenanthrene in Polymethylenic Plant Biopolymers: Proxies for Soil and Sedimentary Organic Matter. PhD Dissertation, Ohio State University, Columbus, OH, 2003.

32. Rushton, M. Lignol Innovations, Burnaby, BC, Canada. Personal communication, April 21, 2010.

33. Gunnarson, Jonas. *Abstract J-03*, in: G.S. Durell and E.A. Foote (Conference Chairs), Remediation of Contaminated Sediments—2009, Fifth International Conference on Remediation of Contaminated Sediments, Jacksonville, Florida, February 2–5, 2009; Battelle Memorial Institute: Columbus, OH, 2009; ISBN 978-0-9819730-0-5

34. Osman, S.F. et al. Preparation, Isolation, and Characterization of Cutin Monomers and Oligomers from Tomato Peels. *J. Agric. Food Chem.* **1999**, 47 (2), 799-802.

35. Heredia, A. Biophysical and Biochemical Characteristics of Cutin, a Plant Barrier Biopolymer. *Biochimica et Biophysica Acta*. **2003,** 1620, 1 – 7.

36. Cordeiro et al. Cork Suberin as a New Source of Chemicals: 1. Isolation and Chemical Characterization of its Composition. *International Journal of Biological Macromolecules*. **1998**, 22, 71-80.

37. Pacchiano, R.A. et al. Isolation and Spectral Characterization of Plant-Cuticle Polyesters. *J. Agric. Food Chem*. **1993**, 41 (1), 78-83.

38. Rocha, S.M. et al. Enzymatic Isolation and Structural Characterization of Polymeric Suberin of Cork from *Quercus Suber L*. *International Journal of Biological Macromolecules*. **2001**, 28, 107-119.

39. Kazlev, A.M. Paleos: The History of Life on Earth: Plants. http://www.palaeos.com/Plants/ (accessed April 2010).

40. Osman, S.F. et al. Method for the Production and Characterization of Tomato Cutin Oligomers. *J. Agric. Food Chem*. **1995**, 43 (8), 2134-2137.

41. Tian, S. et al. Isolation and Identification of Oligomers from Partial Degradation of Lime Fruit Cutin. *J. Agric. Food Chem*. **2008**, 56 (21), 10318-10325.

42. Fang, X. et al. NMR Studies of Molecular Structure in Fruit Cuticle Polyesters. *Phytochemistry*. **2001**, 57, 1035-1042.

43. Heredia-Guerrero, J.A. et al. Chemical Reactions in 2D: Self-Assembly and Self-Esterification of 9(10),16-Dihydroxypalmitic Acid on Mica Surface. *Langmuir*. **2009**, 25 (12), 6869-6874.

44. Cetin, N.; Ozmen, N. Use of Organosolv Lignin in Phenol-Formaldehyde Resins for Particleboard Production. I. Organosolv Lignin Modified Resins. *International Journal of Adhesion and Adhesives*. **2002**, *22*, 477-480.

45. Ibrahim, M.N. et al. Formulation of Lignin Phenol Formaldehyde Resins as a Wood Adhesive. *Malaysian J. Anal. Sci.* **2007**, *11*, 1, 213-218.

46. Clarke, M.R.; Dolenko, A.J. Methylolated Kraft Lignin Polymer Resin. U.S. Patent 4, 113, 675, September 12, 1978.

47. Schneider, M.H.; Phillips, J.G. Furfuryl Alcohol and Lignin Adhesive Composition. U.S. Patent 6,747,076 B2, June 8, 2004.

48. Viikari, L. et al. Lignin Based Adhesives and a Process for the Preparation Thereof. International Publication Number WO 98/31763, July 23, 1998.

49. Lora, J.H. and Glasser, W.G. Recent Industrial Applications of Lignin: A Sustainable Alternative to Nonrenewable Materials. *Journal of Polymers and the Environment.* **2002**. 10 (1/2).

50. Bolle, R. and Wolfgang, A. Lignin Based Coating. U.S. Patent 6,217,942, Apr. 17, 2001.

51. Debons, F.E. et al. Oxidized Alkali Lignins and Their Use in Enhanced Oil Recovery. U.S. Patent 4,611, 659, Sept. 16, 1986.

52. Debons, F.E. et al. Use of Lignin/Amine/Surfactant Blends in Enhanced Oil Recovery. U.S. Patent 4,822,501, Apr. 18, 1989.

53. Nadif, A. et al. Sulfur-Free Lignins from Alkaline Pulping Tested in Mortar for Use as Mortar Additives. *Bioresource Technology*. **2002**, 84, 49-55.

54. Rachor, D.G.; Ludwig, C.H. Lignin Composition and Process for its Preparation. U.S. Patent 3,912,706, Oct. 14, 1975.

55. Allan, G.G. Reaction Products of Lignin and Bark Extracts and Process for Same. U.S. Patent 3,470,148, Sept. 30, 1969.

56. DelliColli, H.T. et al. Cross-Linked Lignin Gels. U.S. Patent 4,244,728, Jan. 13, 1981.

57. Brown, W. Process for Making Lignin Gels in Bead Form. U.S. Patent 4,131,573, Dec. 26, 1978.

58. Meister, J.J. and Patil, D.R. Water Soluble Graft Copolymers of Lignin-(2-Propenamide)-(Sodium 2,2-Dimethyl-3-Imino-4-Oxohex-5-Ene-1-Sulfonate), Methods of Making the Same and Uses Therefor. U.S. Patent 4,687,828, Aug. 18, 1987.

59. Morrow, L.R. Enhanced Oil Recovery Using Alkylated, Sulfonated, Oxidized Lignin Surfactants. U.S. Patent 5,094, 295, Mar. 10, 1992.

60. Boerjan, W. et al. Lignin Biosynthesis. *Annu. Rev. Plant Biol.* **2003**, *54*, 519-546.

61. Biorenew. Biorenew: The Complex Lignin Polymer: What We Can Learn Using Modern Analytical Techniques. http://www.biorenew.org/ (accessed July 2008).

62. Ralph, J. *Lignin Structure: Recent Developments*; US Dairy Forage Research Center, USDA-Agricultural Research Service: Madison, WI, 1999.

63. Baucher, M. et al. Lignin: Genetic Engineering and Impact on Pulping. *Critical Reviews in Biochemistry and Molecular Biology* **2003**, *38*, 305-350.

64. Rio, J. et al. Occurrence of Naturally Acetylated Lignin Units. *J. Agric. Food Chem.* **2007**, *55*, 5461-5468.

65. Grabber, J.H. et al. Cross-Linking of Maize Walls by Ferulate Dimerization and Incorporation into Lignin. *J. Agric. Food Chem.* **2000**, *48*, 6106-6113.

66. Hatfield, R.D. et al. Review: Cell Wall Cross-Linking by Ferulates and Diferulates in Grasses. *J. Sci. Food Agric.* **1999**, *79*, 403-407.

67. Quideau, S.; Ralph, J. Lignin-Ferulate Cross-Links in Grasses. Part 4.[1-3] Incorporation of 5-5-Coupled Dehydrodiferulate Into Synthetic Lignin. *J. Chem. Soc., Perkin Trans.* **1997**, *1*, 2351-2358.

68. Ralph J. et al. Peroxidase-Dependent Cross-Linking Reactions of P-Hydroxycinnamates in Plant Cell Walls. *Phytochem. Reviews.* **2004**, *3*, 79-96.

69. Grabber, J. How do Lignin Composition, Structure, and Cross-Linking Affect Degradability? A Review of Cell Wall Model Studies. *Crop Sci.* **2005**, *45*, 820-831.

70. Chabannes, M. et al. In Situ Analysis of Lignins in Transgenic Tobacco Reveals a Differential Impact of Individual Transformations on the Spatial Patterns of Lignin Deposition at the Cellular and Subcellular Level. *The Plant Journal*. **2001**, 28 (3), 271-282.

71. Dominguez, J.C. et al. Thermal Stability and Pyrolysis Kinetics of Organosolv Lignins Obtained from *Eucalyptus Globulus*. *Industrial Crops and Products*. **2008**, 27, 150-156.

72. Fengel, D. et al. Studies on the Delignification of Spruce Wood by Organosolv Pulping Using SEM-EDXA and TEM. *Wood Sci. Technol*. **1989**, 23, 123-130.

73. Gilarranz, M.A. et al. Acid Precipitation and Purification of Wheat Straw Lignin. *Separation Science and Technology*. **1998**, 33 (9), 1359-1377.

74. Hongzhang, c. and Liying, L. Unpolluted Fractionation of Wheat Straw by Steam Explosion and Ethanol Extraction. *Bioresource Technology*. **2007**, 98, 666-676.

75. Li, J. et al. Lignin Depolymerization/Repolymerization and Its Critical Role for Delignification of Aspen Wood by Steam Explosion. *Bioresource Technology*. **2007**, 98, 3061-3068.

76. Pye, E.K. *Industrial Lignin Production and Applications*, in: Biorefineries-Industrial Processes and Products: Status Quo and Future Directions; Kamm, B. et al, Eds.; Wiley-VCH Verlag GmbH: Weinheim, Germany, 2008.

77. Sahin, H.T. and Young, R.A. Auto-Catalyzed Acetic Acid Pulping of Jute. *Industrial Crops and Products*. **2008**, 28, 24-28.

78. Vazquez, G. et al. Kinetics and Mechanism of Acetic Acid Pulping of Detannined *Pinus Pinaster* Bark. *Wood Sci. Technol*. **1994**, 28, 403-408.

79. Phillips, M. The Chemistry of Lignin. II. Fractional Extraction of Lignin from Corn Cobs. *J. Amer. Chem. Soc*. **1928**, 50 (7), 1986-1989.

80. Hatfield, R. and Fukushima, R.S. Can Lignin Be Accurately Measured? *Crop Sci*. **2005**, 45, 832-839.

81. Hatfield, R.D. et al. A Comparison of the Insoluble Residues Produced by the Klason Lignin and Acid Detergent Lignin Procedures. *J. Sci. Food Agric*. **1994**, 65 (1), 51-58.

82. Hussain, M.A. et al. Estimation of Lignin in Jute by Titration Method. *Pakistan J. Bio. Sci*. **2002**, 5 (5), 521-522.

83. Jung et al. Accuracy of Klason Lignin and Acid Detergent Lignin Methods as Assessed by Bomb Calorimetry. *J. Agric. Food Chem*. **1999**, 47 (5), 2005-2008.

84. Ritchie, P.F. and Purves, C.B. Periodate Lignins. Their Preparation and Properties. *Pulp and Paper Magazine of Canada*. **1947**, 74-82.

85. Rodrigues, J. et al. Improvement of the Acetylbromide Method for Lignin Determination Within Large-Scale Screening Programmes. *Holz als Roh- und Werkstoff*. **1999**, 57, 341-345.

86. Wald, W.J. et al. The Elementary Composition of Lignin in Northern Pine and Black Spruce Woods, and of the Isolated Klason and Periodate Lignins. *J. Amer. Chem. Soc*. **1947**, 69 (6), 1371-1377.

87. Brauns, F.E. Native Lignin 1. Its Isolation and Methylation. *J. Amer. Chem. Soc*. **1939**, 61 (8), 2120-2127.

88. Bjorkman, A. Studies on Finely Divided Wood. Part 1. Extraction of Lignin with Neutral Solvents. *Svensk Papperstidning*. **1956**, 13, 59.

89. Chang et al. Comparative Studies on Cellulolytic Enzyme Lignin and Milled Wood Lignin of Sweetgum and Spruce. *Holtzforschung*. **1975**, 29 (5), 153-159.

90. de Stevens, G. and Nord, F.F. Investigations on Lignin and Lignification. VIII. Isolation and Characterization of Bagasse Native Lignin. *J. Amer. Chem. Soc*. **1951**, 73 (10), 4622-4625.

91. de Stevens, G. and Nord, F.F. *A Study of Lignin Formation Based on the Oxidation of Native and Enzymatically Liberated Lignins*, in: Proceedings of the National Academy of Sciences of the United States of America, **1953**, 39 (2), 80-84.

92. Bjorkman, A. Lignin and Lignin-Carbohydrate Complexes. *Ind. Eng. Chem*. **1957**, 49 (9), 1395-1398.

93. Iverson, T. Lignin-Carbohydrate Bonds in a Lignin-Carbohydrate Complex Isolated from Spruce. *Wood Sci. Technol*. **1985**, 19, 243-251.

94. Chen, J.-Y. et al. A Method for Isolation of Milled-Wood Lignin Involving Solvent Swelling Prior to Enzyme Treatment. *Wood Sci. Technol*. **1995**, 29, 295-306.

95. Holtman, K.M. et al. Solution State Nuclear Magnetic Resonance Study of the Similarities Between Milled Wood Lignin and Cellulolytic Enzyme Lignin. *J. Agric. Food Chem*. **2004**, 52 (4), 720-726.

96. Hu, Z. et al. Elucidation of the Structure of Cellulolytic Enzyme Lignin. *Holtzforshung*. **2006**, 60, 389-397.

97. Polcin, J. and Bezuch, B. Investigation on Enzymic Hydrolysis of Lignified Cellulosic Materials. *Wood Sci. Technol*. **1977**, 11, 275-290.

98. Polcin, J. and Bezuch, B. Enzymic Isolation of Lignin from Wood and Pulps. *Wood Sci. Technol*. **1978**, 12, 149-158.

99. Schubert, W.J. and Nord, F.F. *Investigations on Lignin and Lignification. XV. Heterogeneity of Native and Enzymatically Liberated Lignins as Established by Electrophoresis and Paper Chromatography*, in: Proceedings of the National Academy of Sciences of the United States of America, **1955**, 41 (3), 122-127.

100. Kosikova, B. and Polcin, J. Isolation of Lignin from Spruce by Acidolysis in Dioxane. *Wood Sci. Technol*. **1973**, 7, 308-316.

101. Lu, F. and Ralph, J. Non-Degradative Dissolution and Acetylation of Ball-Milled Plant Cell Walls: High-Resolution Solution-State NMR. *The Plant Journal*. **2003**, 35, 535-544.

102. Deng, L. et al. Green Solvent for Flash Pyrolysis Oil Separation. *Energy and Fuels*. **2009**, 23, 3337-3338.

103. Vignes, R. *Dimethyl Sulfoxide (DMSO) A "New" Clean, Unique, Superior Solvent*, in: American Chemical Society Annual Meeting, Washington, D.C., August 20-24, 2000.

104. Wypych, G. *New Trends Based on Patent Literature*, in: unknown publication, Chemtec Laboratories, Inc., Toronto, Canada, year unknown, 1637-1652.

105. Fengel, D. et al, Studies on Milled Wood Lignin from Spruce. Part II. Electron Microscopic Observations on the Milled Wood. *Wood Sci. Tech*. **1978**, 12, 141-148.

106. Fujimoto, A. et al. Quantitative Evaluation of Milling Effects on Lignin Structure During the Isolation Process of Milled Wood Lignin. *J. Wood Sci*. **2005**, 51, 89-91.

107. Holtman, K.M. et al. Quantitative ^{13}C NMR Characterization of Milled Wood Lignins Isolated by Different Milling Techniques. *J. Wood Chem. Technol*. **2006**, 26, 21-34.

108. Ikeda, T. et al. Studies on the Effect of Ball Milling on Lignin Structure Using a Modified DFRC Method. *J. Agric. Food Chem*. **2002**, 50 (1), 129-135.

109. Wegener, G. and Fengel, D. Studies on Milled Wood Lignins from Spruce. Part1. Composition and Molecular Properties. *Wood Sci. Technol*. **1977**, 11, 133-145.

110. Wegener, G. and Stoll, M. Eine schnelle Isolierung von Milled-Wood-Lignin mit Hilfe von Ultraschall. *Cellulose Chem. Technol*. **1976**, 10, 611-616.

111. Gralen, N. and Berg, St. Treatment of Wood with Ultrasonic Waves. *J. Polym. Sci*. **1951**, 6, 503-507.

112. Kudzin, S.F. and Nord, F.F. Investigations on Lignin and Lignification. IV. Studies on Hardwood Lignin. *J. Amer. Chem. Soc*. **1951**, 73 (2), 690-693.

113. Powell, W.J. and Whittaker, H. XXII- The Chemistry of Lignin. Part II. A Comparison of Lignins Derived from Various Woods, in: Powell and Whittaker:

The Chemistry of Lignin; Research Department, Royal Arsenal: Woolwich, 1924, pp. 132-137.

114. Landucci, L.L. Application of Modern Liquid-State NMR to Lignin Characterization. *Holzforshung*. **1991**, 45, 55-60.

115. Ralph, J. et al. Solution-State NMR of Lignins. In *Advances in Lignocellulosics Characterization*; Argyropoulos, Dimitris, S., Eds.: TAPPI Press, Atlanta, GA, year unknown; pp. 55-108.

116. Lin, S.Y. Method for Polymerization of Lignin. U.S. Patent 4,221,708, Sept. 9, 1980.

117. Askvik, K.M. et al. Complexation Between Lignosulphonates and Cationic Surfactants and Its Influence on Emulsion and Foam Stability. *Colloids and Surfaces A: Physicochemical and Engineering Aspects*. **1999**, 159, 89-101.

118. Garcia-Valls, R. and Hatton, T.A. Metal Ion Complexation with Lignin Derivatives. *Chemical Engineering Journal*. **2003**, 94, 99-105.

119. Guo, X. et al. Adsorption of Metal Ions on Lignin. *Journal of Hazardous Materials*. **2008**, 151, 134-142.

120. Liu, M.-H. and Huang, J.-H. Removal and Recovery of Cationic Dyes from Aqueous Solutions Using Spherical Sulfonic Lignin Adsorbant. *J. Applied Poly. Sci*. **2006**, 101, 2284-2291.

121. Lu, Y. and Allen, H.E. Characterization of Copper Complexation with Natural Dissolved Organic Matter (DOM)- Link to Acidic Moieties of DOM and Competition by Ca and Mg. *Water Research*. **2002**, 36, 5083-5101.

122. Merdy, P. et al. Copper Sorption on a Straw Lignin: Experiments and EPR Characterization. *Journal of Colloid and Interface Science*. **2002**, 245, 24-31.

123. Leiviska, T. and Ramo, J. Coagulation of Wood Extractives in Chemical Pulp Bleaching Filtrate by Cationic Polyelectrolytes. *Journal of Hazardous Materials*. **2008**, 153, 525-531.

124. Masion, A. et al. Coagulation-Flocculation of Natural Organic Matter with Al Salts: Speciation and Structure of the Aggregates. *Environ. Sci. Technol*. **2000**, 34, 3242-3246.

125. Ritter, A.V. et al. Removal of Natural Organic Matter by Coagulation-Flocculation: A Pyrolysis-GC-MS Study. *Environ. Sci. Technol*. **1999**, 33, 3027-3032.

126. Zoumpoulakis, L. and Simitzis, J. Ion Exchange Resins from Phenol/Formaldehyde Resin-Modified Lignin. *Polymer International*. **2001**, 50, 277-283.

127. Allard, B. et al. Chapter V Binding Models for Humic Substances. In *Modelling in Aquatic Chemistry*; Grenthe, I. and Puigdomenech, I., Eds.: OECD Publications, 1997; pp. 153-206.

128. Koopal, L.K. et al. Humic Matter and Contaminants. General Aspects and Modeling Metal Ion Binding. *Pure Appl. Chem*. **2001**, 73 (12), 2005-2016.

129. Benedetti, M.F. et al. Metal Ion Binding to Humic Substances: Application of the Non-Ideal Competitive Adsorption Model. *Environ. Sci. Technol*. **1995**, 29, 446-467.

130. Borrok, D.M. and Fein, J.B. The Impact of Ionic Strength on the Adsorption of Protons, Pb, Cd, and Sr onto the Surfaces of Gram Negative Bacteria: Testing Non-Electrostatic, Diffuse, and Triple-Layer Models. *Journal of Colloid and Interface Science*. **2005**, 286, 110-126.

131. Borrok, D. et al. Significance of Ternary Bacteria-Metal-Natural Organic Matter Complexes Determined Through Experimentation and Chemical Equilibrium Modeling. *Chemical Geology*. **2007**, 238, 44-62.

132. M. de Wit J.C. et al. Proton Binding to Humic Substances. 1. Electrostatic Effects. *Environ. Sci. Technol*. **1993**, 27 (10).

133. Kinniburgh, D. G. et al. Metal Ion Binding by Humic Acid: Application of the NICA-Donnan Model. *Environ. Sci. Technol*. **1996**, 30, 1687-1698.

134. Milne, C.J. et al. Generic NICA-Donnan Model Parameters for Proton Binding by Humic Substances. *Environ. Sci. Technol*. **2001**, 35, 2049-2059.

135. Milne, C.J. et al. Generic NICA-Donnan Model Parameters for Proton Binding by Humic Substances. *Environ. Sci. Technol*. **2003**, 37, 958-971.

136. Pandy, A.K. et al. Stability Constants of Metal-Humic Acid Complexes and Its Role in Environmental Detoxification. *Ecology and Environmental Safety*. **2000**, 47, 195-200.

137. Perdue, E.M. and Lytle, C.R. Distribution Model for Binding of Protons and Metal Ions by Humic Substances. *Environ. Sci. Technol*. **1983**, 17, 654-660.

138. Tipping, E. and Hurley, M.A. A Unifying Model of Cation Binding by Humic Substances. *Geochimica et Cosmochimica Acta*. **1992**, 56, 3627-3641.

139. Tipping, E. Humic Ion-Binding Model VI: An Improved Description of the Interactions of Protons and Metal Ions with Humic Substances. *Aquatic Geochemistry*. **1998**, 4, 3-48.

140. Zeeberg, B. New Approach for Studying Macromolecular-Ligand Binding. *The Journal of Biological Chemistry*. **1980**, 255 (7), 3062-3067.

141. Lu, Y. and Pignatello, J.J. Sorption of Apolar Compounds to Soil Humic Acid Particles Affected by Aluminum(III) Ion Cross-Linking. *J. Environ. Qual*. **2004**, 33, 1314-1321.

142. Pignatello, J.J. et al. Nonlinear and Competitive Sorption of Apolar Compounds in Black Carbon-Free Natural Organic Materials. *J. Environ. Qual*. **2006**, 35, 1049-1059.

143. Polubesova, T. Binding of Pyrene to Hydrophobic Fractions of Dissolved Organic Matter: Effect of Polyvalent Metal Complexation. *Environ. Sci. Technol*. **2007**, 41, 5389-5394.

144. Wang, X. et al. Sorption of Aromatic Contaminants by Biopolymers: Effects of pH, Copper (II) Complexation, and Cellulose Coating. *Environ. Sci. Technol*. **2007**, 41, 185-191.

145. Yuan, G. and Xing, B. Effects of Metal Cations on Sorption and Desorption of Organic Compounds in Humic Acids. *Soil Science*. **2001**, 166 (2), 107-115.

146. El Mansouri, N. et al. Lignin-Based Wood Panel Adhesives Without Formaldehyde. *Holz Roh Werkst*. **2007**, 65, 65-70.

147. Oudgenoeg, G. et al. Peroxidase-Mediated Cross-Linking of a Tyrosine-Containing Peptide with Ferulic Acid. *J. Agric. Food Chem*. **2001**, 49, 2503-2510.

148. Cao, N. et al. Mechanical Properties of Gelatin Films Cross-Linked, Respectively, by Ferulic Acid and Tannin Acid. *Food Hydrocolloids*. **2007**, 21, 575-584.

149. Oosterveld, A. et al. Formation of Ferulic Acid Dehydrodimers Through Oxidative Cross-Linking of Sugar Beet Pectin. *Carbohydrate Research*. **1997**, 300, 179-181.

150. Blanchard, C.R. et al. Keratin-Based Hydrogel for Biomedical Applications and Method of Production. U.S. Patent 5,932,552, Aug. 3, 1999.

151. Timmons, S.F. et al. Method of Making and Cross-Linking Keratin-Based Films and Sheets. U.S. Patent 6,124,265, Sept. 26, 2000.

152. Van Dyke, M.E. Methods for Producing, Films Comprising, and Methods for Using Heterogeneous Crosslinked Protein Networks. U.S. Patent 6,989,437 B2, Jan. 4, 2006.

153. Hong, C.K. and Wool, R.P. Development of a Bio-Based Composite Material from Soybean Oil and Keratin Fibers. *Journal of Applied Polymer Science*. **2005**, 95, 1524-1538.

154. Anker, C.A. Method of Preparing Keratin-Containing Films and Coatings. U.S. Patent 3,642,498, Feb. 15, 1972.

155. Savolainen, J.E.T. Procedure for Hydrolyzing Keratin. U.S. Patent 5,262,307, Nov. 16, 1993.

156. Wool, R.P. and Sun, X.S. *Bio-Based Polymers and Composites*; Academic Press: Burlington, MA, 2005.

157. Iqbal, M. Dyes and Fiber Polymer System, in: *Textile Dyes*; Rahber Publishers, 2008.

158. Price, H. University of Bristol: School of Chemistry: Undergraduate Web Projects 2002: The Chemistry of Dyes. http://www.chm.bris.ac.uk/webprojects2002/ (accessed June 2010).

159. Block, R.J. The Composition of Keratins: The Amino Acid Composition of Hair, Wool, Horn, and Other Eukeratins. *J. Biol. Chem*. **1939,** 128, 181-186.

160. Author Unknown. Chapter 6: Proteins: Three-Dimensional Structure. http://biochem118.stanford.edu/Papers/Protein%20Papers/Voet%26Voet%20chapter6.pdf (accessed June 2010).

161. Feughelman, M. *Mechanical Properties and Structure of Alpha-Keratin Fibres: Wool, Human Hair and Related Fibres*; UNSW Press, 1997, 164 pages.

162. Fraser, R.D.B et al. Keratins: Their Composition, Structure, and Biosynthesis, in: *American Lecture Series, Publication No. 831*; Thomas, 1972, 304 pages.

163. Yamada, M. et al. Process for Solubilizing Animal Hair. U.S. Patent 5,276,138, Jan. 4, 1994.

164. Jones, C.B. Method of Dispersing Keratin Proteins with Amides and the Composition Resulting Therefrom. U.S. Patent 2,445,028, July, 13, 1948.

165. Saoji et al, A.M. Remazol Brilliant Blue as a Pre-Stain for the Immediate Visualization of Human Serum Proteins on Polyacrylamide Gel Disc Electrophoresis. *Clin. Chem*. **1983**, 29 (1), 42-44.

166. Suwanruji, P. The Design, Synthesis, and Application of Easy Wash Off Reactive Dyes. PhD Dissertation, North Carolina University, North Carolina, 2004.

167. Rouette, H.K. et al. Dye-Fiber Bond Stabilities of Some Reactive Dyes with Wool. *Textile Research Journal*. **1971**, 518-525.

168. Ball, P. et al. Cross-Linking Effects in Reactive Dyeing of Protein Fibers. *Textile Research Journal*. **1986**, 447-456.

169. Shore, J. Mechanism of Reaction of Proteins with Reactive Dyes: 1-Literature Survey. *Journal of the Society of Dyers and Colourists*. **1968**, 84 (8), 408-412.

170. Chang, S.-H. et al. Comparative Study on the Degradation of I.C. Remazol Brilliant Blue R and I.C. Acid Black 1 by Fenton Oxidation and Fe^0/Air Process and Toxicity Evaluation. *Journal of Hazardous Materials*. **2009**, 166, 1279-1288.

171. Saquib, M. and Muneer, M. Semiconductor Mediated Photocatalysed Degradation of an Anthraquinone Dye, Remazol Brilliant Blue R Under Sunlight and Artificial Light Source. *Dyes and Pigments*. **2002**, 53, 237-249.

172. Verma, M. and Ghaly, A.E. Treatment of Remazol Brilliant Blue Dye Effluent by Advanced Photo Oxidation Process in TiO_2/UV and H_2O_2/UV Reactors. *American Journal of Engineering and Applied Sciences*. **2008**, 1 (3), 230-240.

173. Mahmoud, A.S. et al. Decolorization of Remazol Brilliant Blue Dye by Advanced Photo Oxidation process (H_2O_2/UV System). *American Journal of Applied Sciences*. **2007**, 4 (12), 1054-1062.

174. Stahl, W.H. et al. Decomposition of Cystine and Wool by Treatment in the Ball Mill and Autoclave. *J. Biol. Chem*. **1949**, 69-73.

175. McWhorter, D. and Sunada, D.K. *Groundwater Hydrology and Hydraulics*; Water Resources Publications: Littleton, Colorado, 1977.

176. Chang, Joseph (Ed.). ICIS: Indicative Chemical Prices A-Z. http://www.icis.com/StaticPages/a-e.htm (accessed November, 2010).

177. Choy, B. and Reible, D.D. *Diffusion Models of Environmental Transport*; Lewis Publishers: Boca Raton, 2000.

178. Logan, B.E. *Environmental Transport Processes*; John Wiley and Sons: New York, 1999.

179. Reible, D.D. *Fundamentals of Environmental Engineering*; Lewis Publishers: Boca Raton, 1999.

180. Thibodeaux, L.J. *Environmental Chemodynamics*; Wiley: New York, 1996.

181. Spalding, D.B. A Novel Finite-Difference Formulation for Different Expressions Involving both First and Second Derivatives. *Int. J. Numer. Meth. Engng.*,**1972,** 4, 551-559.

182. Patankar, S.V. (author), Minkowycz, W.J. and Sparrow, E.M. (Eds.). *Numerical Heat Transfer and Fluid Flow: Series in Computational Methods in Mechanics and Thermal Sciences*; Hemisphere Publishing Corporation: Cambridge, 1980.

183. Smith, G.D. (author), Crank, J. and Ritchie, C.C. (Eds.). *Numerical Solution of Partial Differential Equations, Oxford Mathematical Handbooks*; Oxford University Press: London, 1965.

184. Ferziger, J.H. and Peric, M. *Computational Methods for Fluid Dynamics*, 3rd Ed. (rev); Springer-Verlag: Berlin, 2002.

185. Golub, G.H. and van Loan, C.F. *Matrix Computations*, 3rd Ed.; Johns Hopkins University Press: Baltimore, 1996.

186. Van Genuchten, M.Th. and Alves, W.J. *Analytical Solutions of the One-Dimensional Convective-Dispersive Solute Transport Equation*. U.S. Dept. of Agriculture, Technical Bulletin No. 1661, 151 pp, 1982.

187. Felder, R.M. and R.W. Rousseau. *Elementary Principles of Chemical Processes, 2nd Edition*; Wiley, 1986.

188. Reid, R.C. et al. *The Properties of Gases and Liquids, 3rd Ed*.; McGraw-Hill, 1977.

189. Montgomery, J.H. and L.M Welkom. *Groundwater Chemicals Desk Reference*; Lewis, 1990.

190. Multimedia Environmental Pollutant Assessment System, Batelle, Inc., 1995.

191. United States Department of Labor. Bureau of Labor Statistics: Consumer Price Index. http://www.bls.gov/cpi/ (accessed November 2010).

192. Manuszak, M.A. et al. The Kinetics of Disulfide Bond Reduction in Hair by Ammonium Thioglycolate and Dithiodiglycolic Acid. *J. Soc. Cosmet. Chem*. **1996**, 47, 49-58.

193. Wakida, T. et al. Dyeing Properties of Wool Treated with Liquid Ammonia. *Journal of the Society of Dyers and Colourists*. **1993**, 109, 393–397.

194. Manuszak, M.A. et al. Reduction of Human Hair by Cysteamine and Ammonium Thioglycolate: A Correlation of Amino Acid Analysis and Single-Fiber Tensile Kinetic Data. *J. Soc. Cosmet. Chem*. **1996**, 47, 213-227.

195. Press, W.H. et al. Numerical Recipes in C: The Art of Scientific Computing, 3rd Ed.; Cambridge University Press, 2007.

Vita

Ryan Ziegler Sitzes was born in Cape Girardeau, Missouri and attended Jackson High School in Jackson, Missouri. He graduated Magna Cum Laude from the Missouri University of Science and Technology in the year 2008 with a Bachelor of Science in Environmental Engineering and an Academic Minor in Mathematics. During his undergraduate career, he also served as President of the Missouri University of Science and Technology student chapter of the Water Environment Federation. He intends to graduate from the University of Texas at Austin with a Master of Science in Engineering in Environmental and Water Resources Engineering.

Permanent address: 114 Wellington Drive, Jackson, Missouri 63755

Email: ryan.sitzes@mail.utexas.edu

This thesis was typed by Ryan Z. Sitzes